# Synthesis of Ruthenium Metathesis Catalysts: Small Cyclic (Alkyl)(Amino)Carbene and Fluorophore-Tagged Ligands for Frontier Applications in Olefin Metathesis

Pedro da Silva

Thesis submitted in partial fulfillment of the requirements
for the Master's degree in Chemistry

Center for Catalysis Research and Innovation
Department of Chemistry and Biomolecular Science
Ottawa-Carleton Chemistry Institute
Faculty of Science
University of Ottawa

# Table of Contents

# List of Figures

# List of Schemes

# List of Tables

# Abstract

Olefin metathesis has emerged as a versatile tool with important potential applications in the production of pharmaceuticals, specialty polymers, and crucial building-block chemicals from biomass sources. Ruthenium metathesis catalysts shine in these contexts, due to their remarkable functional-group tolerance and superior resistance to moisture and oxygen compared to catalysts based on earlier transition metals. Nevertheless, deployment of molecular olefin metathesis catalysts on the scale required for industrial production has been hampered by low catalyst productivity.

Increased productivity has been achieved by the incorporation of cyclic (alkyl)(amino)carbene (CAAC) stabilizing ligands. Targeted in this thesis work was the adaptation of CAAC catalysts to better enable metathesis of internal olefins. Even the cis-configured olefins present in plant or algal oils are more challenging than 1-olefin substrates, owing to their greater steric hindrance. Efforts were undertaken to enhance catalyst performance by reducing the bulk of the CAAC ligand. Indeed, this approach is expected to be broadly relevant to the metathesis of internal olefins and other crowded substrates. The first part of this thesis explores the challenges in preparing Hoveyda-type catalysts of the general form $RuCl_2(CAAC)(=CH_2C_6H_4$-*o*-$O^iPr)$, in which small CAACs are present. Specifically targeted was a complex containing the smallest current CAAC ligand, in which the carbene carbon is flanked by an N-mesityl group and a dimethyl-substituted carbon. Meagre yields in the synthesis of this catalyst have been achieved to date, with a maximum of 14% in the open literature. Acting on the hypothesis that a major, overlooked problem lies in abstraction of the [Ru]=CHR ligand by free CAAC or $PCy_3$ present during catalyst synthesis, a new route was established via ligand exchange of the $RuI_2(PCy_3)(=CH_2C_6H_4$-*o*-$O^iPr)$ platform with the small CAAC indicated above. The bulk of the iodide ligands inhibits nucleophilic attack at the benzylidene, conferring the necessary steric protection to prevent catalyst decomposition. Ensuing halide exchange then afforded access to the desired chloride catalyst. This strategy was successful, giving access to the target complex in 55% yield. It offers a potentially generalizable methodology for the preparation of ruthenium metathesis catalysts bearing small stabilizing ligands.

Also examined was the synthesis of a fluorophore-tagged olefin metathesis catalyst. Such catalysts are of interest for their potential to enable real-time monitoring of catalyst behaviour at concentrations too low for NMR analysis. While challenges remain in optimizing yields in the synthesis of a known dansyl-tagged catalysts, the methodology developed (particularly the synthesis of a dansyl-tagged benzylidene) provides a solid foundation for future advances.

In sum, this thesis presents advances in the synthesis of designed catalysts for frontier applications in olefin metathesis. Ruthenium catalysts bearing small CAAC ligands and fluorophore tags are anticipated to enable new applications and new insights relevant to materials science, renewable feedstocks, and process chemistry.

# List of Contributions

**Presentations (O = Oral, presenting author in bold)**

**O1. P. H. L. da Silva,** D. E. Fogg. "Establishing a Route to Ruthenium Metathesis Catalysts Bearing Small Cyclic Alkyl Amino Carbene (CAAC) Ligands" Ottawa-Carleton Chemistry Institute (OCCI) Day, Ottawa, ON, June 8th, 2022.

**Publications**

**Pedro H. L. da Silva** and Deryn E. Fogg. "An Enabling Route to Ruthenium Metathesis Catalysts Bearing Small Cyclic Alkyl Amino Carbene (CAAC) Ligands". Manuscript in preparation.

# Acknowledgments

Firstly, I would like to thank God for all the strength and all the achievements obtained so far. Without his presence, none of this would be possible. To my parents, Miguel Teixeira and Ana Creuma Luciano, as well to my sister, Jully Luciano. For the support, encouragement and affection that built the man I became and pushed me to be more than what our unequal society expected.

To my wife, Jennefer Torres, with my deepest love and gratitude, I thank you for being by my side over all the challenges presented in the last few years. It was your affection, friendship and dedication that kept me firm on the arduous journey of this work and many other moments in my life. Above all, for supporting my dreams and aspirations.

I extend my deepest thanks to Eliza-Jayne, Christian, Samantha and Harrison for their essential roles in guiding and supporting me and supporting my research. Coworkers who became valuable friends who captivated a place in my heart and that I wish to take with me for life. Of course, to all the other friends I found in UOttawa, in many coffees and chats in the hallways.

To all the other wonderful colleagues who have been part of my journey in the Fogg group, I extend my sincere appreciation. Each of you has contributed to making this chapter in my life truly memorable, and for that, I am truly thankful.

Above all, I want to express my deepest gratitude to my supervisor, Prof. Deryn Fogg, for her unwavering guidance, support, and patience throughout my graduate journey. I am profoundly thankful for her mentorship, which has surely enriched my scientific thinking. The invaluable skills and knowledge I have acquired during my tenure in her group will undoubtedly be assets that I carry from now on.

Thank you so much for everything.

# List of Compounds

Organic and main-group compounds

| Compound | Structure | Compound | Structure |
|---|---|---|---|
| $H_2$IMes | 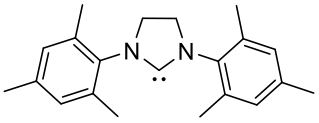 | IMes | 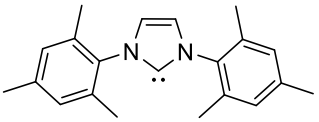 |
| **1** | 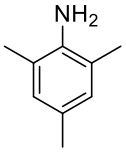 | **2** |  |
| **3** | 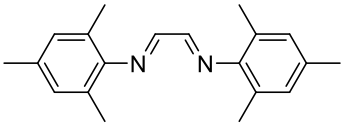 | **4** | 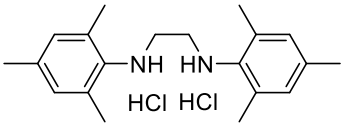 |
| **5** | 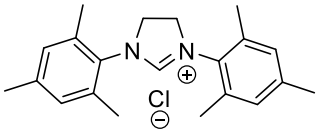 | **6** | 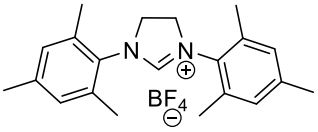 |
| **Z-MO** | 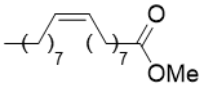 | **E-MO** | 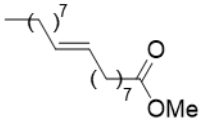 |
| **7** |  | **8** |  |
| **9** | 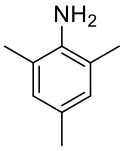 | **10** | 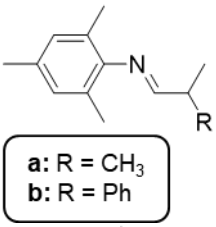 |
| **11** | 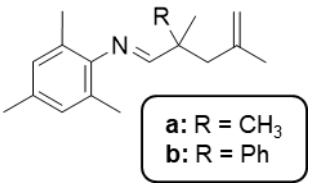 | **12** | 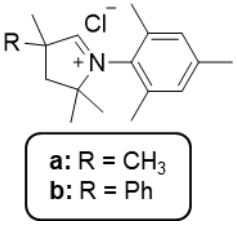 |
| **13** | 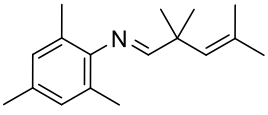 | **14** | 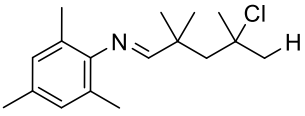 |

| | | | |
|---|---|---|---|
| **15** | 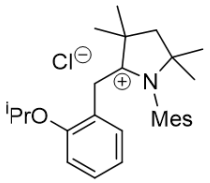 | **16** | 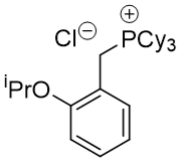 |

Transition-metal complexes

| Compound | Structure | Compound | Structure |
|---|---|---|---|
| **Ta-I** | 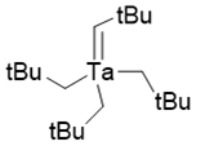 | **Mo-I** | 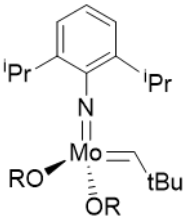 |
| **W-I** | 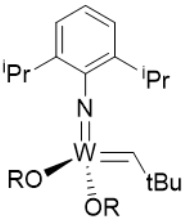 | **Ru-1** | 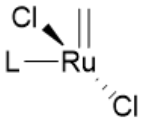 |
| **Ru-1'** | 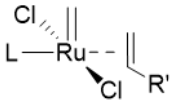 | **Ru-2** | 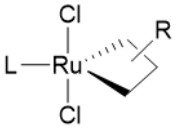 |
| **Ru-3** | 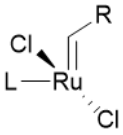 | **Ru-4** | 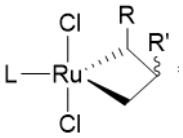 |
| **Ru-5** | 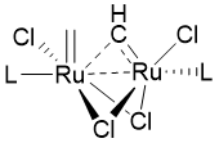 | **Ru-6** | 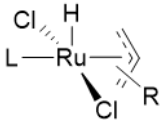 |
| **Ru-7** | 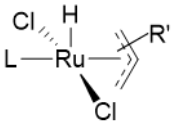 L=$H_2$IMes | **Ru-8** | 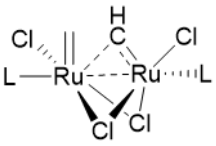 L=$H_2$IMes |

| | | | |
|---|---|---|---|
| **GI** | 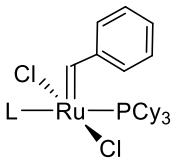 | **GII** | 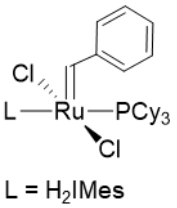 |
| **GII-IMes** | 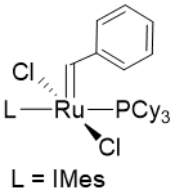 | **HI** | 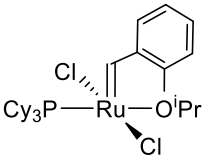 |
| **HII** | 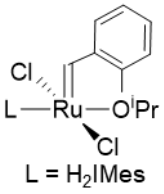 | **HII-IMes** | 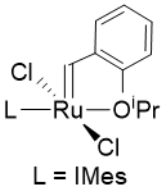 |
| **Ru-m** | 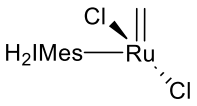 | **UC$^{Mes}$** | 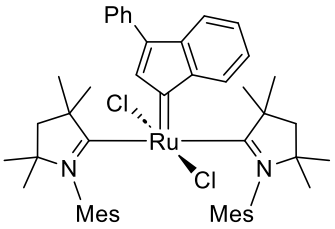 |
| **Ru-9** | 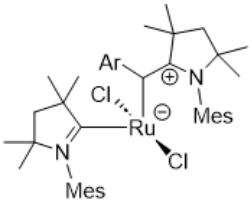 | **Ru-10** | 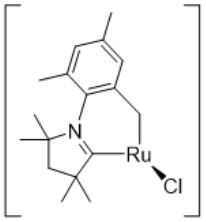 |
| **Ru-11** | 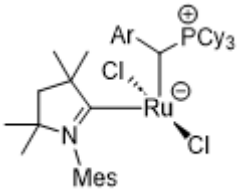 | **HI-I$_2$** | 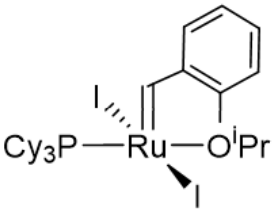 |

# List of Abbreviations

| | |
|---|---|
| ADMET | acyclic diene metathesis |
| BMC | bimolecular coupling |
| CAAC | cyclic (alkyl)(amino)carbene |
| CM | cross-metathesis |
| Cy | cyclohexyl |
| Equiv | equivalents |
| GC | gas chromatography |
| $H_2$IMes | N,N'-bis-(2,4,6-trimethylphenyl)imidazolin-2-ylidene |
| HOMO | highest occupied molecular orbital |
| IMes | N,N'-bis-(2,4,6-trimethylphenyl)imidazol-2-ylidene |
| IS | internal standard |
| KOtBu | tert-butoxide |
| KTp | potassium hydrotris(pyrazolyl)borate |
| LiHMDS | lithium hexamethyldisilazane |
| LUMO | lowest unoccupied molecular orbital |
| MCB | metallacyclobutane |
| Mes | mesityl, 2,4,6-trimethylphenyl |
| **MO** | methyl oleate |
| NHC | N-heterocyclic carbene |
| NMR | nuclear magnetic resonance |
| ppm | parts per million (μg/g) |
| py | pyridine |
| RCM | ring-closing metathesis |
| ROMP | ring-opening metathesis polymerization |
| RT | room temperature |
| SM | self-metathesis |
| TON | turnover number |

# Chapter 1 Introduction

## 1.1 Olefin Metathesis

### 1.1.1 General Background

Olefin metathesis is a powerful chemical reaction that involves the rearrangement of carbon-carbon double bonds catalyzed by a transition-metal carbene complex (Scheme 1.1).[1,2] Even though reports of the associated products can be tracked to the early 1930s, the first catalyzed reaction was only reported in the late 1950s by industrial chemists at DuPont, Standard Oil and Phillips Petroleum.[3] In 1956, the DuPont team observed the $TiCl_4$-catalyzed ring-opening metathesis polymerization (ROMP) of norbornene.[3] Simultaneously, a separate investigation led by Eleuterio[4] at DuPont revealed a remarkable occurrence. On passing propylene gas through a molybdenum-on-aluminum catalyst bed, the unexpected formation of propylene, ethylene, and 1-butene was observed.

**Scheme 1.1.** General representation for the olefin metathesis reaction.

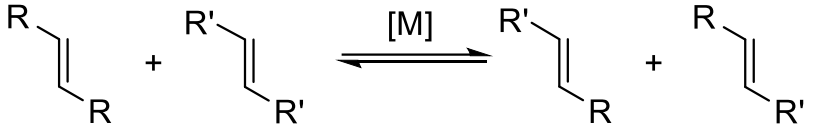


This intriguing reactivity drew attention from many chemists who sought to decipher the mechanism. In 1967, a breakthrough resulted from the efforts of Calderon at Goodyear Tire & Rubber.[5] Calderon's experiments with a 1:1 mixture of 2-pentene and $WCl_6$ in EtOH yielded 2-butene, 2-pentene, and 3-hexene, in a ratio of 1:2:1. Based on this finding, Calderon proposed that the olefinic products arose from an intermolecular exchange of alkylidene groups, for which he coined the term 'olefin metathesis'.

In 1974, as a member of DuPont's Central Research and Discovery unit, Schrock designed and synthesized the first well-defined metal-alkylidene olefin metathesis catalyst.[6] In this seminal discovery, he prepared a stable and isolable Ta(V) neopentylidene complex, **Ta-I** (Figure 1.1). The high oxidation state of the metal center results in a highly polarized M=CHR bond, with a partial positive charge on the tantalum center and a partial negative charge on the alkylidene carbon. These characteristics rendered **Ta-I** exceptionally reactive in metathesis.[7] However, they also conferred undesired, non-metathetical reactivity toward carbonyl functionalities (including ketones) and protic groups such as those present in alcohols or water. Subsequent discoveries revealed bimolecular decomposition pathways, discussed in more detail in Section 1.1.4. Much effort thus focused on introducing bulky ligands to block the latter pathways. Schrock catalysts containing bulky imido and alkoxide or aryloxide ligands (exemplified by **W-I** and **Mo-I** in Figure 1.1) attain high metathesis activity. However, they remain susceptible to oxygen and water. Their thermal sensitivity[8,9] is also problematic, particularly for commercial production and shipping, as it affects their long-term shelf stability.

**Figure 1.1.** Selected Schrock olefin metathesis catalysts.

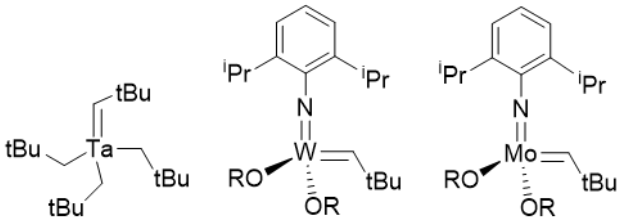


**Ta-I** **W-I** **Mo-I**

Olefin metathesis reactions represent versatile tools for the synthesis of both molecules and materials. The ring-closing metathesis (RCM) of α,ω-dienes to form cyclic olefins (Figure 1.2), for example, holds promise in the pharmaceuticals sector.[10–12] Production of polymers can be achieved through acyclic diene metathesis (ADMET)[1,13] or ring-opening metathesis polymerization (ROMP)[13–15] of strained cyclic olefins. In the feedstocks arena, intermolecular cross-metathesis (CM) reactions offers important opportunities for the conversion of plant oils into essential building-block chemicals and the transformation of essential oils into valuable, enhanced products.[16–18]

**Figure 1.2.** Common olefin metathesis reactions.

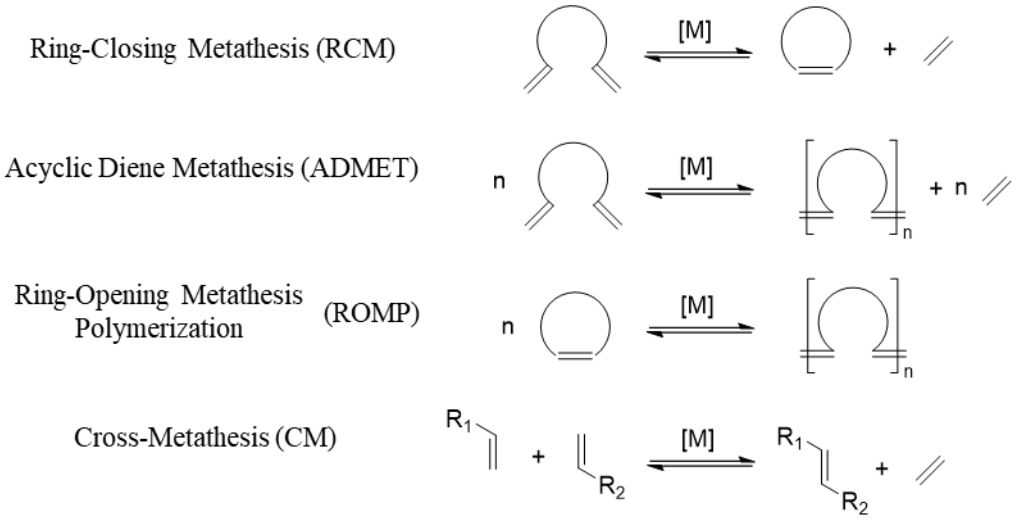


### 1.1.2 Ruthenium-Catalyzed Olefin Metathesis

Ruthenium catalysts offer an attractive alternative to the group 6 catalysts, owing to their enhanced tolerance for air (both oxygen and water), and various functional groups,[19,20] as well as excellent shelf-stability. In 1995, Schwab, Grubbs and their coworkers published a catalyst with breakthrough reactivity, now known as the "first-generation Grubb's catalyst" (**GI**, Figure 1.3).[21] This discovery led to intensive research on ruthenium metathesis catalysts, turning the focus away from group 6 complexes. Grubbs later shared the Nobel Prize with Schrock and Chauvin.[22–24] Among the most significant subsequent advances in catalyst design was the development of

"second-generation" Grubbs catalysts (for example, **GII**, Figure 1.3), in which an N-heterocyclic carbene (NHC) replaced one or both $PCy_3$ ligands. Such catalysts were reported nearly simultaneously by the groups of Herrmann, Grubbs, and Nolan in 1998-1999.[25–27] The most extensively investigated variants are those reported by the Grubbs and Nolan groups, containing an $H_2$IMes or IMes ligand (**GII**, **GII-IMes**, respectively), which afforded significant increases in metathesis activity.[25]

**Figure 1.3.** Selected olefin metathesis catalysts and NHC ligands.

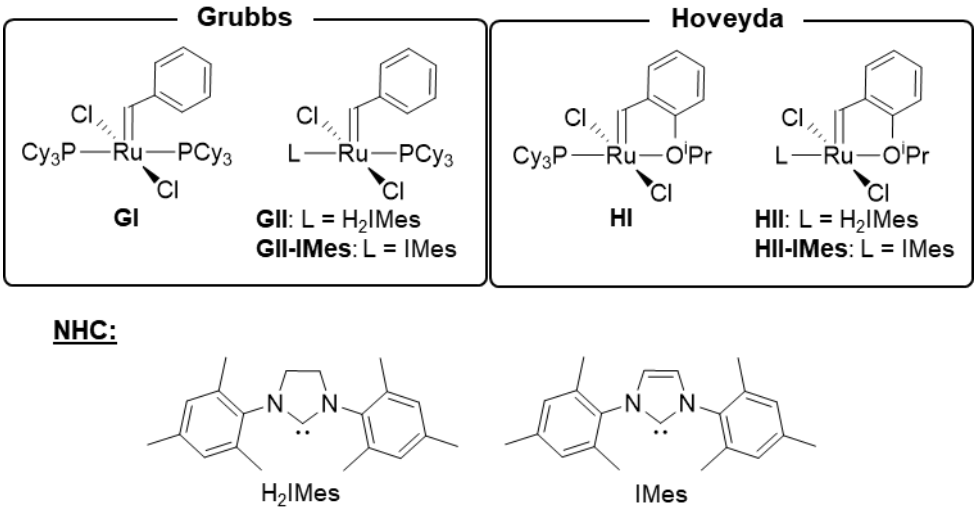


A further significant development was the introduction of the phosphine-free Hoveyda-class catalysts, in which the benzylidene moiety bears a chelating *o*-ether group (see **HI**,[28] **HII**,[29,30] Figure 1.3) that replaces one $PCy_3$ ligand. As with the Grubbs catalysts, replacing the second $PCy_3$ ligand with a strongly σ-donating NHC ligand greatly improved catalyst activity.[30] Improved productivity also resulted, because this design circumvents the low lability of the phosphine ligand noted above, as well as decomposition of the active species by free $PCy_3$ (see below).[31–33] These second-generation complexes are among the most studied and used catalysts for olefin metathesis, highlighting the importance of carbene ligands in the field.[2,34]

### 1.1.2.1 Synthesis of NHCs and Hoveyda-Class catalysts

The synthesis of NHC ligands from commercially available materials is well established, offering access to their imidazol(in)ium salts in overall yields of 55-80%.[35] A typical synthetic route to the imidazolium salt of $H_2$IMes is depicted in Scheme 1.2. Arguably the most important step, liberation of the free carbene, is achieved by deprotonating the imidazolium salt with a strong base such as lithium hexamethyldisilazane (LiHMDS), potassium tert-butoxide (KOtBu) or NaH. Many NHCs are sufficiently stable to isolate as the free carbene,[36,37] in principle enabling their installation on the catalyst via ligand exchange with (e.g.) a Ru-phosphine precursor. Very commonly, however, the imidazolium salt is generated in situ for reasons of convenience,[2,34] despite the negative impacts of residual salt or excess base on catalyst purity.[36,37]

**Scheme 1.2.** Synthetic route for $H_2$IMes and **HII**.

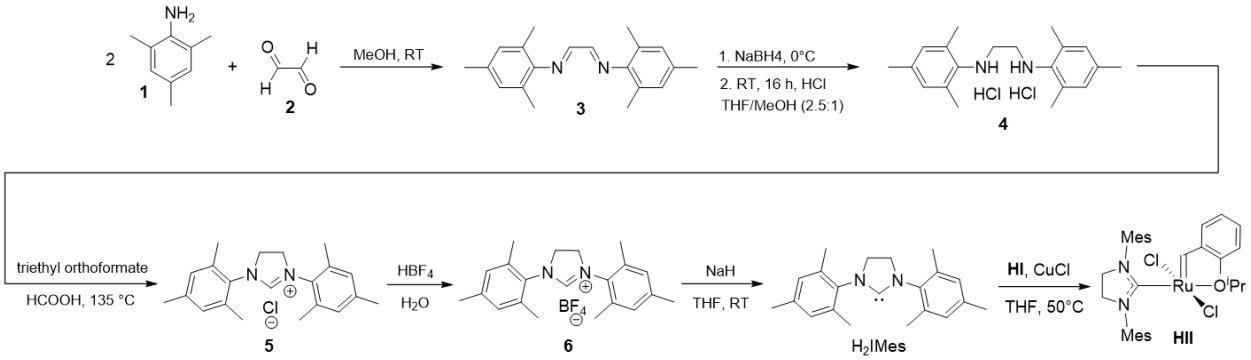


### 1.1.3 Mechanism of Transition-Metal Catalyzed Olefin Metathesis

From the early studies in olefin metathesis, various hypotheses emerged to explain its mechanism. Possible intermediates were proposed, including a four-centered cyclobutane-metal species, a tetra(methylene)metal complex, and a metallocyclopentane intermediate.[38–40] In 1971, Chauvin[41] postulated a series of steps that are now accepted as the mechanism of olefin metathesis.[42] Initially, the incoming olefin coordinates to a metal species bearing an alkylidene moiety (**Ru-1**) through the pi bond. Next, a metallacyclobutane (**Ru-2**) is formed via a [2+2] cycloaddition of the olefin and M=CHR species (Scheme 1.3). This metallacyclobutane undergoes a [2+2] cycloreversion, which can reconstitute the starting alkylidene and olefin (unproductive metathesis), or liberate a new olefin (Olefin A) and a new metal-alkylidene species (**Ru-3**) in a productive metathesis step. After repeating the process with another incoming olefin (**Ru-4**), the second olefinic product (Olefin B) is released, and the active species is restored. Chauvin's elucidation of this mechanism was essential for advancing and comprehending olefin metathesis.

**Scheme 1.3.** General catalytic cycle for olefin metathesis.

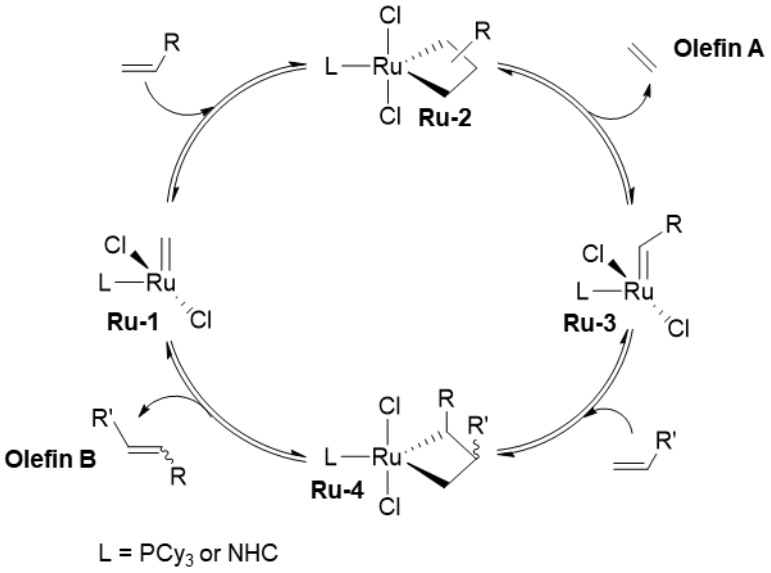

In contrast to the four-coordinate Schrock catalysts, the ruthenium precatalysts are generally five-coordinate, square pyramidal complexes in which the high trans-effect alkylidene ligand occupies the apical site. Release of a basal ligand is required to form the four-coordinate active species,[43] and permit the incoming olefin to bind cis to the alkylidene. Then, the coordinated olefin undergoes a cycloaddition that gives rise to the **MCB** intermediate (Scheme 1.4). The first step involves only initiation to form the actual active catalyst, which continues to turn over in the presence of olefin.[43–45]

Initially, Grubbs attributed the enhanced activity of second-generation vs first-generation catalysts to 'increased labilization' of the $PCy_3$ ligand due to the trans effect of the NHC.[25] In fact, the precatalyst **GII** initiates more than 100-fold slower than **GI**.[46–48] Indeed, the off-cycle resting state, methylidene species **Ru-m**, dissociates $PCy_3$ to re-enter the active cycle 41,000 times slower than **GI**.[49] This initially puzzling phenomenon was shown by our group to arise from an *inverse* trans effect exerted by the NHC ligand,[46] a function of strong NHC donicity in conjunction with the long-dismissed acceptor ability of the phosphine ligand.[48] The higher metathesis activity of Ru-NHC catalysts is now known to arise from the impact of strong NHC σ-donation in reducing the energy barrier to cycloaddition,[50,51] which enables faster reaction with olefin than reuptake of $PCy_3$. Similarly, phosphine-free **HII** undergoes dissociation of the chelating *o*-propoxide group in the first metathesis step to generate the active catalyst (**Ru-m**; Scheme 1.4).

**Scheme 1.4.** Initiation of **GII** and **HII** catalysts.

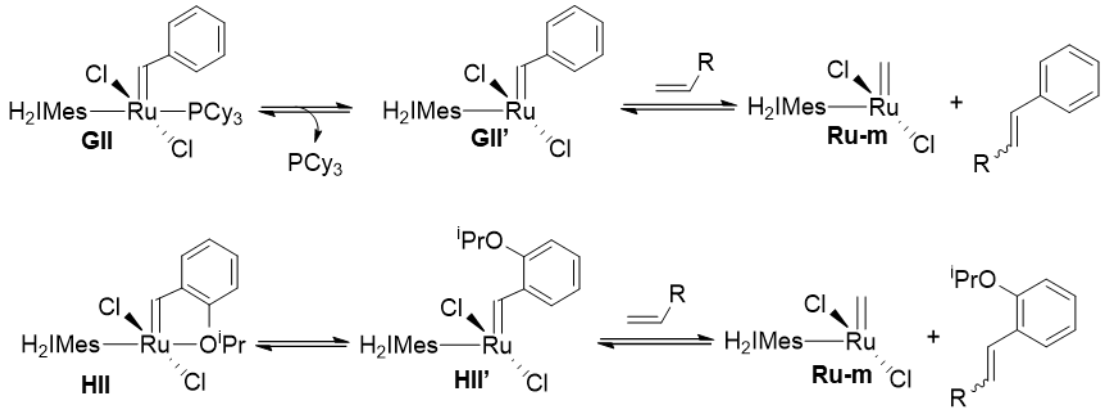


### 1.1.4 Decomposition of Metathesis Catalysts: Intrinsic Pathways

Two pathways by which the vast majority of metathesis catalysts decompose are shown in Scheme 1.5 (exemplified with the Ru catalysts). The first involves bimolecular coupling (BMC) of two molecules of the four-coordinate $RuCl_2(L)(=CHR)$ intermediate (**Ru-1**). BMC was widely accepted for first-generation Grubbs catalysts (where L = $PCy_3$ or other phosphines), based on the observation of RCH=CHR products during catalyst synthesis or use.[52–54] Its operation in second-generation systems was thought to be blocked by NHC bulk, in conjunction with low phosphine lability, and hence limited concentrations of **Ru-1**. However, Bailey and Fogg demonstrated BMC of second-generation catalysts by quantifying the ethylene produced by coupling of transiently-

stabilized methylidene complexes.[52] These experiments firmly established BMC as a prominent decomposition pathway for both second- and first-generation Ru catalysts. The importance of alkylidene bulk in inhibiting bimolecular coupling was also demonstrated.[52] In particular, methylidene complexes such as **Ru-1** were shown to undergo significantly faster coupling than their benzylidene counterparts, although the latter do undergo BMC (if slowly) when phosphine ligands are absent or trapped.[55,56] Nascimento and Fogg demonstrated that carbene bulk is also critical.[56]

**Scheme 1.5.** Bimolecular coupling and β-H elimination decomposition pathways.

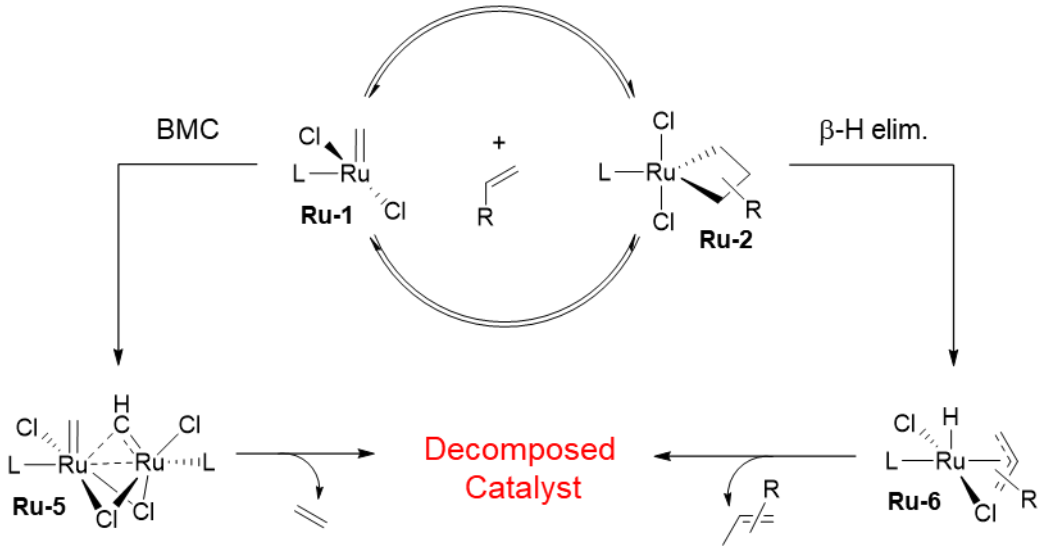


A second decomposition pathway intrinsic to nearly all metathesis catalysts involves β-hydride elimination from the MCB ring (**Ru-2**).[57] In this process, a hydrogen atom is transferred from the β-$CH_2$ group of the MCB to the metal, forming an allyl hydride intermediate (**Ru-6**). This intermediate can undergo reductive elimination to yield the substituted propene ($H_2C$=$CHCHR_3$ or $RCH_2$=$CHCH_3$).[58] In experiments using a $^{13}C$-labelled MCB in $CD_2Cl_2$, Piers and coworkers tracked the release of labelled propene on raising the temperature from -40 °C to -10 °C, providing the most compelling evidence for β-H elimination in the ruthenium catalysts.[59–61]

### 1.1.5 CAAC Ligands: Advances Arising from Electronic Differences vs NHCs

Notwithstanding the advances arising from incorporating NHC ligands in olefin metathesis (Section 1.1.2), catalyst productivity has remained a major challenge. Catalysts containing cyclic (alkyl)(amino)carbene (CAAC) ligands were hence a breakthrough, enabling increased productivity in cross-metathesis with ethylene ("ethenolysis") and macrocyclization via ring-closing metathesis (mRCM).[55] In 2015, the Grubbs and Bertrand groups reported turnover numbers (TONs) of 340,000 using Ru-CAAC catalysts in ethenolysis of methyl oleate, 100-fold higher than the best TONs observed for Ru-$H_2$IMes catalysts.[55,62] The improved performance originates in the difference in electronic properties.[62,63] In the CAAC ligands, one σ-withdrawing

and π-donating N-aryl group is replaced by an σ-donating quaternary alkyl group (e.g., $CMe_2$). This structural change renders the highest occupied molecular orbital (HOMO) of the CAAC slightly higher in energy, and the lowest unoccupied molecular orbital (LUMO) lower in energy than the corresponding NHC (Figure 1.4). This confers higher nucleophilicity and electrophilicity on the CAACs than traditional NHCs. Overall, CAAC carbenes are more σ-donating and π-accepting than NHCs.[17,64,65]

**Figure 1.4.** Structures and Frontier molecular orbitals for NHC and CAAC ligands.

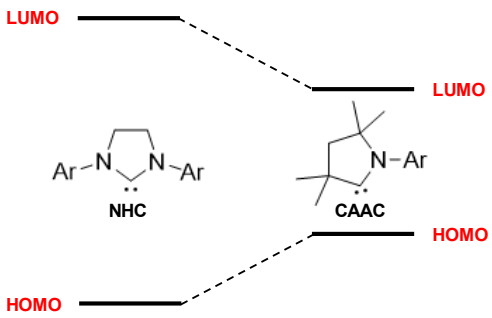


Nascimento and Fogg established that the productivity breakthrough is due to improved catalyst robustness.[66] Specifically, they established that the CAAC catalysts are essentially immune to decomposition via β-H elimination of the metallacyclobutane (MCB). In a comparative study of the $RuCl_2(L)(=CHAr)$ catalysts (L= CAAC or $H_2IMes$; Ar = *o*-$C_6H_4$-O$^i$Pr), they tracked the propenes produced by β-H elimination of **Ru-2** (Scheme 1.6) by $^1$H NMR analysis. They showed that the CAAC catalysts generate ≤2% propenes, based on the starting catalyst charge. Crucially, however, they also demonstrated that the CAAC catalysts are more susceptible to bimolecular decomposition of the methylidene intermediates **Ru-1** generated by loss of pyridine from $RuCl_2(L)(py)(=CH_2)$.[56,66] In 2022, the Jensen and Fogg groups uncovered the common factor that unites the increased stability of the CAAC catalysts to β-elimination and their increased susceptibility to bimolecular decomposition.[47] The stronger σ-donating and π-back-donating orbital interactions noted above strengthen the Ru-CAAC covalent bond. Donation of the β-C–H bond of the metallacycle involves the same orbitals, as this interaction is essentially trans to the carbene. The higher energy of the transition state for C–H activation during β-elimination (trans effect), as well as the Ru-olefin intermediate **Ru-1'** (trans influence), disfavor β-elimination, accounting for the resistance of CAAC catalysts to this decomposition pathway. In addition, the CAAC catalysts were shown to be less susceptible to non-productive metathesis with ethylene, the coproduct in the metathesis of terminal olefin. Greater engagement in the productive cycle limits catalyst decomposition during unproductive turnovers, thus also improving TONs.

**Scheme 1.6.** Intrinsic decomposition pathways for phosphine-free metathesis catalysts.

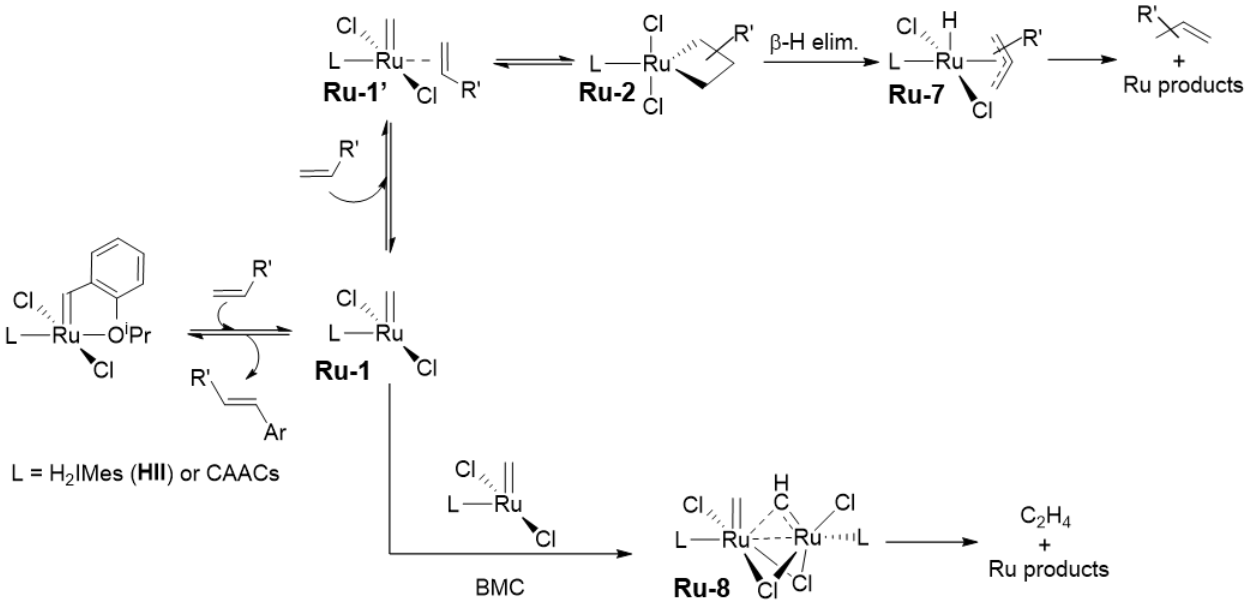


The high trans influence of the CAAC ligand, while advantageous in preventing β-elimination of the CAAC catalysts, destabilizes the coordinated olefin in species **Ru-1'**. The higher instantaneous concentration of the methylidene species (**Ru-1**) promotes faster decomposition via formation of dimer **Ru-8**.[47,56]

### 1.1.6 Strategies to Prevent Bimolecular Coupling

One potential strategy to limit BMC of the Ru metathesis catalysts is using bulkier CAAC or other auxiliary ligands, which could sterically disfavour coupling of four-coordinate **Ru-**1 (Scheme 1.6). Nascimento and Fogg explored the relationship between increased catalyst bulk and robustness in a study of $RuX_2$(CAAC)(py)(=$CH_2$) complexes (Figure 1.5; py = pyridine; X = Cl or I ). In that work, they compared rates of BMC decomposition of different Ru-CAAC catalysts by $^1$H NMR analysis.[56] Increasing bulk by replacing the chloride ligands by iodide (see **RuCAAC-1** and **RuCAAC-1-I$_2$**) slowed BMC by 40-fold. Alternatively, replacing the CAAC α-methyl group with a phenyl group (see **RuCAAC-1** and **RuCAAC-2**) led to eight times slower BMC. The same tendency can be observed on decreasing N-aryl bulk. Thus, **RuCAAC-3**, containing a mesityl group, decomposed at double the rate of **RuCAAC-1**. Where the metathesis of crowded substrates is desired, however, catalyst bulk can significantly limit performance (a point explored in more detail in Chapter 2). More general ways to reduce BMC decomposition are thus employing very low (sub-micromolar) catalyst concentrations to retard the second-order pathway, or anchoring the catalyst to a solid support.

**Figure 1.5.** BMC experiments and CAAC ligands discussed by Nascimento and Fogg.[56]

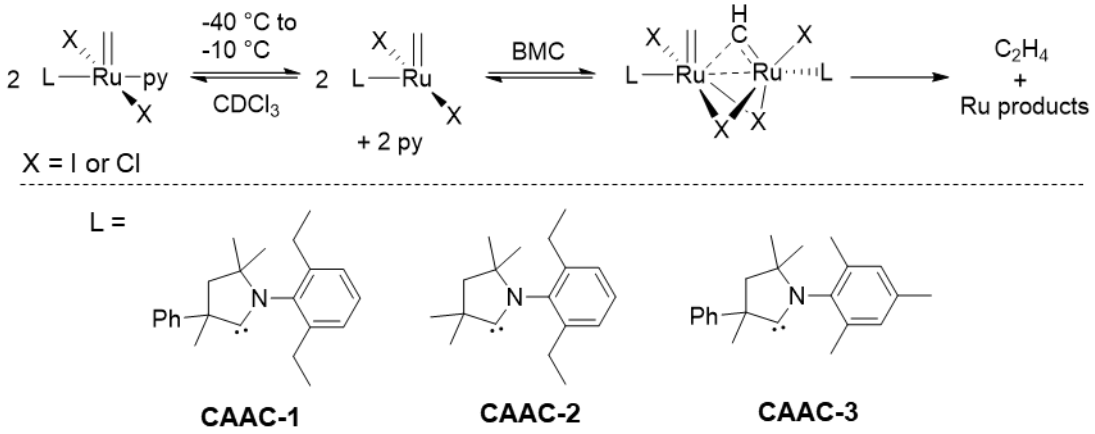


## 1.2 Scope of Thesis

Despite the power of the ruthenium catalysts, improved performance for specific applications remains a challenge. The implementation of CAACs as stabilizing ligands for the metathesis of hindered substrates is one such opportunity. Chapter 2 considers the potential to improve metathesis of such substrates by employing catalysts bearing small CAAC ligands. A decomposition pathway is proposed to account for the low synthetic yields of such catalysts, a new route to an exemplary catalyst is described, and the enhanced productivity of this catalyst in self-metathesis of methyl oleate is described, in an advance that contributes to the valorization of renewable fatty acids.

Described in Chapter 3 is a complementary approach to the development of improved catalysts, with a mechanistic focus. Catalysts bearing fluorophore tags enable the use of fluorimetry to track catalyst behaviour in practical operational scenarios, in which catalyst concentrations are typically in the micromolar range. Fluorimetry offers a solution to the elevated catalyst concentration required for NMR analysis, which can alter the decomposition pathways. Bimolecular decomposition serves as a clear illustration of this phenomenon. An improved synthetic route to a dansyl-tagged alkylidene ruthenium catalyst is presented.

Finally, Chapter 4 presents an overview of results and recommendations for future work.

## 1.3 References


(1) Grubbs, R. H. *Handbook of Metathesis, Second Edition, Volume I: Catalyst Development and Mechanism*; Grubbs, R. H., Wenzel, A. G., Eds.; Wiley-VCH, 2015; Vol. 1.

(2) Vougioukalakis, G. C.; Grubbs, R. H. Ruthenium-Based Heterocyclic Carbene-Coordinated Olefin Metathesis Catalysts. *Chem. Rev.* **2010**, *110*, 1746–1787.

(3) Anderson, A. W.; Merckling, N. G. Polymeric Bicyclo-(2,1)-2-Heptene. US2721189A, 1956.

(4) Eleuterio, H. S. Olefin Metathesis: Chance Favors Those Minds That Are Best Prepared. *J. Mol. Catal.* **1991**, *65*, 55–61.

(5) Calderon, N.; Chen, H. Y.; Scott, K. W. Olefin Metathesis - A Novel Reaction for Skeletal Transformations of Unsaturated Hydrocarbons. *Tetrahedron Lett.* **1967**, *8*, 3327–3329.

(6) Schrock, R. R.; Copéret, C. Formation of High-Oxidation-State Metal–Carbon Double Bonds. *Organometallics* **2017**, *36*, 1884–1892.

(7) Schrock, R. R. Multiple Metal-Carbon Bonds. 5. The Reaction of Niobium and Tantalum Neopentylidene Complexes with the Carbonyl Function. *J. Am. Chem. Soc.* **1976**, *98*, 5399–5400.

(8) Schrock, R. R.; DePue, R. T.; Feldman, J.; Schaverien, C. J.; Dewan, J. C.; Liu, A. H. Preparation and Reactivity of Several Alkylidene Complexes of the Type W(CHR')(N-2,6-C6H3-Iso-Pr2)(OR)2 and Related Tungstacyclobutane Complexes. Controlling Metathesis Activity through the Choice of Alkoxide Ligand. *J. Am. Chem. Soc.* **1988**, *110*, 1423–1435.

(9) Schrock, R. R.; Murdzek, J. S.; Bazan, G. C.; Robbins, J.; DiMare, M.; O'Regan, M. Synthesis of Molybdenum Imido Alkylidene Complexes and Some Reactions Involving Acyclic Olefins. *J. Am. Chem. Soc.* **1990**, *112*, 3875–3886.

(10) Lu, X.; Fan, L.; Phelps, C. B.; Davie, C. P.; Donahue, C. P. Ruthenium Promoted On-DNA Ring-Closing Metathesis and Cross-Metathesis. *Bioconjug. Chem.* **2017**, *28*, 1625–1629.

(11) Higman, C. S.; Lummiss, J. A. M.; Fogg, D. E. Olefin Metathesis at the Dawn of Implementation in Pharmaceutical and Specialty-Chemicals Manufacturing. *Angew. Chem. Int. Ed.* **2016**, *55*, 3552–3565.

(12) Giordanetto, F.; Kihlberg, J. Macrocyclic Drugs and Clinical Candidates: What Can Medicinal Chemists Learn from Their Properties? *J. Med. Chem.* **2014**, *57*, 278–295.

(13) Knall, A.; Slugovc, C. Olefin Metathesis Polymerization. In *Olefin Metathesis*; Wiley, 2014; pp 269–284.

(14) Feist, J. D.; Xia, Y. Enol Ethers Are Effective Monomers for Ring-Opening Metathesis Polymerization: Synthesis of Degradable and Depolymerizable Poly(2,3-Dihydrofuran). *J. Am. Chem. Soc.* **2020**, *142*, 1186–1189.

(15) Cormier, S. K.; Fogg, D. E. Probing Catalyst Degradation in Metathesis of Internal Olefins: Expanding Access to Amine-Tagged ROMP Polymers. *ACS Catal.* **2023**, *13*, 11834–11840.

(16) Yelchuri, V.; Srikanth, K.; Prasad, R. B. N.; Karuna, M. S. L. Olefin Metathesis of Fatty Acids and Vegetable Oils. *J. Chem. Sci.* **2019**, *131*, 39–55.

(17) Morvan, J.; Mauduit, M.; Bertrand, G.; Jazzar, R. Cyclic (Alkyl)(Amino)Carbenes (CAACs) in Ruthenium Olefin Metathesis. *ACS Catal.* **2021**, *11*, 1714–1748.

(18) Marvey, B. B.; Segakweng, C. K.; Vosloo, M. H. C. Ruthenium Carbene Mediated Metathesis of Oleate-Type Fatty Compounds. *Int. J. Mol. Sci.* **2008**, *9*, 615–625.

(19) Nguyen, S. T.; Grubbs, R. H.; Ziller, J. W. Syntheses and Activities of New Single-Component, Ruthenium-Based Olefin Metathesis Catalysts. *J. Am. Chem. Soc.* **1993**, *115*, 9858–9859.

(20) Wolf, J.; Stüer, W.; Grünwald, C.; Werner, H.; Schwab, P.; Schulz, M. Ruthenium Trichloride, Tricyclohexyl- Phosphane, 1-Alkynes, Magnesium, Hydrogen, and Water—Ingredients of an Efficient One-Pot Synthesis of Ruthenium Catalysts for Olefin Metathesis. *Angew. Chem. Int. Ed.* **1998**, *37*, 1124–1126.

(21) Schwab, P.; France, M. B.; Ziller, J. W.; Grubbs, R. H. A Series of Well-Defined Metathesis Catalysts–Synthesis of[RuCl2(□CHR′)(PR3)2] and Its Reactions. *Angew. Chem. Int. Ed. English* **1995**, *34*, 2039–2041.

(22) Grubbs, R. H. Olefin-Metathesis Catalysts for the Preparation of Molecules and Materials (Nobel Lecture). *Angew. Chem. Int. Ed.* **2006**, *45*, 3760–3765.

(23) Schrock, R. R. Multiple Metal–Carbon Bonds for Catalytic Metathesis Reactions (Nobel Lecture). *Angew. Chem. Int. Ed.* **2006**, *45*, 3748–3759.

(24) Chauvin, Y. Olefin Metathesis: The Early Days (Nobel Lecture). *Angew. Chem. Int. Ed.* **2006**, *45*, 3740–3747.

(25) Scholl, M.; Ding, S.; Lee, C. W.; Grubbs, R. H. Synthesis and Activity of a New Generation of Ruthenium-Based Olefin Metathesis Catalysts Coordinated with 1,3-Dimesityl-4,5-Dihydroimidazol-2-Ylidene Ligands. *Org. Lett.* **1999**, *1*, 953–956.

(26) Huang, J.; Stevens, E. D.; Nolan, S. P.; Petersen, J. L. Olefin Metathesis-Active Ruthenium Complexes Bearing a Nucleophilic Carbene Ligand. *J. Am. Chem. Soc.* **1999**, *121*, 2674–2678.

(27) Weskamp, T.; Schattenmann, W. C.; Spiegler, M.; Herrmann, W. A. A Novel Class of Ruthenium Catalysts for Olefin Metathesis. *Angew. Chem. Int. Ed.* **1998**, *37*, 2490–2493.

(28) Kingsbury, J. S.; Harrity, J. P. A.; Bonitatebus, P. J.; Hoveyda, A. H. A Recyclable Ru-Based Metathesis Catalyst. *J. Am. Chem. Soc.* **1999**, *121*, 791–799.

(29) Gessler, S.; Randl, S.; Blechert, S. Synthesis and Metathesis Reactions of a Phosphine-Free Dihydroimidazole Carbene Ruthenium Complex. *Tetrahedron Lett.* **2000**, *41*, 9973–9976.

(30) Garber, S. B.; Kingsbury, J. S.; Gray, B. L.; Hoveyda, A. H. Efficient and Recyclable Monomeric and Dendritic Ru-Based Metathesis Catalysts. *J. Am. Chem. Soc.* **2000**, *122*, 8168–8179.

(31) McClennan, W. L.; Rufh, S. A.; Lummiss, J. A. M.; Fogg, D. E. A General Decomposition

Pathway for Phosphine-Stabilized Metathesis Catalysts: Lewis Donors Accelerate Methylidene Abstraction. *J. Am. Chem. Soc.* **2016**, *138*, 14668–14677.

(32) Lummiss, J. A. M.; Ireland, B. J.; Sommers, J. M.; Fogg, D. E. Amine-Mediated Degradation in Olefin Metathesis Reactions That Employ the Second-Generation Grubbs Catalyst. *ChemCatChem* **2014**, *6*, 459–463.

(33) Lummiss, J. A. M.; Botti, A. G. G.; Fogg, D. E. Isotopic Probes for Ruthenium-Catalyzed Olefin Metathesis. *Catal. Sci. Technol.* **2014**, *4*, 4210–4218.

(34) Ogba, O. M.; Warner, N. C.; O'Leary, D. J.; Grubbs, R. H. Recent Advances in Ruthenium-Based Olefin Metathesis. *Chem. Soc. Rev.* **2018**, *47*, 4510–4544.

(35) Benhamou, L.; Chardon, E.; Lavigne, G.; Bellemin-Laponnaz, S.; César, V. Synthetic Routes to N-Heterocyclic Carbene Precursors. *Chem. Rev.* **2011**, *111*, 2705–2733.

(36) van Lierop, B. J.; Reckling, A. M.; Lummiss, J. A. M.; Fogg, D. E. Clean, Convenient, High-Yield Access to Second-Generation Ru Metathesis Catalysts from Commercially Available Precursors. *ChemCatChem* **2012**, *4*, 2020–2025.

(37) Nascimento, D. L.; Davy, E. C.; Fogg, D. E. Merrifield Resin-Assisted Routes to Second-Generation Catalysts for Olefin Metathesis. *Catal. Sci. Technol.* **2018**, *8*, 1535–1544.

(38) Lewandos, G. S.; Pettit, R. Mechanism of the Metal-Catalyzed Disproportionation of Olefins. *J. Am. Chem. Soc.* **1971**, *93*, 7087–7088.

(39) Grubbs, R. H.; Brunck, T. K. Possible Intermediate in the Tungsten-Catalyzed Olefin Metathesis Reaction. *J. Am. Chem. Soc.* **1972**, *94*, 2538–2540.

(40) Calderon, N.; Ofstead, E. A.; Ward, J. P.; Judy, W. A.; Scott, K. W. Olefin Metathesis. I. Acyclic Vinylenic Hydrocarbons. *J. Am. Chem. Soc.* **1968**, *90*, 4133–4140.

(41) Jean-Louis, P.; Hérisson Chauvin, Y. Catalyse de Transformation Des Oléfines Par Les Complexes Du Tungstène. II. Télomérisation Des Oléfines Cycliques En Présence d'oléfines Acycliques. *Makromol. Chem.* **1971**, *141*, 5–7.

(42) Adlhart, C.; Chen, P. Mechanism and Activity of Ruthenium Olefin Metathesis Catalysts: The Role of Ligands and Substrates from a Theoretical Perspective. *J. Am. Chem. Soc.* **2004**, *126*, 3496–3510.

(43) Sanford, M. S.; Love, J. A.; Grubbs, R. H. Mechanism and Activity of Ruthenium Olefin Metathesis Catalysts. *J. Am. Chem. Soc.* **2001**, *123*, 6543–6554.

(44) Bates, J. M.; Lummiss, J. A. M.; Bailey, G. A.; Fogg, D. E. Operation of the Boomerang Mechanism in Olefin Metathesis Reactions Promoted by the Second-Generation Hoveyda Catalyst. *ACS Catal.* **2014**, *4*, 2387–2394.

(45) Vorfalt, T.; Wannowius, K.-J.; Plenio, H. Probing the Mechanism of Olefin Metathesis in Grubbs-Hoveyda and Grela Type Complexes. *Angew. Chem. Int. Ed.* **2010**, *49*, 5533–5536.

(46) Lummiss, J. A. M.; Higman, C. S.; Fyson, D. L.; McDonald, R.; Fogg, D. E. The Divergent Effects of Strong NHC Donation in Catalysis. *Chem. Sci.* **2015**, *6*, 6739–6746.

(47) Occhipinti, G.; Nascimento, D. L.; Foscato, M.; Fogg, D. E.; Jensen, V. R. The Janus Face of High Trans-Effect Carbenes in Olefin Metathesis: Gateway to Both Productivity and Decomposition. *Chem. Sci.* **2022**, *13*, 5107–5117.

(48) (a) Fey, N.; Orpen, A. G.; Harvey, J. N. Building Ligand Knowledge Bases for Organometallic Chemistry: Computational Description of Phosphorus(III)-Donor Ligands and the Metal–Phosphorus Bond. *Coord. Chem. Rev.* **2009**, *253*, 704–722. (b)

(49) Lummiss, J. A. M.; Perras, F. A.; McDonald, R.; Bryce, D. L.; Fogg, D. E. Sterically Driven Olefin Metathesis: The Impact of Alkylidene Substitution on Catalyst Activity. *Organometallics* **2016**, *35*, 691–698.

(50) Adlhart, C.; Chen, P. Comparing Intrinsic Reactivities of the First- and Second-Generation Ruthenium Metathesis Catalysts in the Gas Phase. *Helv. Chim. Acta* **2003**, *86*, 941–949.

(51) Paredes-Gil, K.; Solans-Monfort, X.; Rodriguez-Santiago, L.; Sodupe, M.; Jaque, P. DFT Study on the Relative Stabilities of Substituted Ruthenacyclobutane Intermediates Involved in Olefin Cross-Metathesis Reactions and Their Interconversion Pathways. *Organometallics* **2014**, *33*, 6065–6075.

(52) Bailey, G. A.; Foscato, M.; Higman, C. S.; Day, C. S.; Jensen, V. R.; Fogg, D. E. Bimolecular Coupling as a Vector for Decomposition of Fast-Initiating Olefin Metathesis Catalysts. *J. Am. Chem. Soc.* **2018**, *140*, 6931–6944.

(53) Amoroso, D.; Snelgrove, J. L.; Conrad, J. C.; Drouin, S. D.; Yap, G. P. A.; Fogg, D. E. An Attractive Route to Olefin Metathesis Catalysts: Facile Synthesis of a Ruthenium Alkylidene Complex Containing Labile Phosphane Donors. *Adv. Synth. Catal.* **2002**, *344*, 757.

(54) Amoroso, D.; Yap, G. P. A.; Fogg, D. E. Deactivation of Ruthenium Metathesis Catalysts via Facile Formation of Face-Bridged Dimers. *Organometallics* **2002**, *21*, 3335–3343.

(55) Nascimento, D. L.; Gawin, A.; Gawin, R.; Guńka, P. A.; Zachara, J.; Skowerski, K.; Fogg, D. E. Integrating Activity with Accessibility in Olefin Metathesis: An Unprecedentedly Reactive Ruthenium-Indenylidene Catalyst. *J. Am. Chem. Soc.* **2019**, *141*, 10626–10631.

(56) Nascimento, D. L.; Foscato, M.; Occhipinti, G.; Jensen, V. R.; Fogg, D. E. Bimolecular Coupling in Olefin Metathesis: Correlating Structure and Decomposition for Leading and Emerging Ruthenium−Carbene Catalysts. *J. Am. Chem. Soc.* **2021**, *143*, 11072–11079.

(57) Tsang, W. C. P.; Hultzsch, K. C.; Alexander, J. B.; Bonitatebus, P. J.; Schrock, R. R.; Hoveyda, A. H. Alkylidene and Metalacyclic Complexes of Tungsten That Contain a Chiral Biphenoxide Ligand. Synthesis, Asymmetric Ring-Closing Metathesis, and Mechanistic Investigations. *J. Am. Chem. Soc.* **2003**, *125*, 2652–2666.

(58) Janse van Rensburg, W.; Steynberg, P. J.; Meyer, W. H.; Kirk, M. M.; Forman, G. S. DFT Prediction and Experimental Observation of Substrate-Induced Catalyst Decomposition in Ruthenium-Catalyzed Olefin Metathesis. *J. Am. Chem. Soc.* **2004**, *126*, 14332–14333.

(59) Romero, P. E.; Piers, W. E. Direct Observation of a 14-Electron Ruthenacyclobutane Relevant to Olefin Metathesis. *J. Am. Chem. Soc.* **2005**, *127*, 5032–5033.

(60) Romero, P. E.; Piers, W. E. Mechanistic Studies on 14-Electron Ruthenacyclobutanes: Degenerate Exchange with Free Ethylene. *J. Am. Chem. Soc.* **2007**, *129*, 1698–1704.

(61) van der Eide, E. F.; Piers, W. E. Mechanistic Insights into the Ruthenium-Catalysed Diene Ring-Closing Metathesis Reaction. *Nat. Chem.* **2010**, *2*, 571–576.

(62) Marx, V. M.; Sullivan, A. H.; Melaimi, M.; Virgil, S. C.; Keitz, B. K.; Weinberger, D. S.; Bertrand, G.; Grubbs, R. H. Cyclic Alkyl Amino Carbene (CAAC) Ruthenium Complexes as Remarkably Active Catalysts for Ethenolysis. *Angew. Chem. Int. Ed.* **2015**, *54*, 1919–1923.

(63) Anderson, D. R.; Lavallo, V.; O'Leary, D. J.; Bertrand, G.; Grubbs, R. H. Synthesis and Reactivity of Olefin Metathesis Catalysts Bearing Cyclic (Alkyl)(Amino)Carbenes. *Angew. Chem. Int. Ed.* **2007**, *46*, 7262–7265.

(64) Melaimi, M.; Jazzar, R.; Soleilhavoup, M.; Bertrand, G. Cyclic (Alkyl)(Amino)Carbenes (CAACs): Recent Developments. *Angew. Chem. Int. Ed.* **2017**, *56*, 10046–10068.

(65) Kumar Kushvaha, S.; Mishra, A.; Roesky, H. W.; Chandra Mondal, K. Recent Advances in the Domain of Cyclic (Alkyl)(Amino) Carbenes. *Chem. – An Asian J.* **2022**, *17*.

(66) Nascimento, D. L.; Fogg, D. E. Origin of the Breakthrough Productivity of Ruthenium–Cyclic Alkyl Amino Carbene Catalysts in Olefin Metathesis. *J. Am. Chem. Soc.* **2019**, *141*, 19236–19240.

# Chapter 2 Synthesis of a Ruthenium Metathesis Catalyst Bearing a Small CAAC Ligand

## 2.1 Introduction

### 2.1.1 Renewable Feedstocks via Olefin Metathesis

With the depletion of fossil-fuel-derived feedstocks, the need for renewable alternatives is increasingly urgent. Olefin metathesis is an appealing catalytic reaction for biomass valorization. It offers atom-efficient opportunities for conversion of readily available and accessible renewable resources, such as canola, soybean, or sunflower oil, and particularly non-edible fatty oils sourced from autotrophic entities like algae, into valuable oleochemical products.[1–3] The unsaturated hydrocarbon chains found in such sources are commonly converted into fatty acids (FAs) or fatty acid methyl esters (FAMEs). These fatty oil-derived substances are $CO_2$-neutral due to the capacity of autotrophic organisms to convert carbon dioxide into organic compounds.[3–5]

Metathesis of the long-chain unsaturated esters derived from such lipids generates compounds with potential high market value.[3,4,6] The self-metathesis of FAMEs such as methyl oleate (MO) offers a highly atom-efficient route to (E/Z) 9-octadecene (**7**) and (E/Z) dimethyl-9-octadecenoate (**8**) (Scheme 2.1). The former is reportedly employed for the production of biologically-sourced lubricants, surfactants and plasticizers, while the latter holds potential as a precursor to bio-sourced polymers.[3–5]

**Scheme 2.1.** Production of bio-based products by self-metathesis of **MO**.

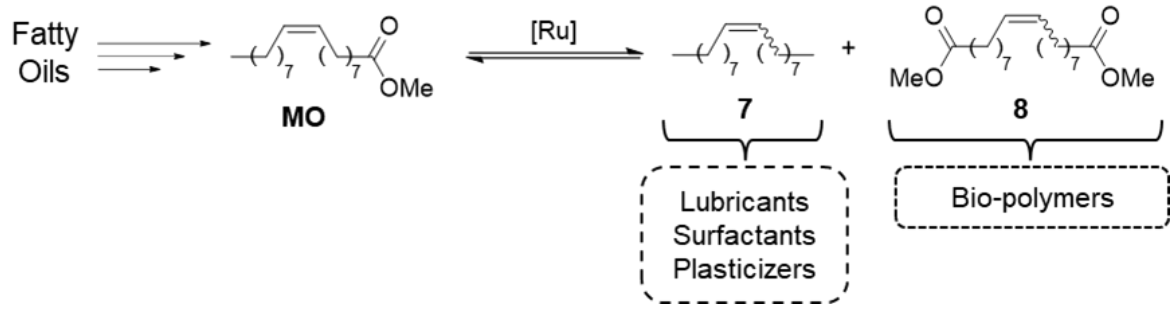


Alternatively, cross-metathesis (CM) with ethylene ("ethenolysis") converts FAMEs into valuable 1-olefins of lower molecular weight.[3–5] In 2015, Grubbs and Bertrand reported a breakthrough in ethenolysis of methyl oleate (**MO**) using Hoveyda-type catalysts containing CAAC ligands. Selected CAACs with different N-Ar and α-carbon groups are shown in Figure 2.1.[7] Turnover numbers (TONs) at catalyst loadings of 3 ppm reached 180,000 for **CAAC-8** and **CAAC-9**. Even higher performance was demonstrated for **CAAC-9** at 1 ppm, with a TON of 340,000, approximately 100-fold more than the highest observed for $H_2$IMes catalysts.[7,8] It should be noted that high-purity ethylene (99.995%) was required to achieve these TONs, as impurities that decompose the catalyst are significant at the low catalyst loadings employed.[7]

**Figure 2.1.** RuCAAC catalyst performance in ethenolysis of **MO**. Values shown are with 99.95% purity ethylene and methyl oleate purified over activated neutral alumina. [a]Not reported – Conv. < 5%

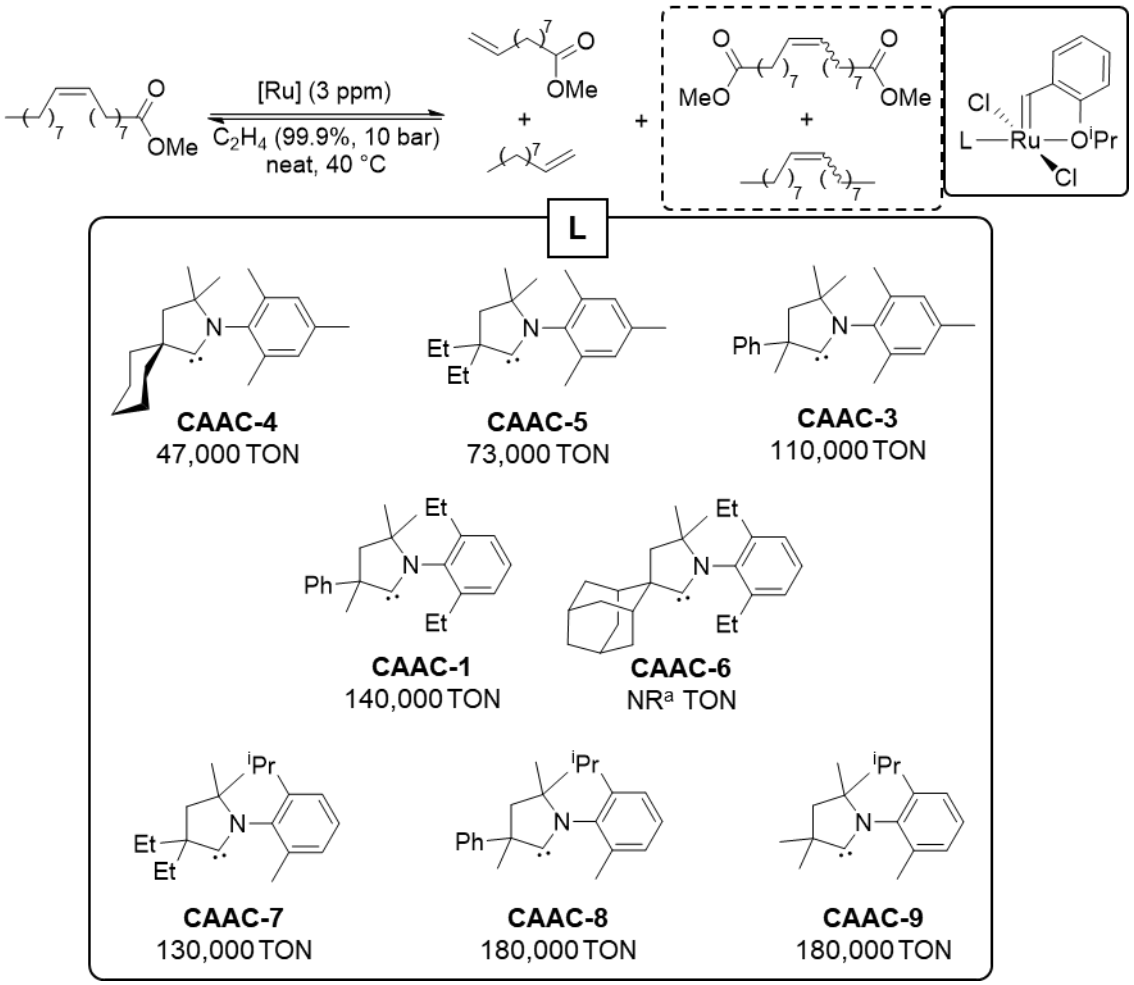


### 2.1.2 Opportunities for Ru-CAAC Catalysts Bearing Small CAAC Ligands

Internal olefins such as that present in **MO** present a challenge to metathesis.[9,10] While steric comparisons in the Grubbs-Bertrand study are hampered by the lack of symmetry or changes to more than one variable, some trends point toward higher TONs for CAACs bearing smaller α-carbon substituents. At the extreme, the bulky C-adamantyl group in **CAAC-6** completely inhibits catalyst activity, resulting in conversion < 5%, which results in TON < 15,000 (TON are not explicitly reported due to the limit of detection), vs 140,000 for its analogue **CAAC-1** in which a α-CMePh group is present. Within the N-mesityl series CAAC **4** and **5**, TONs increased from 47,000 to 73,000 on changing from an α-cyclohexyl to a diethyl substituent. It is crucial to notice that at the 3 ppm catalyst loading used in these experiments, BMC remains significant. The faster BMC of smaller catalysts may mask their advantages in rates of productive metathesis. For example, CAACs **8** and **9**, bearing $CH_3$/$^i$Pr N-Ar, present the same TON (180,000), even though the latter contains a α-CMe group instead of a α-CPh.

Reduced CAAC size would logically translate into a greater ability to access sterically hindered substrates. Reduced bulk is suspected to be critical to performance in metathesis of internal olefins, and, more generally, to success in metathesis of crowded substrates. A challenge, however, lies in the synthesis of catalysts bearing small CAACs, as outlined in the next section.

### 2.1.3 Established Routes to CAAC Aldiminium Salts

Two general synthetic routes to CAAC ligands have been established, with yields ranging from 30-80% (Scheme 2.2).[11–13] Both commence with addition of a suitable strong base (e.g. $^{n}$BuL or lithium diisopropylamide, LDA) to an aldimine to form an aza-allyl anion intermediate. An electrophile is then added: either an epoxide (Route (a)) or an allylic halide (Route (b)). Cyclization of the resulting aldiminium salt is achieved by adding $Tf_2O$ in Route (a), or use of acid to enable an intramolecular 'hydroiminiumation' reaction in Route (b). As Route (b) offers higher yields, it has become the standard method.

To synthesize the target catalysts, the free CAAC ligands are liberated by deprotonation with a strong base such as LiHMDS,[12,14–16] and immediately added to a ruthenium complex.[14] The free CAACs are difficult to isolate relative to the free NHCs, unless bulky N-aryl and α-carbon substituents are present.[17] Their instability is thought to be due to the smaller HOMO/LUMO gap described in Chapter 1, which facilitates dimerization via the Wanzlick equilibrium.[17,18] Moreover, the higher nucleophilic and electrophilic properties of CAACs make the free carbenes more reactive toward trace impurities such as $H_2O$, and potentially more susceptible to cyclization via C-H activation of alkyl groups at the N-aryl or α-carbon.[19] The latter point will be revisited below.

**Scheme 2.2.** General synthetic routes to CAAC ligands.

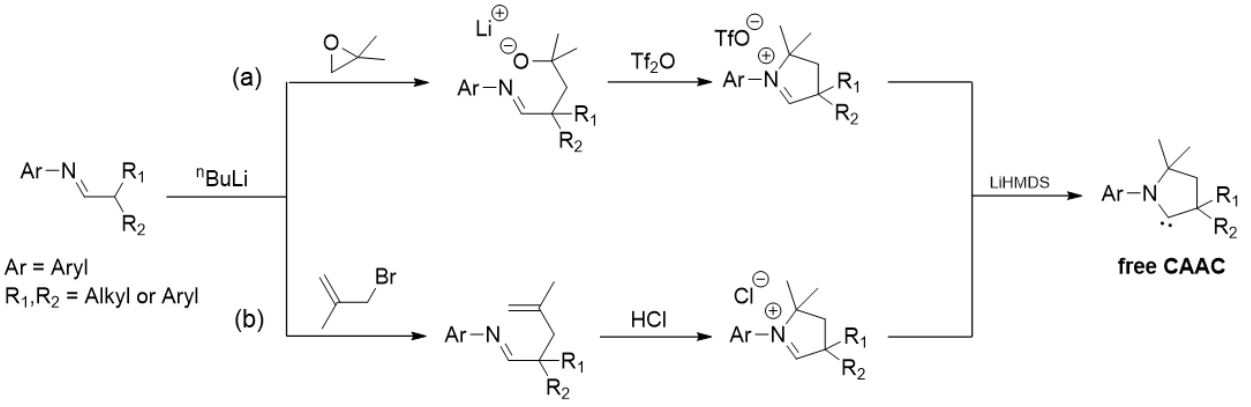


### 2.1.4 Synthesis of Hoveyda-type CAAC Catalysts: Challenges for Small CAAC Ligands

Two synthetic routes to Hoveyda-CAAC catalysts have been developed. Route A (note: a capital letter is used to distinguish synthesis of the catalyst from the ligand synthesis above) involves direct exchange of the $PCy_3$ ligand in **HI** (Scheme 2.3a) with a CAAC ligand generated in situ. Route B commences with synthesis of the indenylidene complex $RuCl_2(CAAC)_2$(ind) **UC**, followed by metathesis with the chelating isopropoxy-styrene to afford the Hoveyda catalyst

(Scheme 2.3b).[7,20] Route A delivers yields of up to 91% for CAAC ligands containing bulky N-aryl or N-heterocyclic rings (see **1, 11** and **12**; Table 2.1). However, yields are poor when these substituents are small (18% or 29% for CAACs **2** and **3**, respectively), and this approach fails completely for **RuCAAC-10**, which bears an N-mesityl group and only dimethyl substituents at the α-carbon.[7,14,21] Route B is more efficient, but is still sub-optimal for the smallest CAACs. Reported yields for **CAAC-10**, for example, range from 14% to 40% (the latter appearing in a 2017 patent claim by Skowerski and coworkers).[22,23] Moreover, this method is time-consuming and requires use of a sacrificial CAAC to synthesize the bis-indenylidene complex.

**Scheme 2.3.** Dominant routes to Ru-CAAC metathesis catalysts. Route A: via the first-generation Hoveyda catalyst **HI**. (b) Route B: via the bis(CAAC)-indenylidene catalysts Ultracat, **UC$^{Mes}$**.

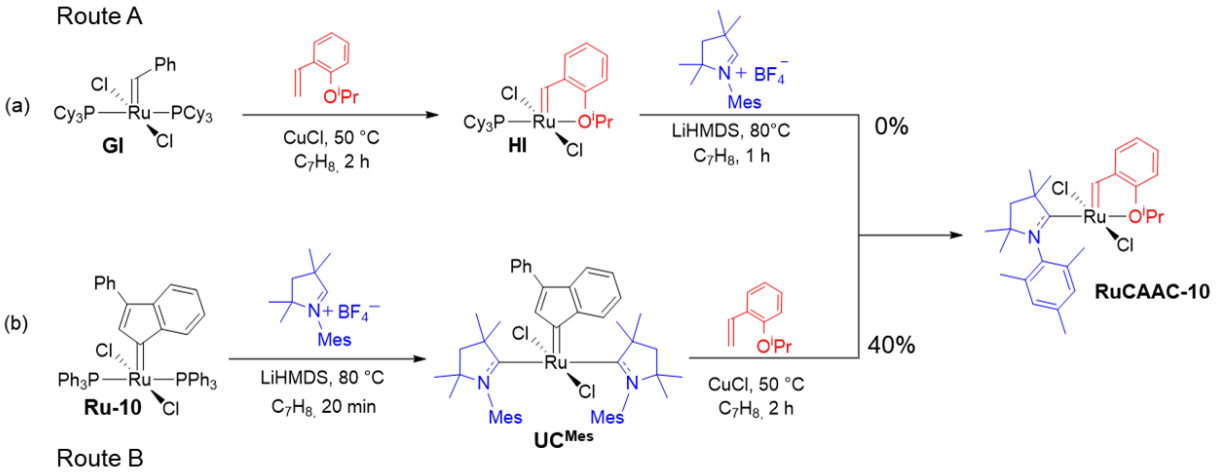


**Table 2.1.** Reported yields of Ru-CAAC catalysts synthesized via routes (a) or (b).

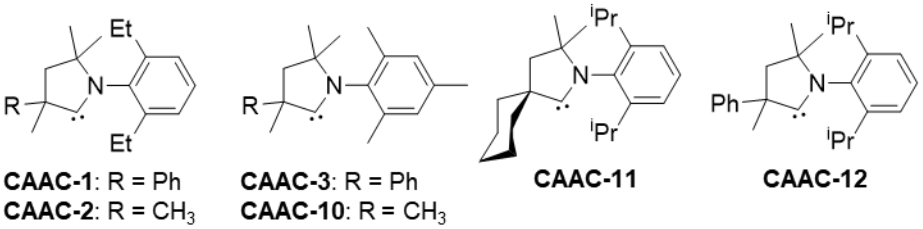


| | Route A (%) | Route B (%) | References |
|---|---|---|---|
| **CAAC-1** | 45 | 52 | 7,20 |
| **CAAC-2** | 18 | 59 | |
| **CAAC-3** | 29 | 37 | |
| **CAAC-11** | 91 | N.R. | |
| **CAAC-12** | 70 | N.R. | |
| **CAAC-10** | 0 | 40 | |

The drop in productivity for small CAACs in both routes has several potential reasons. First, as noted above, they are sterically unprotected against dimerization via the Wanzlick equilibrium[17,18] (Scheme 2.4a). Second, they are potentially more susceptible to side-reactions: intramolecular cyclization for *o*-methyl N-aryl C($sp^3$)-H activation (Scheme 2.4b) or intermolecular insertion of toluene (Scheme 2.4c).[14,24] Bulkier aryl groups are thought to inhibit these side reactions by forcing the aromatic ring to adopt an orientation perpendicular to the N-heterocyclic ring, preventing the ortho substituents from approaching the carbene center.

**Scheme 2.4.** Side-reactions suggested in the literature for small carbenes, exemplified with **CAAC-10**.

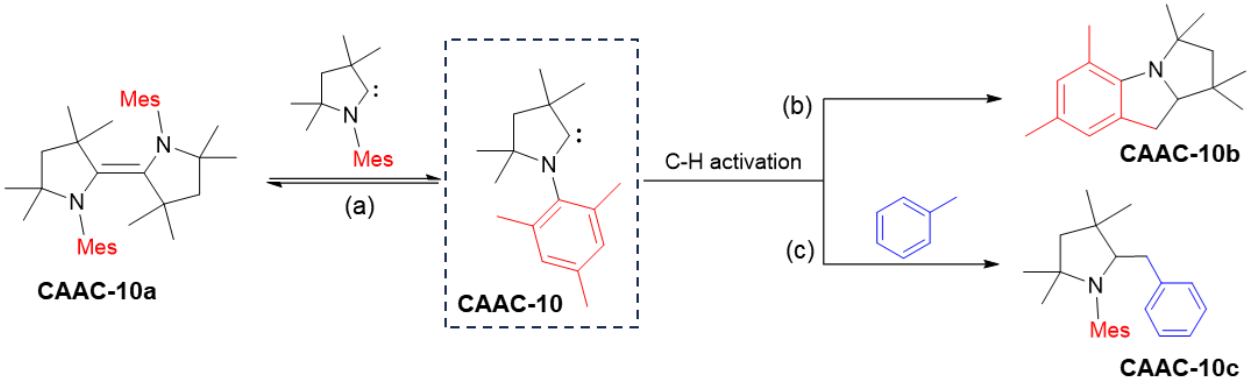


Of note in this context, however, is the high-yield synthesis of **RuCAAC-10-$I_2$**, an iodide catalyst containing the small **CAAC-10** ligand, by Blanco and Fogg (Scheme 2.5).[25] The product was isolated in 80% yield and high purity from **HI-$I_2$**, suggesting that the instability of the free carbene is not the real impediment. Attempts to access the chlorinated analogue led to decomposition, implying that the bulk of the Ru-iodide complex is critical. This observation suggests that the problem is not trapping of the free CAAC by the Ru species, but decomposition of the ruthenium product. The potential pathways will be considered in more detail in the relevant section of the Results and Discussion.

**Scheme 2.5.** Synthesis of **RuCAAC-10-$I_2$** by Blanco and Fogg using a Merrifield iodide resin to capture the $PCy_3$ ligand liberated from **GI**.

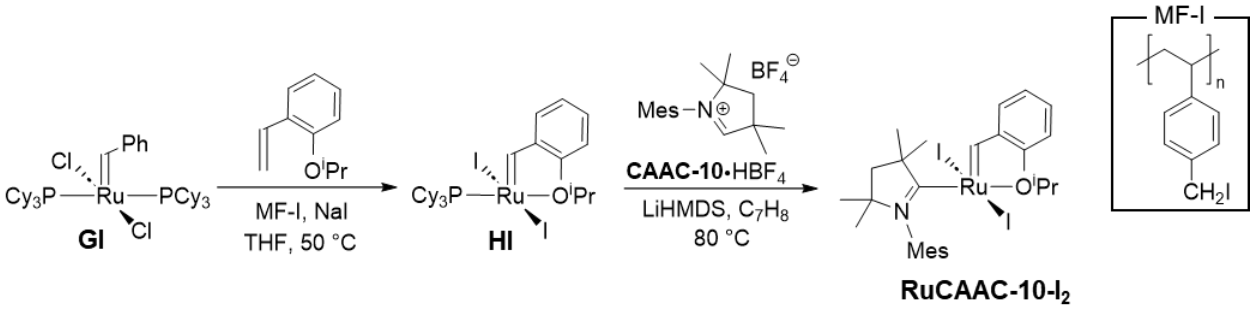

To date, the limited synthetic accessibility of catalysts bearing small CAAC ligands has severely restricted advances in the metathesis of crowded olefins. The smallest CAAC ligand employed so far in the open literature on olefin metathesis is the N-mesityl derivative **CAAC-10**, with a 5-membered ring core. Given the challenges outlined above for in situ synthesis and installation of **CAAC-10** on the Hoveyda catalyst platform, the present work aimed to identify new routes capable of providing small CAAC Ru catalysts in better yields. The complex **RuCAAC-10** was selected as a target because it is on the verge of success by current synthetic methods, and its superiority in the metathesis of encumbered olefins is already established.[13,22]

## 2.2 Results and Discussion

To explore the hypothesis outlined above, this work commenced with synthesis of the **CAAC-10** salt. A number of issues emerged during its preparation. These and work-arounds to address them will be discussed prior to the key step of CAAC installation.

### 2.2.1 Synthesis of CAAC Precursors

The detailed synthesis of **CAAC-10•HX** is described in only two research articles published in 2007, one a joint paper from the Grubbs and Bertrand groups, and the other by the Bertrand group alone. The two routes correspond to those shown in Scheme 2.2. Route (a) afforded **CAAC-10•HOTf** in 61% overall yield,[21] while Route (b) afforded the corresponding hydrochloride salt, **CAAC-10•HCl**, in 76% overall yield.[11] While the method of Route (b) was selected in the present work, the $HBF_4$ salt was pursued in preference to the triflate or chloride salts, given its higher solubility in toluene,[26,27] the solvent used in the catalyst synthesis. Moreover, the $[BF_4]^-$ anion is a weakly coordinating counter-ion , reducing the risk of its unintended ligation.[28] The analogous α-phenyl CAAC salt, **CAAC-3•HBF$_4$**, was also prepared, with the intention of assessing the impact of CAAC bulk on catalyst performance. Both routes are considered in detail in this section.

**S**ynthesis of **CAAC-10•HBF$_4$** commenced with amination of the aldehyde with 2,4,6-trimethylaniline (Scheme 2.6). The aldimine product **10a** was isolated as a yellow oil in 80% yield, following which treatment with 3-chloro-2-methylpropene and $^n$BuLi (to generate the nucleophile for halide substitution) afforded alkenyl imine **11a**. The latter was isolated as a dark yellow viscous oil in 70% yield. Initial attempts to cyclize **11a** in $Et_2O$ using 2 equiv aqueous HCl, as in Bertrand's 2016 route,[29] gave meagre yields of **12a** (<10%). The salt was isolated as a precipitate, accompanied by an amber oil that afforded no further product on extracting with $CH_2Cl_2$ or ethyl acetate.

**Scheme 2.6.** Overview of synthetic route to **CAAC-3•HBF$_4$** and its phenyl analogue **CAAC-10•HBF$_4$**. For the original approach, see Scheme 2.2b.

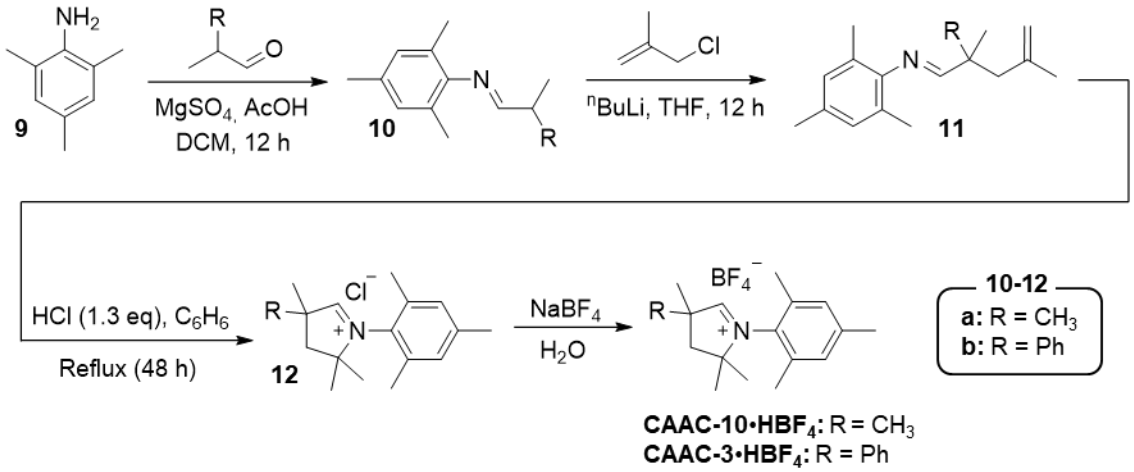


The problem in this reaction may be an early sign of difficulties associated with the reduced steric bulk of the target carbenes. HCl is required for cyclization to form the CAAC salts (Scheme 2.7a). The Bertrand and Apeiron groups reported the successful use of excess HCl (2–2.5 equiv vs **11**) to cyclize alkenyl imines bearing large substituents at the quaternary carbon or N-aryl moiety.[23,29] However, Bertrand pointed out in 2022 that high proportions of HCl (>2 equiv) triggered partial to complete isomerization of the terminal olefin in attempted cyclization of phenyl and cyclohexyl α-carbon substituted alkenyl imines.[30]

In our hands, cyclization of **11a** in proportions of HCl higher than 1.5 equivalents failed completely. Excess HCl may be a particular problem where the substituents are small, whether due to isomerization or another well-known reaction for alkenes in the presence of HCl, electrophilic addition to form the alkyl chloride (Scheme 2.7b).[31] Alkenyl imines bearing large substituents may resist such isomerization and addition reactions, by favouring positioning of the aliphatic chain to place the olefin closer to the imine moiety. This would plausibly reduce the energy for spatial rearrangement in the cyclization step, and hence accelerate cyclization relative to these competing side-reactions.

**Scheme 2.7.** (a) Synthesis of **CAAC-10•HCl** and (b) potential side-reactions of alkenyl imine **11a** promoted by HCl.

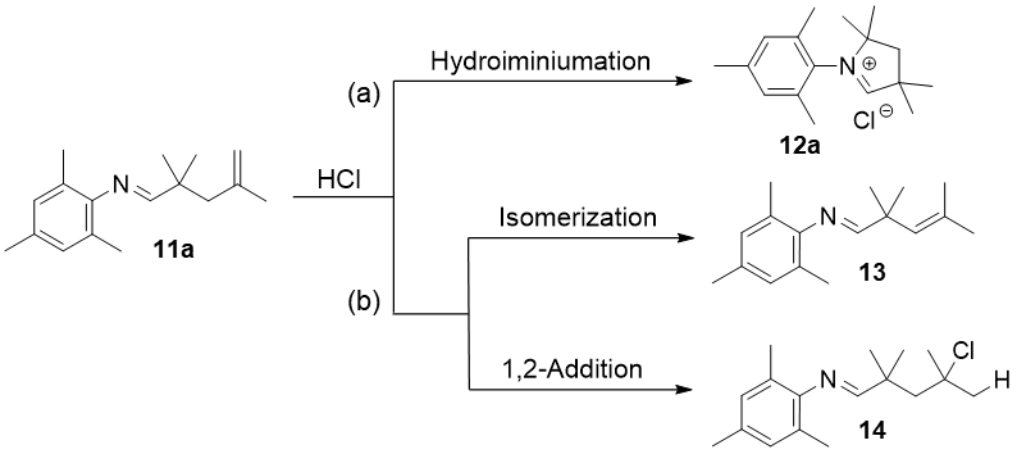


To test the hypothesis that the side-products originate in the use of excess acid, the proportion of HCl was reduced from 2 equiv to 1.3 equiv (Scheme 2.8). As well, the solvent was switched to hexanes, given success in the production of a related iminium heterocycle in hexanes by Ms. Eliza-Jayne Boisvert of the Fogg group. Cyclization of **11a** was complete in 48 h, as indicated by the integrated intensity of the N=C*H* signal observed by $^{1}$H NMR analysis (7.52 ppm). Evaporation of the solvent and stirring the crude residue in $Et_2O$ to remove organic side products yielded a pale yellow solid. As the hygroscopic nature of the solid hampered filtration (a viscous paste formed on exposure to air), the workup was limited to washing several times with $Et_2O$. Conversion to the more tractable $[BF_4]^-$ salt was then carried out by anion exchange with $NaBF_4$ in water.

**Scheme 2.8.** Cyclization of **11a** to form **CAAC-10•HBF$_4$** using a lower proportion of HCl.

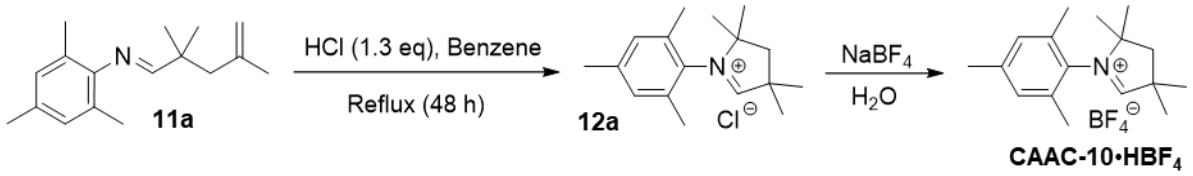


The final step in preparation of the desired CAAC salt involved exchange of the chloride counter-ion for $BF_4$. In a 2020 report, Mauduit and coworkers described preparation of bulky **CAAC•HBF$_4$** salts by anion exchange by stirring in water for 12 h before filtering off. This procedure was reportedly successful for CAAC salts bearing a 2,6-diisopropylphenyl N-aryl group and different α-carbon substituents; 3,5-dimethylphenyl, 2,6-diisopropylphenyl and naphthalen-2-yl.[27] Attempts to duplicate this reaction with **CAAC-10•HBF$_4$** failed. The white precipitate formed on addition of $NaBF_4$ redissolved over a few hours in water, and no product could be isolated, perhaps indicating hydrolysis of the C=N bond. To inhibit degradation, the precipitate was stirred in water for only 30 min, after which the product was filtered off, washed with $Et_2O$, and dried. This approach afforded **CAAC-10•HBF$_4$** in 45% yield.

The same approach was used to prepare **CAAC-3•HBF$_4$** (see Figure A.4 for $^1$H NMR spectrum of iminium salt). The yields for the first two steps were similar to those for **CAAC-10•HBF$_4$**, but cyclization yields were ca. 10% higher relative to the methyl-substituted analogue, again pointing toward a steric role in side-reactions.

### 2.2.2 Synthesis of a Hoveyda-CAAC Catalyst Bearing CAAC-10•HBF$_4$

As noted in the Introduction, Grubbs and coworkers reported failure in ligand exchange between the first-generation Hoveyda catalyst **HI** and **CAAC-10**,[7,21] while the Apeiron group claimed the synthesis of **RuCAAC-10** from **UC** in 40% yield in a patent.[22] While the basis of these difficulties has not been considered in the literature, these outcomes contrast with the ca. 80% yield of the iodide analogue **RuCAAC-10-I$_2$** achieved by Blanco and Fogg on reacting the iodo-Hoveyda platform **HI-I$_2$** with **CAAC-10**.[25] It is therefore worth considering the pathways that could account for the greater vulnerability of the chloride complexes.

In an earlier study, Stephanie Rufh of this research group discovered that a small N-methyl NHC is able to attack at the methylidene carbon of $RuCl_2(PCy_3)_2(=CH_2)$.[32] Given the low steric profile of the "protecting" CAAC ligand in **RuCAAC-10**, we speculated that a similar vulnerability may be at play within chloride complexes bearing a small carbene. That is, the alkylidene ligand may be abstracted by either $PCy_3$ or the free CAAC released during ligand exchange from **HI** or **UC**, respectively (Scheme 2.9). Catalysts bearing small CAACs, such as **RuCAAC-10**, would be more prone to the initial nucleophilic attack. Ensuing C-H activation to eliminate the benzylidene moiety may also occur more readily, given the closer proximity of the CAAC alkyl groups to the Ru core and the alkylidene moiety.

**Scheme 2.9.** Hypothesized decomposition of **Ru-CAAC-10** by nucleophilic abstraction of the alkylidene. Top: Attack by the free **CAAC-10**. Bottom: Attack by free $PCy_3$.

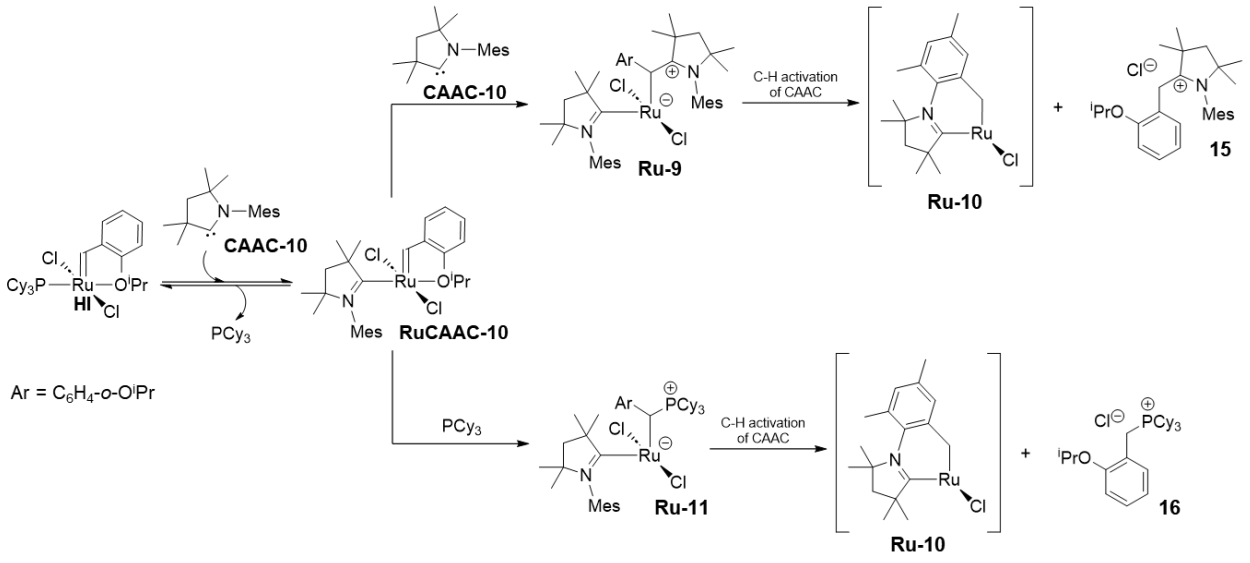

We conceived of the bulkier iodo platform as an alternative that could potentially block attack by phosphine or the free CAAC on the alkylidene, and thereby enable improved access to catalysts bearing small CAAC ligands. After isolation of **RuCAAC-10-I$_2$**, halide exchange under conditions with no deleterious nucleophiles present could enable access to **RuCAAC-10**: Scheme 2.10.

**Scheme 2.10.** Proposed route to **RuCAAC-10**.

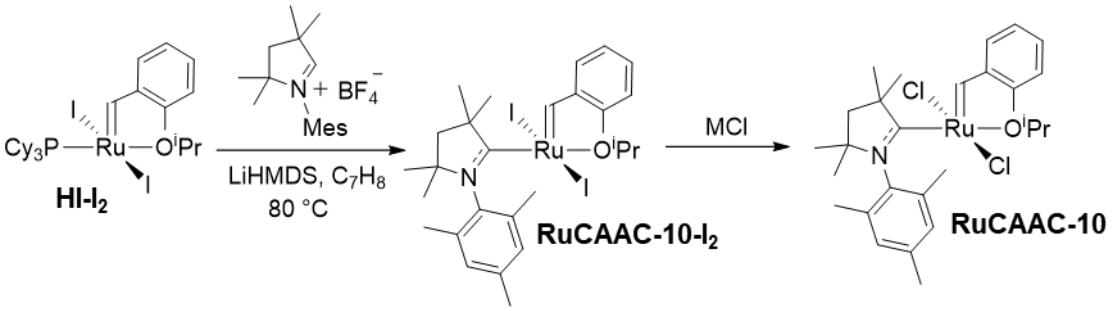


Accordingly, synthesis of **RuCAAC-10-I$_2$** was undertaken according to the method developed by Blanco. Solid LiHMDS was added to a solution of **CAAC-10•HBF$_4$** in toluene at 80 °C and heated briefly (2-3 min) to deprotonate the iminium salt and generate the free carbene (Scheme 2.11). The mixture – that is, the putative free CAAC, and any residual LiHMDS and/or **CAAC-10•HBF$_4$** – was then added to a stirred green solution of **HI-I$_2$** in toluene in a second Schlenk tube, likewise held at 80 °C. Analysis after 1 hour indicated complete conversion, as inferred from the loss of the $^{31}$P NMR signal for **HI-I$_2$** at 72.2 ppm. Solvent removal under vacuum afforded the crude residue which was purified by silica-gel chromatography in air to remove residual CAAC and $PCy_3$, together with side products. As the product was obtained in high purity, the washes with cold hexanes from the original methodology were not performed to avoid product loss. The iodide complex **RuCAAC-10-I$_2$** was thus isolated in 70% yield. It should be noted that yields of the ruthenium product declined to 10-30% if the initial LiHMDS–**CAAC-10•HBF$_4$** solution was heated for an additional 10–15 min, possibly owing to dimerization of the free carbene.[17,33]

**Scheme 2.11.** Synthesis of **RuCAAC-10-I$_2$**.

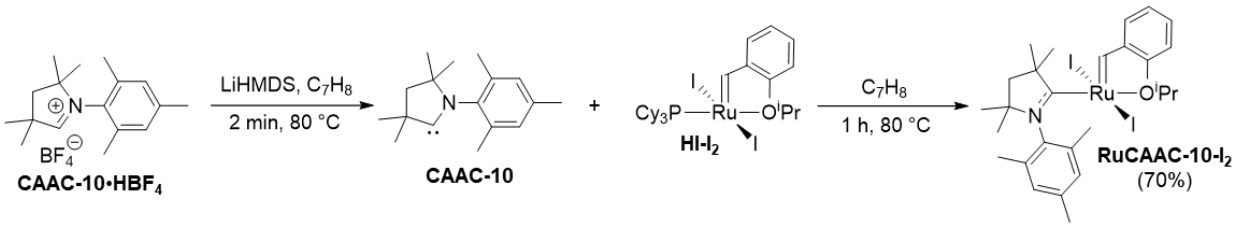


The final step, transformation of the Hoveyda-class iodide complex **RuCAAC-10-I$_2$** into the desired chloride catalyst, was undertaken via salt metathesis with different chloride salts. The reaction progress was determined from the disappearance of the alkylidene singlet for **RuCAAC-10-I$_2$**, and emergence of that for **RuCAAC-10** (chemical shifts 15.10 and 16.38 ppm, respectively). Aliquots were assayed hourly for the first 3 hours, and after 24 h for those that did not fully convert within that period.

Reaction with NaCl in THF gave no conversion over 24 h (Table 2.2, entry 1). The failure of this reaction is unsurprising, given the 0.1 mM solubility of NaCl in THF,[26] which severely restricts the availability of chloride in solution. Use of 150 equiv LiCl (for which the solubility in THF is 0.9 M)[26] resulted in 90% consumption of the iodide complex after 24 h (entry 2). Two new alkylidene singlets, at 15.70 ppm (80%) and 16.30 ppm **(**10%), were respectively assigned to **RuCAAC-10-I/Cl** and **RuCAAC-10**.To effect complete conversion of the latter, a higher proportion of LiCl was used (300 equiv), the reaction was heated at 50 °C for 1.5 h, and the entire procedure was then repeated (entry 3). That is, the residue was taken up in benzene, filtered through Celite to remove LiI, the solvent was removed, and the residue was redissolved in THF with a further 300 equiv LiCl for an additional 1.5 h at 50 °C. This treatment enabled full conversion of **RuCAAC-10-I$_2$**, but 20% of the mono-iodide catalyst remained.

**Figure 2.2.** Tracking salt metathesis of **RuCAAC-10-I$_2$** with LiCl (150 equiv) by $^1$H NMR analysis (300 MHz, $C_6D_6$). Only the alkylidene region is shown. (a) Initial spectrum. (b) Spectrum at 24 h.

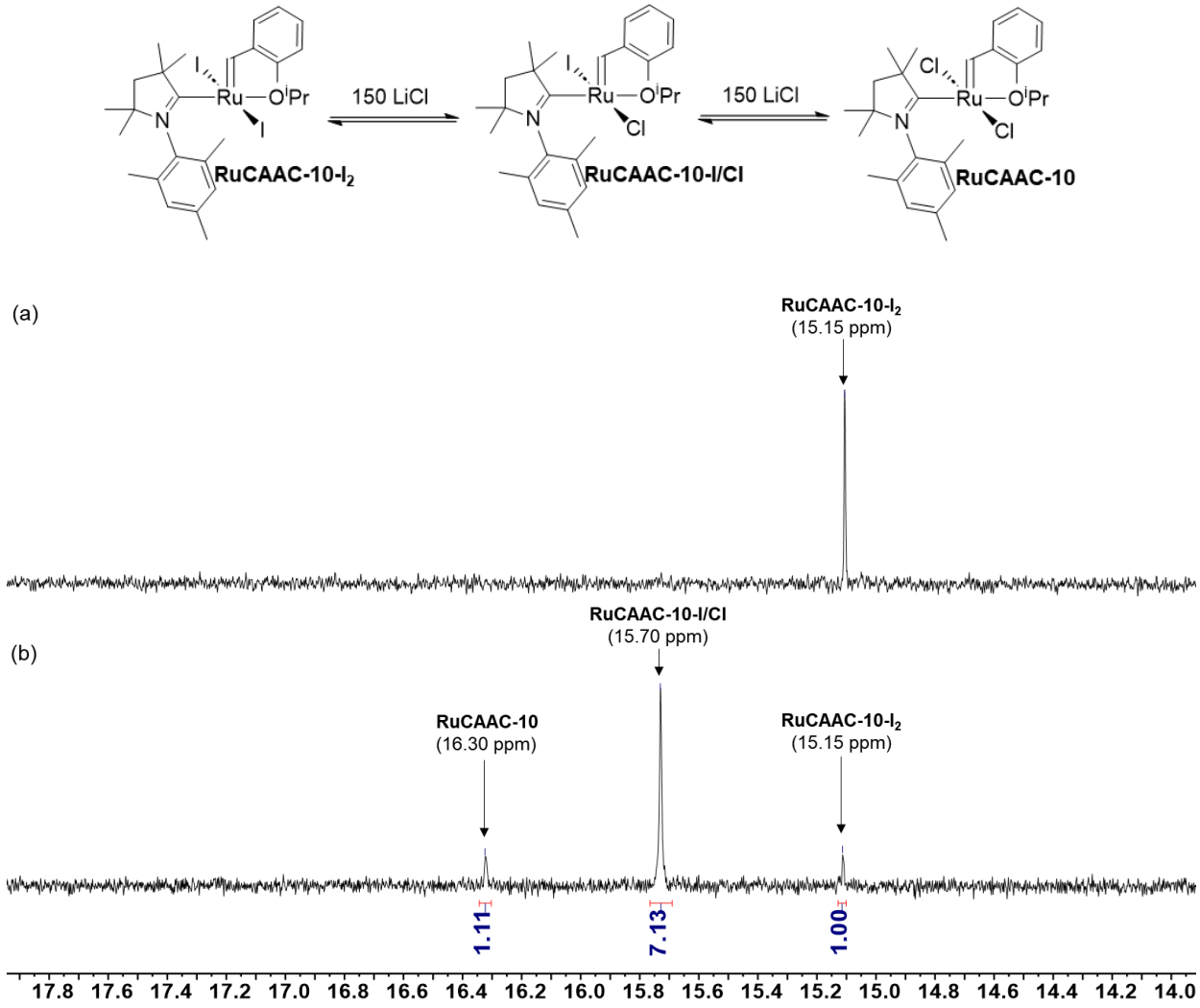

Alternative chloride sources were examined in the hope of increasing the yield and eliminating the need for multiple cycles of halide exchange. Transmetalation with AgCl was attempted, given its success in related reactions,[34] but conversions reached only 50% (entry 4), and a colour change to yellow over a few hours indicated catalyst decomposition. More successful was the use of ammonium salts (entries 5 and 6). Use of 20 equiv $N^tBu_4Cl$ enabled complete conversion of **RuCAAC-10-I$_2$** into **RuCAAC-10** in 2 h, with no decomposition. Similar results could be achieved with $NEt_4Cl$, albeit in 3-4 hours. Increasing the proportion of $NEt_4Cl$ to 40 equiv reduced the reaction time to 2 hours. An advantage to use of the tetraethylammonium salt is the insolubility of $NEt_4Cl$ and $NEt_4I$ in benzene, which enables their facile removal.

**Table 2.2.** Summary of screening reactions in salt metathesis of **RuCAAC-10-I$_2$**.

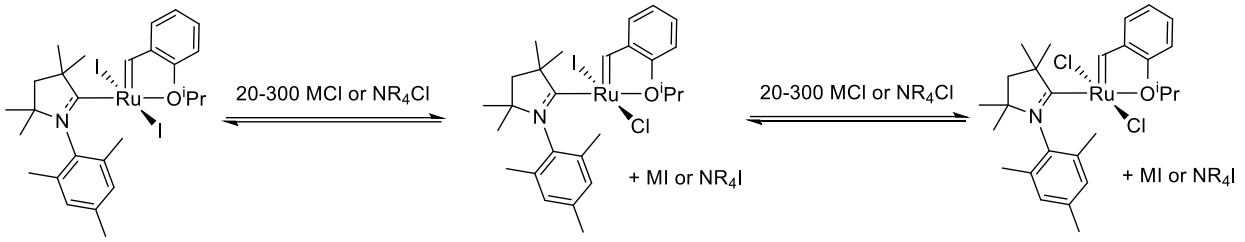


| Entry | Salt | Equiv | Solvent | T (°C) | Time (h) | Conv. (%) | RuCAAC-10 I/Cl (%) | RuCAAC-10 (%) |
|---|---|---|---|---|---|---|---|---|
| **1** | NaCl | 40 | THF | RT | 24 | 0 | N/A | N/A |
| **2** | LiCl | 150 | THF | RT | 24 | 90 | 80 | 10 |
| **3** | LiCl | 300 (2×) | THF | 50 | 3 | quant. | 20 | 80 |
| **4**[b] | AgCl | 2.2 | $CH_2Cl_2$ | 40 | 24 | 50 | 50 | 0 |
| **5**[a] | $N^tBu_4Cl$ | 20 | $CH_2Cl_2$ | RT | 2 | quant | 0 | >95 |
| **6**[a] | $NEt_4Cl$ | 40 | $CH_2Cl_2$ | RT | 2 | quant | 0 | >95 |

[a.] DMT used as internal standard (IS) for $^1$H NMR analysis. [b.] Possible decomposition.

Given the easier product purification, $NEt_4Cl$ was selected to synthesize **RuCAAC-10** (Scheme 2.12). Synthesis was undertaken on 100 mg in $CH_2Cl_2$ at room temperature, with 40 equiv of $NEt_4Cl$. Tracking reaction by $^1$H NMR, observing the decrease of **RuCAAC-10-I$_2$** alkylidene peak (15.15 ppm) showed full conversion after 2 h reaction. No formation of **RuCAAC-10-I/Cl** was observed under such conditions. The excess chloride salt and the $NEt_4I$ product were removed by extracting the product into benzene. The desired **RuCAAC-10** was isolated as a dark green solid in 85% yield.

**Scheme 2.12.** Optimized synthesis of **RuCAAC-10**.

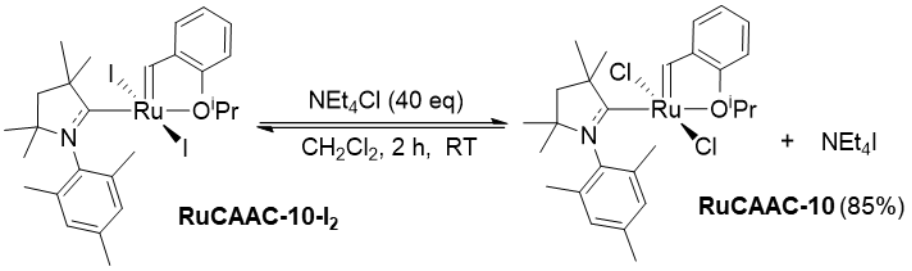


In summary, the most successful prior methodology for preparation of metathesis catalysts bearing small CAAC ligands was from the indenylidene complex (Scheme 2.13a). This approach was time-consuming, and delivered low overall yields, only 14-40%.[22,23] Moreover, it requires use of a sacrificial CAAC ligand. Direct installation on the Hoveyda platform, the most common method used for larger CAACs, failed completely (Scheme 2.13 b).[13] In the present work, use of a diiodide ruthenium complex increased catalyst robustness under the synthetic conditions, enabling an increase in overall yield to 55% for **RuCAAC-10** (Scheme 2.13 c), without a sacrificial CAAC ligand.

**Scheme 2.13.** Overall view of productivity in the synthetic routes to **RuCAAC-10**. (a) Skowerski route from indenylidene precursor. (b) Grubbs route from **GI**. (c) Route developed in this thesis work.

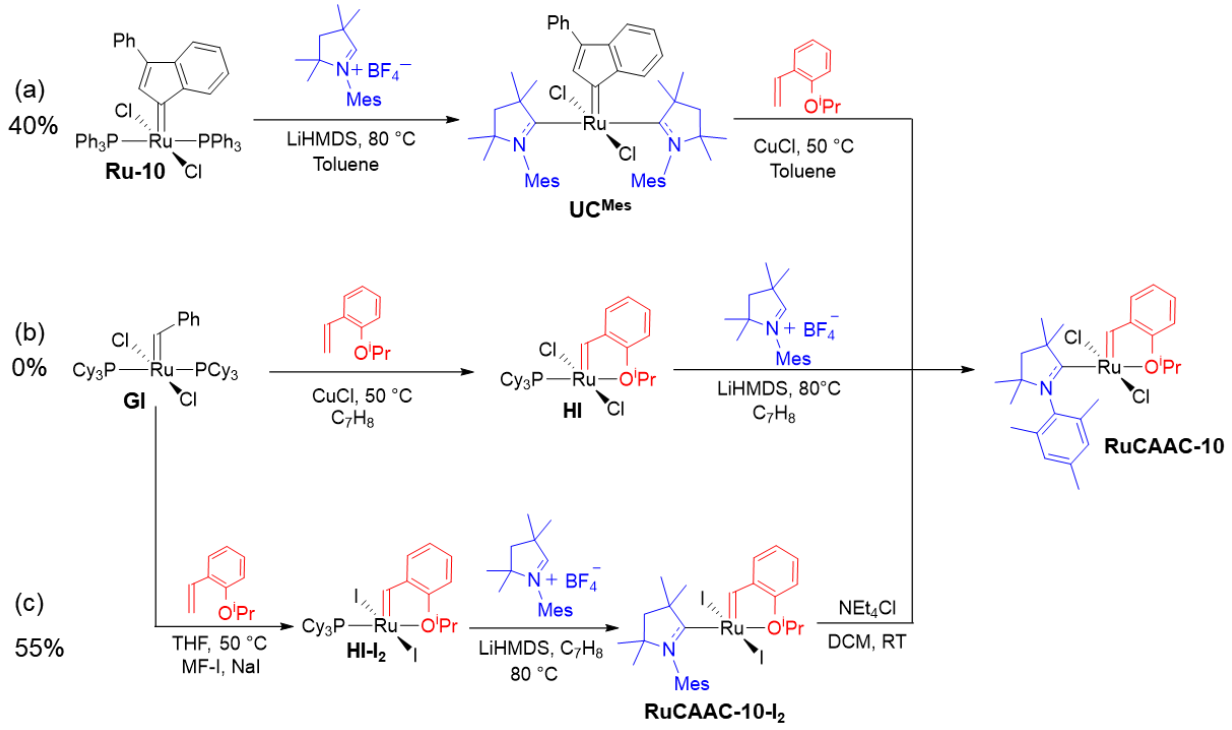

### 2.2.3 Validation of the Strengths of a Small Carbene: Self-Metathesis of Methyl Oleate

The self-metathesis of methyl oleate (Table 2.3) was selected as a model transformation of an internal olefin to examine the impact on productivity of a small CAAC ligand. Methyl oleate is of intense interest in the valorization of renewable lipids via self-metathesis, as noted in the Introduction.[2,35] To date, the top-performing catalyst for this reaction remains **GII**. In a 2002 study, the Mol group reported a total TON of 440,000 for **GII** at a loading of 1 ppm (Entry 1).[36] Competing E/Z isomerization resulted in a selectivity of ca. 91%, however, meaning that the productive TON for the desired reaction was 410,000, if solely the Z-isomer is desired. It should be noted that positional isomerization is undetectable by the analytical method used (GC-FID).

The TON for **GII-IPr** (Entry 2) was nearly an order of magnitude lower, behaviour attributed to the bulk of **GII-IPr** and its restricted access to the internal olefin. However, the fourfold higher catalyst concentration could also contribute to this difference. More recently, Mauduit reported an overall TON of 744,000 for a **HII-IPr** catalyst at a loading of 1 ppm (Entry 3).[3] Comparisons are difficult given that 85% pure **MO** was used along with different purification protocols, but the TON for formation of the desired product was 359,000.

**Table 2.3.** Top-performing catalysts for **MO** self-metathesis.

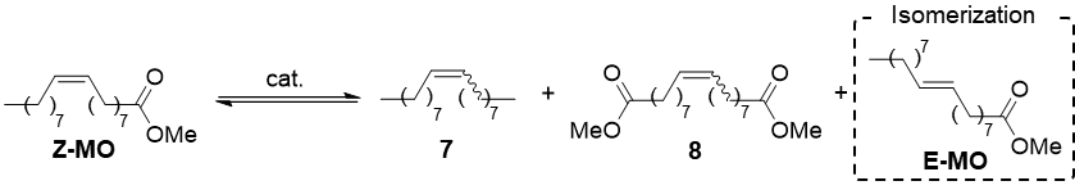


| Entry | Catalyst | Loading | Conv. (Yield[a]) | Total TON (E/Z mixture) | Productive TON (Z-products) | Ref. |
|---|---|---|---|---|---|---|
| 1 | **GII** | 1 ppm | 45% (41%) | 440,000 | 410,000 | 36 |
| 2 | 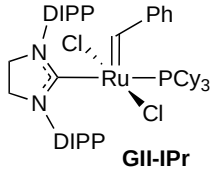 **GII-IPr** | 4 ppm | 46% | 46,000 | 46,000 | 36 |
| 3 | 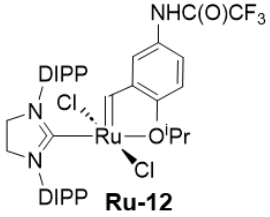 **Ru-12** | 1 ppm | 65% (31%) | 744,000 | 359,000 | 3 |

[a] Conditions: 50 °C, neat **MO**. For entries 1-2, >99% pure **MO** was passed through an alumina column before use. For entry 3, 85% **MO** was purified by first heating at 185 °C under vacuum for 2 h to eliminate volatile contaminants such as water and oxides, then treating with aluminosilicates ("bleaching earth") at 50 °C for 15 min.

In the present work, self-metathesis of 99% **MO** was carried out neat, using 1 ppm of catalyst (2 μM Ru) to minimize bimolecular decomposition. The performance of **RuCAAC-10** was tested relative to **HII**, **RuCAAC-3** and **RuCAAC-10-I$_2$**. Temperatures of RT and 40 °C were chosen, given the potential for isomerization at higher temperatures.[36,37] The results in Figure 2.3 show no E/Z isomerization for any of the CAAC catalysts: that is, solely productive catalysis occurred. The outstanding performance of **RuCAAC-10** is evident from the TONs of 430,000 over 24 h. In comparison, the iodide catalyst **RuCAAC-10-I$_2$** was completely inactive at RT, but reached 160,000 TON at 40 °C. Comparable performance (TON 150,000 at 40 °C) was observed for **RuCAAC-3**, the α-phenyl CAAC analogue of **RuCAAC-10**. Finally, while **HII** fell short of the productivity of **RuCAAC-10**, it out-performed both **RuCAAC-10-I$_2$** and **RuCAAC-3** at elevated temperature, despite the susceptibility of such NHC catalysts to decomposition via β-H elimination of the metallacyclobutane.[38,39]

Comparison with Table 2.3 indicates that the productivity of the small-CAAC catalyst **RuCAAC-10** surpasses the most productive catalysts reported to date, for which productive TONs of 410,000 and 359,000 were reported. Its high selectivity is an outstanding feature in offering access to high-purity products. Also notable is the fact that this performance was achieved in metathesis of a cis-internal olefin. Trans-internal olefins are anticipated to show even more dramatic improvements. These results clearly indicate the potential of small Ru-CAAC catalysts for crowded substrates.

**Figure 2.3.** Performance of **RuCAAC-10** relative to **HII** and bulkier CAAC catalysts in self-metathesis of **MO**.

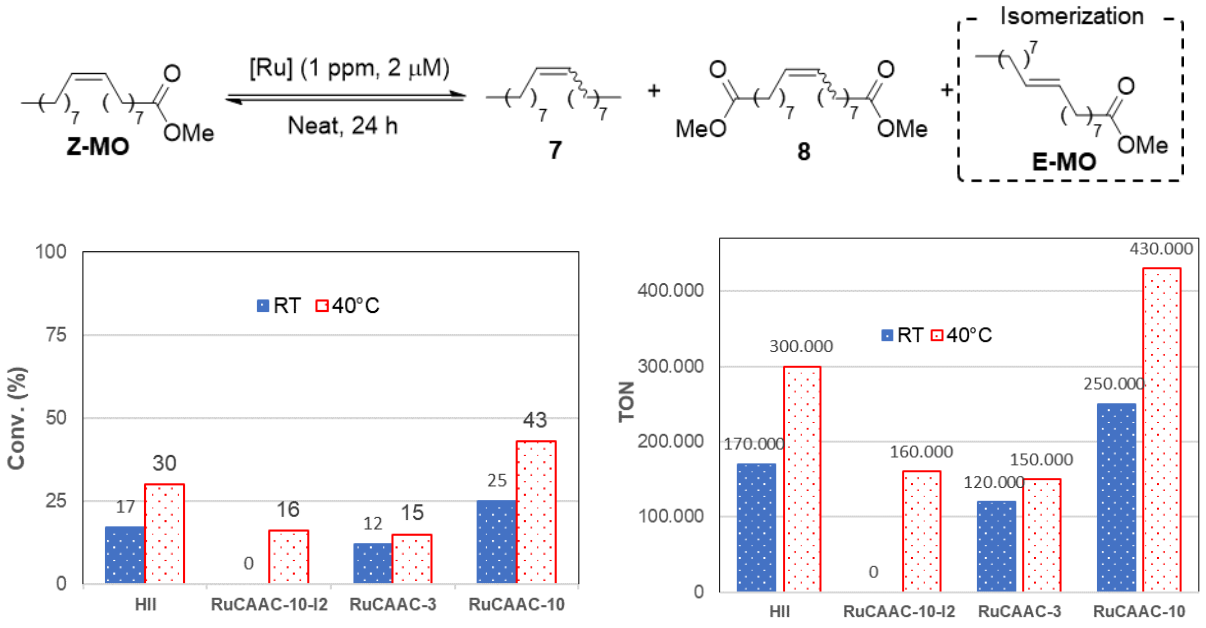

## 2.3 Conclusions

Challenges in the synthesis of small-CAAC catalysts emerge first in synthesis of the CAAC salts. In cyclization of the iminium precursor to **CAAC-10•HBF$_4$**, control of acid concentration proved essential to minimize side reactions. Decomposition of the chlorinated salt in water also occurred for reaction times above 1 h. Neither of these sensitivities applies so drastically to larger CAACs.

The installation of **CAAC-10** on the Hoveyda platform presents a second synthetic challenge, plausibly associated with attack of $PCy_3$ or a free CAAC on the alkylidene ligand. Use of iodide substituted precursor (**HI-I$_2$**) to protect the catalyst circumvented these suspected side-reactions, affording **RuCAAC-10** in an overall yield of 55%, as compared to 40% yield in a patent claim. Thus, the route developed in this thesis offers a more practical, viable, and efficient method to prepare Ru catalysts bearing smaller CAAC ligands.

To probe the capacity of **RuCAAC-10**, bearing a N-mesityl group and a dimethyl-substituted α-carbon, to improve performance in metathesis of a crowded olefin, the self-metathesis of methyl oleate was examined. **RuCAAC-10** delivered a TON of 430,000, with complete selectivity for the target olefin. It outperformed not only **HII**, diiodide **RuCAAC-10-I$_2$** and **RuCAAC-3,** but the best cases reported to date. Its performance demonstrates the advantage of reducing catalyst bulk for crowded substrates.

## 2.4 Experimental Procedures

### 2.4.1 General Procedures:

HPLC-grade $CH_2Cl_2$, $C_6H_6$, hexanes, and THF were dried and degassed using a Glass Contour solvent purification system and stored under $N_2$ over 4 Å molecular sieves. $CDCl_3$ and $C_6D_6$ (Cambridge Isotopes), were freeze-pump-thaw degassed (4×) and stored under $N_2$ in the glovebox. Deuterated solvents were stored over sieves as above. 2-Isopropoxystyrene was stored in the glovebox freezer at –35 °C. Dimethyl terephthalate (DMT, internal standard for NMR experiments; Sigma-Aldrich) was used as received. Methyl oleate (>98.5%) was purchased from Sigma-Aldrich and stored over alumina in glovebox freezer (–35 °C). The Merrifield resin **MF-I**,[40] 2-isopropoxystyrene,[4] and catalysts **RuCAAC-3**,[7] **HI-I$_2$**[25] and **GI**[41] were prepared by literature methods.

NMR spectra were recorded on a Bruker Avance 300 MHz spectrometer at 25 ± 2 °C. Chemical shifts are given in ppm and referenced to the residual proton of the deuterated solvent ($^1$H NMR). Air-sensitive NMR experiments (salt metathesis and catalyst synthesis) were carried out using either screw-capped NMR tubes equipped with PTFE septa (Rotoflo), or valved J. Young NMR tubes.

Quantitation in the self-metathesis of methyl oleate was carried out using an Agilent 7890A gas chromatograph (GC) equipped with auto-sampler, flame ionization detector (FID) and Agilent HP-5 polysiloxane column (30 m length, 320 µm diameter). Helium (UHP grade) was used as the carrier gas to maintain column pressure at 11.5 psi. Calibration curves of peak areas versus

concentration were established for methyl oleate and dodecane as internal standard in the relevant concentration regimes.

### 2.4.2 Synthesis of Small CAAC•$HBF_4$ Salts

#### 2.4.2.1 Synthesis of Aldimines (10a)

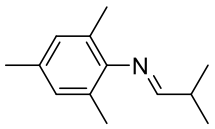

2,4,6-Trimethylaniline (8.15 g, 60.3 mmol, 1 equiv) was added to a solution of aldehyde (6.5 g, 90.1 mmol, 1.5 equiv) in dry hexanes (100 mL) under a flow of $N_2$. To the stirred mixture was added $MgSO_4$ (14.60 g, 121.2 mmol, 2 equiv) and 5 drops of glacial acetic acid. The reaction was heated at 55 °C for 12 h. The reaction was filtered through alumina and the filtrate was stripped to dryness under vacuum to afford the products as yellow oils. Yield: 80%. $^1$H NMR (300 MHz, $CDCl_3$): δ 7.52 (d, $^3J_{HH}$ = 4.9 Hz, 1H, C*H*=N), 6.83 (s, 2H, $H_{aryl}$), 2.69 (sept, $^3J_{HH}$ = 6.9, $^3J_{HH}$ = 4.9 Hz, 1H, C*H*Me$_2$), 2.26 (s, 3H, Mes *p*-C$H_3$), 2.05 (s, 6H, Mes *o*-C$H_3$), 1.22 (d, $^3J_{HH}$ = 6.9 Hz, 6H, C$H_3$).

#### 2.4.2.2 Synthesis of Alkenyl Imines (11a)

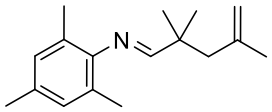

A solution of aldimine **10a** (4.92 g, 26.4 mmol, 1 equiv) in dry THF (15 mL) was cooled to –78 °C in acetone/dry ice. A 2.5 M solution of $^n$BuLi in hexanes (14.0 mL, 35.0 mmol, 1.3 equiv) was added dropwise under $N_2$ flow on a Schlenk line. After 5 min, the mixture was warmed to RT and left to stir for 3 h. 3-Chloro-2-methylpropene (3.0 g, 33.1 mmol, 1.2 equiv) was then slowly added at -78 °C. The solution was stirred at RT for 24 h. The volatiles were removed under vacuum and the resulting crude oil was dissolved in 20 mL hexanes. The lithium salt precipitated as white solid was filtered off through an alumina plug. The filtrate was concentrated under vacuum to yield the products as viscous oils. Yield: 70%. $^1$H NMR (300 MHz, $CDCl_3$): δ 7.59 (s, 1H, C*H*=N), 6.90 (s, 2H, $H_{aryl}$), 4.96 (s, 1H, C=C$H_2$), 4.82 (s, 1H, C=C$H_2$), 2.29 (s, 2H, C-C$H_2$-C), 2.25 (s, 3H, Mes *p*-C$H_3$), 2.05 (s, 6H, Mes *o*-C$H_3$), 1.78 (s, 3H, C$H_3$), 1.25 (s, 6H, C$H_3$); For fully assigned $^1$H NMR spectrum, see Figure A.2.

#### 2.4.2.3 Synthesis of Small CAAC•$HBF_4$ Salts (CAAC-10•$HBF_4$ and CAAC-3•$HBF_4$)

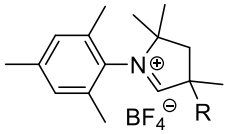

To a solution of alkenyl imine (12.3 mmol, 1 equiv) in 150 mL dry benzene at 0 °C was added 2 M HCl in $Et_2O$ (8.0 mL, 16.0 mmol, 1.3 equiv) under $N_2$ flow. After 10 min stirring, the reaction was heated to reflux overnight, then at 50 °C for 24 h. The solvent was removed under vacuum and the crude product washed with $Et_2O$ (3 × 15 mL) under $N_2$ flow to remove contaminants. To the resulting light yellow solid was added a minimum volume of water until complete dissolution of the chlorinated salt. $NaBF_4$ (2.7 g, 24.5 mmol, 2 equiv) was slowly added to precipitate the solid product. The solid was filtered off and washed several times with $Et_2O$ to obtain the off-white pure product.

In cases where the chlorinated solid did not precipitate in ether at room temperature, the mixture was heated at 50 °C for 30 min to promote solubilization of the amber oil.

R = Me. Yield: 45%. $^1$H NMR (300 MHz, $CDCl_3$) δ 9.08 (s, 1H, C*H*=N), 7.06 (s, 2H, $H_{aryl}$), 2.41 (s, 2H, backbone C$H_2$), 2.36 (s, 3H, Mes *p*-C$H_3$), 2.28 (s, 6H, Mes *o*-C$H_3$), 1.72 (s, 6H, N-C$Me_2$), 1.60 (s, 6H, C$H_3$). For fully assigned $^1$H NMR spectrum, see Figure A.3.

R = Ph. Yield: 55%. $^1$H NMR (300 MHz, $CDCl_3$) δ 9.51 (s, 1H, C*H*=N), 7.47 (m, 4H, overlapping $H_{aryl}$ signals), 7.36 (m, 1H, Ph *p-H* ), 7.05 (s, 1 H), 7.00 (s, 1 H), 3.11 (d, $J_{HH}$ = 13.9 Hz, 1H), 2.67 (d, $J_{HH}$ = 13.8 Hz, 1H), 2.33 (overlapping of 2 singlets, 6H), 2.05 (s, 3H), 2.00 (s, 3H), 1.62 (s, 3H), 1.42 (s, 3H). Values agree with the literature report.[42]

### 2.4.3 Synthesis of Hoveyda-type CAAC-catalysts

#### 2.4.3.1 Synthesis of $RuI_2$(CAAC-10)(=$C_6H_4$-2-O$^i$Pr), RuCAAC-10-$I_2$

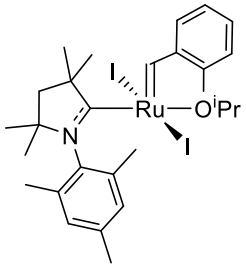


In the glovebox, solid white **CAAC-10•$HBF_4$** (158.8 mg, 0.48 mmol, 2 equiv) and LiHMDS (85.6 mg, 0.48 mmol, 2 equiv) were suspended in 2 mL toluene and stirred at 80 °C for 2 min. The resulting suspension was added dropwise to **HI-$I_2$** (200 mg, 0.24 mmol) in 1 mL toluene. The resulting brown-yellow suspension was stirred at 80 °C for 1 h. Full conversion was confirmed by $^{31}$P NMR analysis. The solvent was evaporated under vacuum and the residue purified by chromatography on silica gel in air (hexanes:$CH_2Cl_2$ 2:1). A green band was isolated. The solvent was stripped off and the product dried in vacuo. Yield of green **RuCAAC-10-$I_2$**: 70%. $^1$H NMR (300 MHz, $C_6D_6$): δ 15.15 (s, 1H, [Ru]=C*H*), 7.15 (m, Ar; integration hampered by overlap with $C_6D_5H$), 6.98 (dd, $^3J_{HH}$ = 7.2, $^4J_{HH}$ = 1.6 Hz, 2H, ArC*H*, Mes *m*-C*H*), 6.58 (m, 1H, ArC*H*), 4.90 (sept, $^3J_{HH}$ = 5.7 Hz, 1H, C*H*$Me_2$), 2.42 (s, 6H, C$H_3$), 2.29 (s, 6H, C$H_3$), 2.15 (s, 3H, Mes *p*-C$H_3$), 1.80 (d, $^3J_{HH}$ = 5.7 Hz, 6H, $^i$PrC$H_3$), 1.76 (s, 2H, CAAC backbone C$H_2$), 1.02 (s, 6H, Mes *o*-C$H_3$).

#### 2.4.3.2 Salt Metathesis of RuCAAC-10-$I_2$

In a $N_2$-filled glovebox, **RuCAAC-10-$I_2$** (10 mg, 0.013 mmol) in 1.0 mL of $CH_2Cl_2$ in a Schlenk flask. The chloride salt was added as a solid, and the mixture was stirred at RT or heated in an oil bath. Reaction progress was tracked by $^1$H NMR analysis of the alkylidene region from 14–25 ppm. $^1$H NMR samples were prepared by removing solvent under vacuum, solubilizing the residue in $C_6D_6$ and filtering any salt suspension through a small Celite plug.

For the experiments with DMT as internal standard, 10 mg, was added to a solution of **RuCAAC-10-$I_2$** in $C_6D_6$ and analysed by $^1$H NMR to obtain time zero spectrum. Then, solvent was removed under vacuum and redissolved in 1.0 mL $CH_2Cl_2$ or THF before addition of the chloride salt. The **RuCAAC-10-$I_2$** alkylidene signal was normalized to the signal for DMT. Conversion and yields were calculated based on integration vs DMT.

### 2.4.3.3 Synthesis of $RuCl_2$(CAAC-10)(=$C_6H_4$-2-O$^i$Pr), RuCAAC-10

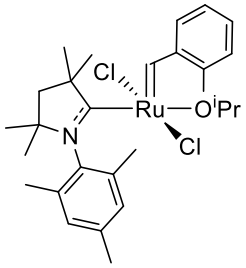


**RuCAAC-10-$I_2$** (100 mg, 0.13 mmol, 1 equiv) was dissolved in 1.0 mL of $CH_2Cl_2$ in a Schlenk flask. $NEt_4Cl$ (880 mg, 5.35 mmol, 40 equiv) was added and solution was stirred at room temperature. Reaction progress was tracked by $^1$H NMR which was fully converted after 2 h. Solvent was stripped off and the residue was dissolved in a minimum amount of benzene. The resulting mixture was filtered through a Celite plug to remove the precipitated ammonium salts, filtrate solvent removed under vacuum and product dried under vacuum for additional 24 h. Yield: 85%. $^1$H NMR (300 MHz, $C_6D_6$) δ 16.38 (s, 1H, [Ru]=C*H*), 7.14 (m, Ar; integration hampered by overlap with $C_6D_5H$), 7.07 (dd, $^3J_{HH}$ = 7.5, $^4J_{HH}$ = 1.6 Hz, 1H, ArC*H*), 6.84 (s, 2H, ArC*H*, Mes *m*-C*H*), 6.69 (td, $^3J_{HH}$ = 7.5, $^4J_{HH}$ = 0.9 Hz, 1H, ArC*H*), 6.46 (d, $^3J_{HH}$ = 8.4 Hz, 1H, ArC*H*), 4.70 (sept, $^3J_{HH}$ = 6.1 Hz, 1H, C*H*Me$_2$), 2.26 (m, 12H, overlapping C$H_3$), 2.19 (s, 3H, Mes *p*-C$H_3$), 1.80 (s, 2H, CAAC backbone C$H_2$), 1.73 (d, $^3J_{HH}$ = 6.1 Hz, 6H, $^i$PrC$H_3$), 1.02 (s, 6H, Mes *o*-C$H_3$).

### 2.4.4 Methyl Oleate Self-Metathesis

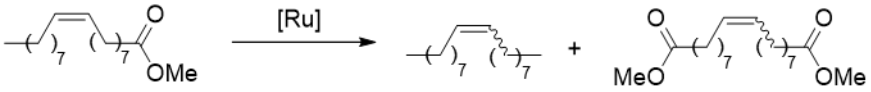


In the glovebox, 200 μL **MO** and 100 μL dodecane (internal standard for GC analysis) were added to a 4 mL vial at RT. The mixture was stirred for 5 min, after which a solution of the catalyst in benzene (45–50 μM) was added to reach the desired loading. Any heated reactions were immediately transferred to a preheated degassed oil bath. After 24 h reaction, a sample was taken, quenched with KTp in THF, and diluted in $CH_2Cl_2$ for GC-FID analysis. In all cases, the GC trace showed only two additional peaks other than **MO** and IS, assigned to the SM products. As no isomerization products were observed, reaction yields correspond to the conversions calculated based on initial and final concentrations of **MO**.

TONs were calculated based on the equation:

$$TON = \frac{yield \times initial\ moles\ \boldsymbol{MO}}{moles\ of\ catalyst}$$

## 2.5 References


(1) Cho, E. J.; Trinh, L. T. P.; Song, Y.; Lee, Y. G.; Bae, H.-J. Bioconversion of Biomass Waste into High Value Chemicals. *Bioresour. Technol.* **2020**, *298*, 122386–122398.

(2) Kajetanowicz, A.; Chwalba, M.; Gawin, A.; Tracz, A.; Grela, K. Non-Glovebox Ethenolysis of Ethyl Oleate and FAME at Larger Scale Utilizing a Cyclic (Alkyl)(Amino)Carbene Ruthenium Catalyst. *Eur. J. Lipid Sci. Technol.* **2020**, *122*, 1900263–1900274.

(3) Allard, J.; Curbet, I.; Chollet, G.; Tripoteau, F.; Sambou, S.; Caijo, F.; Raoul, Y.; Crévisy, C.; Baslé, O.; Mauduit, M. Bleaching Earths as Powerful Additives for Ru-Catalyzed Self-Metathesis of Non-Refined Methyl Oleate at Pilot Scale. *Chem. Eur. J.* **2017**, *23*, 12729–12734.

(4) Nienałtowski, T.; Szczepanik, P.; Małecki, P.; Czajkowska-Szczykowska, D.; Czarnocki, S.; Pawłowska, J.; Kajetanowicz, A.; Grela, K. Large-Scale Synthesis of a Niche Olefin Metathesis Catalyst Bearing an Unsymmetrical N-Heterocyclic Carbene (NHC) Ligand and Its Application in a Green Pharmaceutical Context. *Chem. – A Eur. J.* **2020**, *26*, 15708–15717.

(5) Yelchuri, V.; Srikanth, K.; Prasad, R. B. N.; Karuna, M. S. L. Olefin Metathesis of Fatty Acids and Vegetable Oils. *J. Chem. Sci.* **2019**, *131*, 39–55.

(6) Alexander, K. A.; Paulhus, E. A.; Lazarus, G. M. L.; Leadbeater, N. E. Exploring the Reactivity of a Ruthenium Complex in the Metathesis of Biorenewable Feedstocks to Generate Value-Added Chemicals. *J. Organomet. Chem.* **2016**, *812*, 74–80.

(7) Marx, V. M.; Sullivan, A. H.; Melaimi, M.; Virgil, S. C.; Keitz, B. K.; Weinberger, D. S.; Bertrand, G.; Grubbs, R. H. Cyclic Alkyl Amino Carbene (CAAC) Ruthenium Complexes as Remarkably Active Catalysts for Ethenolysis. *Angew. Chem. Int. Ed.* **2015**, *54*, 1919–1923.

(8) Nascimento, D. L.; Gawin, A.; Gawin, R.; Guńka, P. A.; Zachara, J.; Skowerski, K.; Fogg, D. E. Integrating Activity with Accessibility in Olefin Metathesis: An Unprecedentedly Reactive Ruthenium-Indenylidene Catalyst. *J. Am. Chem. Soc.* **2019**, *141*, 10626–10631.

(9) Wang, Z. J.; Jackson, W. R.; Robinson, A. J. An Efficient Protocol for the Cross-Metathesis of Sterically Demanding Olefins. *Org. Lett.* **2013**, *15*, 3006–3009.

(10) Stewart, I. C.; Ung, T.; Pletnev, A. A.; Berlin, J. M.; Grubbs, R. H.; Schrodi, Y. Highly Efficient Ruthenium Catalysts for the Formation of Tetrasubstituted Olefins via Ring-Closing Metathesis. *Org. Lett.* **2007**, *9*, 1589–1592.

(11) Jazzar, R.; Bourg, J. B.; Dewhurst, R. D.; Donnadieu, B.; Bertrand, G. Intramolecular "Hydroiminiumation and -Amidiniumation" of Alkenes: A Convenient, Flexible, and Scalable Route to Cyclic Iminium and Imidazolinium Salts. *J. Org. Chem.* **2007**, *72*, 3492–3499.

(12) Jazzar, R.; Dewhurst, R. D.; Bourg, J.-B.; Donnadieu, B.; Canac, Y.; Bertrand, G. Intramolecular "Hydroiminiumation" of Alkenes: Application to the Synthesis of Conjugate Acids of Cyclic Alkyl Amino Carbenes (CAACs). *Angew. Chem. Int. Ed.* **2007**, *46*, 2899–2902.

(13) Marx, V. M.; Sullivan, A. H.; Melaimi, M.; Virgil, S. C.; Keitz, B. K.; Weinberger, D. S.; Bertrand, G.; Grubbs, R. H. Cyclic Alkyl Amino Carbene (CAAC) Ruthenium Complexes as Remarkably Active Catalysts for Ethenolysis. *Angew. Chem. Int. Ed.* **2015**, *54*, 1919–1923.

(14) Morvan, J.; Mauduit, M.; Bertrand, G.; Jazzar, R. Cyclic (Alkyl)(Amino)Carbenes (CAACs) in Ruthenium Olefin Metathesis. *ACS Catal.* **2021**, *11*, 1714–1748.

(15) Melaimi, M.; Jazzar, R.; Soleilhavoup, M.; Bertrand, G. Cyclic (Alkyl)(Amino)Carbenes (CAACs): Recent Developments. *Angew. Chem. Int. Ed.* **2017**, *56*, 10046–10068.

(16) Lavallo, V.; Canac, Y.; Präsang, C.; Donnadieu, B.; Bertrand, G. Stable Cyclic (Alkyl)(Amino)Carbenes as Rigid or Flexible, Bulky, Electron-Rich Ligands for Transition-Metal Catalysts: A Quaternary Carbon Atom Makes the Difference. *Angew. Chem. Int. Ed.* **2005**, *44*, 5705–5709.

(17) Grünwald, A.; Goodner, S. J.; Munz, D. Isolating Free Carbenes, Their Mixed Dimers and Organic Radicals. *J. Vis. Exp.* **2019**, *2019*, 1–11.

(18) Wanzlick, H. W. Aspects of Nucleophilic Carbene Chemistry. *Angew. Chem. Int. Ed. Engl.* **1962**, *1*, 75–80.

(19) Baguli, S.; Kundu, A.; Nath, S.; Adhikari, D.; Mukherjee, D. A Donor–Acceptor Cyclopropane by Intramolecular C(Sp 3 )–H Activation at a Cyclic(Alkyl)(Amino)Carbene Center and Its Fascinating Ring-Opening Chemistry. *Org. Lett.* **2023**, *25*, 3141–3145.

(20) Gawin, R.; Kozakiewicz, A.; Guńka, P. A.; Dąbrowski, P.; Skowerski, K. Bis(Cyclic Alkyl Amino Carbene) Ruthenium Complexes: A Versatile, Highly Efficient Tool for Olefin Metathesis. *Angew. Chem. Int. Ed.* **2017**, *56*, 981–986.

(21) Anderson, D. R.; Lavallo, V.; O'Leary, D. J.; Bertrand, G.; Grubbs, R. H. Synthesis and Reactivity of Olefin Metathesis Catalysts Bearing Cyclic (Alkyl)(Amino)Carbenes. *Angew. Chem. Int. Ed.* **2007**, *46*, 7262–7265.

(22) Skowerski, K.; Rafal, G. Process for Producing Ruthenium Complexes and Intermediates Thereof and Their Use in Olefin Metathesis. WO 2017/055945 A1, 2017.

(23) Gawin, R.; Tracz, A.; Chwalba, M.; Kozakiewicz, A.; Trzaskowski, B.; Skowerski, K. Cyclic Alkyl Amino Ruthenium Complexes—Efficient Catalysts for Macrocyclization and Acrylonitrile Cross Metathesis. *ACS Catal.* **2017**, *7*, 5443–5449.

(24) Turner, Z. R. Chemically Non-Innocent Cyclic (Alkyl)(Amino)Carbenes: Ligand Rearrangement, C−H and C−F Bond Activation. *Chem. Eur. J.* **2016**, *22*, 11461–11468.

(25) Blanco, C. O.; Nascimento, D. L.; Fogg, D. E. Routes to High-Performing Ruthenium–Iodide Catalysts for Olefin Metathesis: Ligand Lability Is Key to Efficient Halide Exchange. *Organometallics* **2021**, *40*, 1811–1816.

(26) *CRC Handbook of Chemistry and Physics*, 84th ed.; Lide, D. R., Ed.; Taylor & Francis, 2004.

(27) Morvan, J.; Vermersch, F.; Zhang, Z.; Falivene, L.; Vives, T.; Dorcet, V.; Roisnel, T.; Crévisy, C.; Cavallo, L.; Vanthuyne, N.; Bertrand, G.; Jazzar, R.; Mauduit, M. Optically Pure C 1 -Symmetric Cyclic(Alkyl)(Amino)Carbene Ruthenium Complexes for Asymmetric Olefin Metathesis. *J. Am. Chem. Soc.* **2020**, *142*, 19895–19901.

(28) Strauss, S. H. The Search for Larger and More Weakly Coordinating Anions. *Chem. Rev.* **1993**, *93*, 927–942.

(29) Chu, J.; Munz, D.; Jazzar, R.; Melaimi, M.; Bertrand, G. Synthesis of Hemilabile Cyclic

(Alkyl)(Amino)Carbenes (CAACs) and Applications in Organometallic Chemistry. *J. Am. Chem. Soc.* **2016**, *138*, 7884–7887.

(30) Vermersch, F.; Oliveira, L.; Hunter, J.; Soleilhavoup, M.; Jazzar, R.; Bertrand, G. Cyclic (Alkyl)(Amino)Carbenes: Synthesis of Iminium Precursors and Structural Properties. *J. Org. Chem.* **2022**, *87*, 3511–3518.

(31) Dalton, R. D.; Mascavage, M. L. Halogen Hydride Addition to Alkenes and Alkynes. *Trends Org. Chem.* **1993**, *4*, 303–333.

(32) Rufh, S. A.; Goudreault, A. Y.; Foscato, M.; Jensen, V. R.; Fogg, D. E. Rapid Decomposition of Olefin Metathesis Catalysts by a Truncated N-Heterocyclic Carbene: Efficient Catalyst Quenching and N-Heterocyclic Carbene Vinylation. *ACS Catal.* **2018**, *8*, 11822–11826.

(33) Denk, M. K.; Thadani, A.; Hatano, K.; Lough, A. J. Steric Stabilization of Nucleophilic Carbenes. *Angew. Chem. Int. Ed. Engl.* **1997**, *36*, 2607–2609.

(34) Patrzałek, M.; Piątkowski, J.; Kajetanowicz, A.; Grela, K. Anion Metathesis in Facile Preparation of Olefin Metathesis Catalysts Bearing a Quaternary Ammonium Chloride Tag. *Synlett* **2019**, *30*, 1981–1987.

(35) Schunck, N. S.; Mecking, S. In Vivo Olefin Metathesis in Microalgae Upgrades Lipids to Building Blocks for Polymers and Chemicals. *Angew. Chem. Int. Ed.* **2022**, *61*, e202211285.

(36) Dinger, M. B.; Mol, J. C. High Turnover Numbers with Ruthenium-Based Metathesis Catalysts. *Adv. Synth. Catal.* **2002**, *344*, 671–677.

(37) Butilkov, D.; Frenklah, A.; Rozenberg, I.; Kozuch, S.; Lemcoff, N. G. Highly Selective Olefin Metathesis with CAAC-Containing Ruthenium Benzylidenes. *ACS Catal.* **2017**, *7*, 7634–7637.

(38) Nascimento, D. L.; Foscato, M.; Occhipinti, G.; Jensen, V. R.; Fogg, D. E. Bimolecular Coupling in Olefin Metathesis: Correlating Structure and Decomposition for Leading and Emerging Ruthenium−Carbene Catalysts. *J. Am. Chem. Soc.* **2021**, *143*, 11072–11079.

(39) Nascimento, D. L.; Fogg, D. E. Origin of the Breakthrough Productivity of Ruthenium–Cyclic Alkyl Amino Carbene Catalysts in Olefin Metathesis. *J. Am. Chem. Soc.* **2019**, *141*, 19236–19240.

(40) Nascimento, D. L.; Davy, E. C.; Fogg, D. E. Merrifield Resin-Assisted Routes to Second-Generation Catalysts for Olefin Metathesis. *Catal. Sci. Technol.* **2018**, *8*, 1535–1544.

(41) Schwab, P.; Grubbs, R. H.; Ziller, J. W. Synthesis and Applications of RuCl 2 (CHR‘)(PR 3 ) 2 : The Influence of the Alkylidene Moiety on Metathesis Activity. *J. Am. Chem. Soc.* **1996**, *118*, 100–110.

(42) Mauduit, M.; Morvan, J.; Lorkowski, J.; Vanthuyne, N.; Jazzar, R.; Bertrand, G. Process for the Preparation of Optically Pure Enantiomers of Cyclic Iminium Salts and Their Use as Catalysts. WO2023031335 A1, 2023.

# Chapter 3 Synthesis of a Fluorophore-Tagged Benzylidene Catalyst for Olefin Metathesis

## 3.1 Introduction

Fluorophore-tagged catalysts hold great promise as a tool with the potential to allow visualization and tracking of catalyst behaviour (including decomposition) during reaction. In the broader context of catalysis, they enable reactions to be monitored in real time, delivering mechanistic information under actual operating conditions, particularly at low catalyst loadings.[1,2] The use of fluorophore-tagged metathesis catalysts has the potential to advance the fields of materials science,[3] renewable feedstocks,[4,5] industrial and pharmaceutical chemistry.[6]

### 3.1.1 Advantages of Fluorescence over Nuclear Magnetic Resonance Spectroscopy

At present, catalyst speciation in olefin metathesis is almost invariably monitored by NMR spectroscopy. This is problematic for tracking catalyst decomposition, which relies on quantification of alkylidene (Ru=C*H*R) signals and organic "markers" released in catalyst degradation. Analyte concentrations in the millimolar range are required to achieve detectable and reliable signals for quantitative $^{1}$H NMR analysis.[7–9] Under realistic operating conditions, however, catalyst concentrations are in the millimolar to micromolar range.[10–12] The high metal concentrations required for NMR analysis perturb catalyst speciation, and hence the decomposition pathways (bimolecular decomposition being one obvious example). The high sensitivity of fluorescence spectroscopy, in contrast, permits detection of analytes present in picomolar to micromolar concentrations.

A further asset in fluorimetry is the nanosecond timescale for detection of small molecules, much shorter than the millisecond timescale of NMR experiments. Fluorimetry can hence identify steady states in fast dynamic processes that are averaged on the NMR timescale.[13,14] Finally, fluorimetry can permit selective detection of the target molecule in the presence of a large excess of non-tagged background and substrate.[14,15]

### 3.1.2 Fluorophore Properties and Probe Selection

Considered in this section are the decisions governing the design and synthesis of fluorophore-tagged catalysts for olefin metathesis. The decision of which fluorophore to employ (see Table 3.1) rests on several fundamental properties. Firstly, the fluorophore tag should have minimal impact on catalyst activity during olefin metathesis. That is, it must accurately represent the catalytic process of untagged analogues. Moreover, it must be chemically stable under experimental conditions, to ensure that degradation of the emissive moiety does not interfere.

High quantum yield and high detection sensitivity are essential for accurate and reliable measurements.[14,16] Particularly attractive candidates for metathesis are BODIPY, with its high quantum yields, chemical stability, and versatile applications (Table 3.1, entries 1). Prior studies suggest that it has minimal impact on metathesis catalyst activity.[3–5] The dansyl group has similar advantages, leading to its popularity as a fluorophore in various biochemical and analytical applications.[1,2,17,18] A major further advantage of the dansyl dye is its large Stokes shift (ca. 100

nm): that is, the separation between the UV-vis band in the excitation spectrum vs the emission spectrum (Table 3.1, entries 2).[17,18] A large Stoke shift confers higher accuracy and precision in quantitative fluorescence experiments by minimizing overlap between absorption and emission bands, hence limiting self-absorption via reabsorption of emitted radiation.[3–5]

The other dyes in Table 3.1 were excluded from consideration, given lower quantum yields and a variety of other reasons. Coumarin (entry 3) is a widely used, biocompatible fluorophore,[19,20] but its environment-dependent fluorescence (e.g. varying with pH)[21] would limit accurate quantification for metathesis in biological media, one of our long-term target applications. Pyrene, another well-known fluorophore (entry 4), may participate in intermolecular π-stacking on release, forming excimers and resulting in concentration-dependent emission.[22,23] Rhodamine[24] and fluorescein (entries 5 and 6) are chemically unstable, the latter being particularly susceptible to decay over time on exposure to light.[25] Finally, cyanine dyes (entry 7) have particularly low quantum yields: in addition, the internal olefinic groups are potentially reactive in olefin metathesis.

**Table 3.1.** Fluorophores considered, and their photophysical properties.[14,15,26,27]

| | Fluorophore | Structure[a] | $\lambda max_{(abs)}$ (nm)[b] | $\lambda max_{(em)}$ (nm)[b] | Quantum yield ($\Phi_F$)[b] | Issues for metathesis applications |
|---|---|---|---|---|---|---|
| 1 | BODIPY | 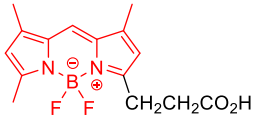 | 505 | 511 | 0.94 | Small Stoke shift |
| 2 | Dansyl | 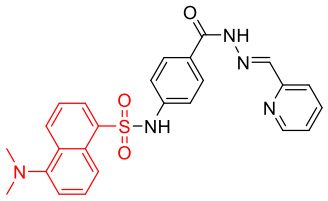 | 350 | 545 | 0.80 | None |
| 3 | Coumarin | 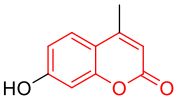 | 360 | 450 | 0.63 | Lower $\Phi_F$ pH sensitivity |
| 4 | Pyrene | 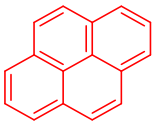 | 340 | 390 | 0.65 | Lower $\Phi_F$ Excimer formation |
| 5 | Rhodamine | 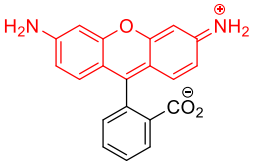 | 497 | 520 | 0.88 | Small Stokes shift Chemically unstable |

| | Fluorophore | Structure[a] | λmax(abs) (nm)[b] | λmax(em) (nm)[b] | Quantum yield ($\Phi_F$)[b] | Issues for metathesis applications |
|---|---|---|---|---|---|---|
| 6 | Fluorescein | 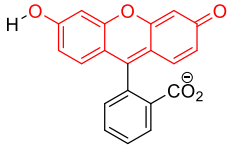 | 491 | 510 | 0.86 | Small Stokes shift<br>Chemically unstable |
| 7 | Cyanine | 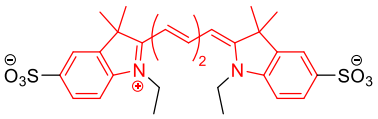 | 647 | 665 | 0.25 | Low $\Phi_F$<br>Small Stokes shift<br>Reactive olefinic sites |

[a] Fluorophore core in red. [b] Approximate values; will vary with solvent and structural changes.

A key consideration for fluorescence measurements is the contrast between emissive and quenched states. For metal-bound fluorophores, quenching may occur by energy exchange through dipole-dipole interactions (the Forster resonance energy transfer or FRET mechanism), and/or collisional electron exchange (the Dexter mechanism). Emission is quenched to varying extents when the tagged ligand is bound to a metal, and restored when the ligand is lost. Complete quenching on the metal is ideal to maximize contrast.

Overall, the combination of chemical stability, high quantum yield, high contrast, large Stoke shift and low perturbation of catalyst activity make the dansyl and BODIPY fluorophores optimal for studies of olefin metathesis. A significant advantage of the dansyl tag lies in its much greater Stokes shift relative to BODIPY, and it was therefore chosen for study in this thesis work.

### 3.1.3 Fluorophore-Tagged Catalysts in Olefin Metathesis

Despite the advantage noted above, the dansyl fluorophore has rarely been employed in olefin metathesis. In the sole report to date, Plenio and coworkers employed a dansyl tag in a 2010 study to examine operation of the so-called 'boomerang', or release-return mechanism, for Hoveyda-type catalysts.[1] In this pathway (Scheme 3.1), recapture of the alkylidene ligand by the four-coordinate active methylidene species is proposed to regenerate the precatalyst as an off-cycle resting state. While flaws in this study (particularly poor mass transfer) limit the validity of its mechanistic conclusions, as pointed out in a robust critique,[28] the key point from the present perspective is the utility of fluorescence spectroscopy to monitor release of the benzylidene ligand (Scheme 3.1b). Minimal impact on metathesis activity was reported for the tagged catalyst relative to the parent **HII**. As binding to ruthenium largely quenched the fluorescence of the dansyl dye, release of the benzylidene ligand as a tagged styrene during initiation was confirmed by increases in fluorescence.[1,14]

**Scheme 3.1.** Release of the fluorophore-tagged probe from **HII-Dansyl** during initiation.

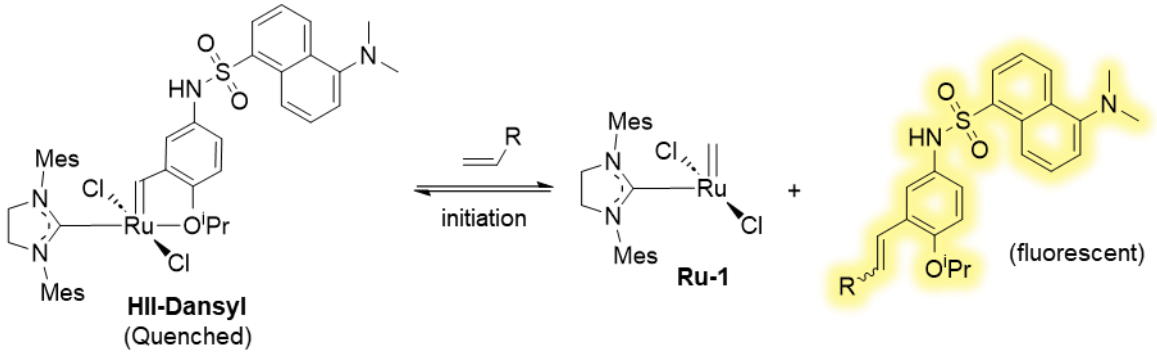


Fluorescence was used similarly, to quantify release of a benzylidene ligand in the first turnover of metathesis, in a 2018 "chemodosimetry" study by Michel and coworkers.[5] In this work, a BODIPY-tagged **HII** analogue (Figure 3.1a) was used as a probe to detect the plant hormone ethylene in the green microalga *Chlamydomonas reinhardtii*. The unique capacity of the neutral BODIPY ligand to pass through the cell membrane was key to successful detection of ethylene in the living cells. Confocal fluorescence microscopy confirmed localization of the BODIPY-tagged styrene in the cells. Selective detection of ethylene was reported. It should be noted that the green BODIPY dye (absorbance at 493 nm; emission at 505 nm) minimizes interference with chlorophyll, which absorbs in the red and blue region of the visible spectrum, and autofluorescences at 650-700 nm.

**Figure 3.1** BODIPY-tagged catalysts used in olefin metathesis.

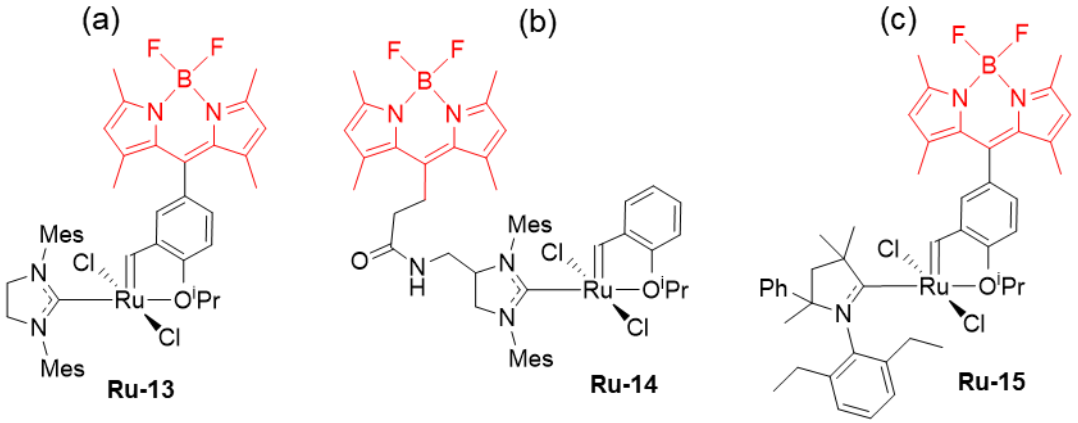


Related BODIPY-tagged catalysts were subsequently used to detect catalyst uptake in a diatom microalga, *Phaeodactylum tricornutum* (Figure 3.1, b-c).[4] Microalgae are of interest for the sustainable production of chemical feedstocks, owing to their ability to capture $CO_2$ as unsaturated fatty acids via photosynthesis. In a 2022 study, Schunck and Mecking showed that *catalytic* olefin metathesis could be achieved inside living microalgae.[4] Fluorescence microscopy was used to

track uptake of the catalyst into the cell, and to confirm its viability for the first turnover of olefin metathesis.

In addition to these reports of fluorophore-tagged benzylidenes, the fluorophore has been appended to the stabilizing carbene ligand. In 2015, the Tour group[3] used a BODIPY-tagged NHC for ROMP. In 2019, Takada and coworkers[29] used a coumarin-tagged $H_2$IMes ligand to detect ethylene in fruits and leaves. Related studies in metathesis polymerization or RCM were reported for BODIPY,[30] coumarin,[31] and pyrene[23] fluorophores. Because of potential applications in catalyst decomposition, a Hoveyda catalyst containing fluorophore-tagged benzylidene ligand was the focus of this thesis work.

### 3.2 Results and Discussion

The **HII-Dansyl** catalyst has potential as a fluorimetry probe in metathesis. However, Plenio's reported synthetic route (Scheme 3.2) delivers **HII-Dansyl** in only ca. 20% yield over 5 steps.[1] The reaction sequence commences with installation of the isopropoxy group on phenol **17**, followed by installation of the terminal olefin **20** via Stille cross-coupling. These steps, which proceed in good yield, were originally established by Mauduit and coworkers (2006) for synthesis of "Grela-class" catalysts containing a nitro-benzylidene.[32] Plenio exploited the nitro functionality in styrene **20** to install the desired dansyl tag. Thus, reduction of the nitro group to an amine with $Na_2S_2O_4$ and an organic mediator (see **21**, Step 3), followed by reaction with dansyl chloride, delivered the fluorophore-tagged styrene **23**. Metathesis with **GII** then generated **HII-Dansyl**.

**Scheme 3.2.** Reported synthetic route for **HII-Dansyl**.[1,32]

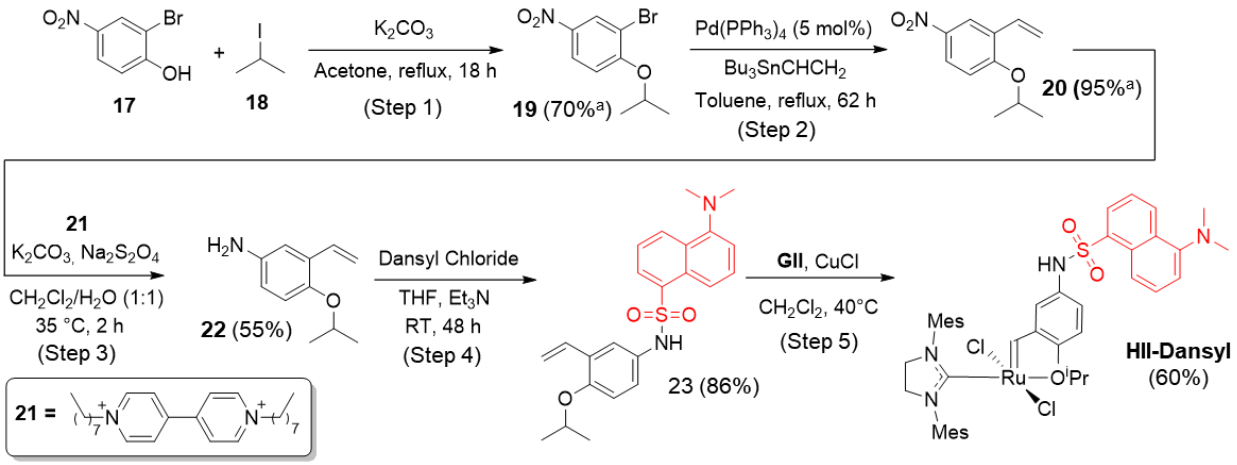


[a]The yield in Step 1 was reported by Mauduit and coworkers.[32]

An alternative route commencing with 5-nitrosalicylaldehyde **24** (Scheme 3.3) was envisaged as a means of improving safety and overall yields. Identified at the outset for improvement was Step 3, the reduction of the nitro group, which proceeded in 55% yield. In addition to the unsatisfactory yield, alternatives to the neuro- and hepatotoxic organotin reagent are desirable.[33,34] In addition,

increases to the 60% yield in Step 5 (installation of the isopropoxy alkylidene) were anticipated to be readily achievable, given that this reaction has been reported in yields above 85%.[35–37]

**Scheme 3.3.** Overview of alternative route to **HII-Dansyl**.

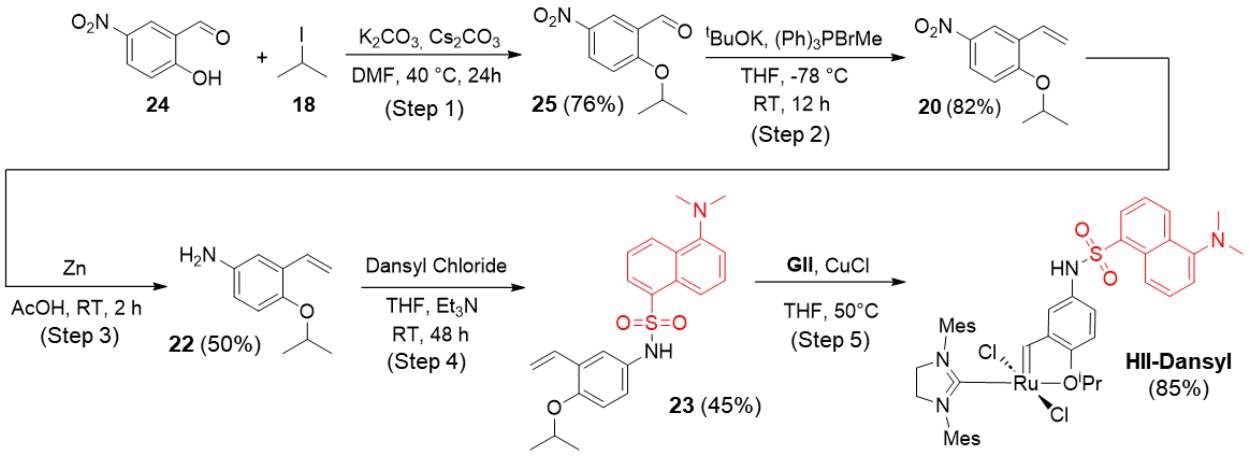


The new reaction sequence commenced with preparation of the isopropoxybenzaldehyde **25** by nucleophilic substitution of 2-iodopropane **18** and phenol **24**. The reaction afforded known[38] **25** as a yellow solid in 76% yield. Transformation of the benzaldehyde into styrene **20** was undertaken by Wittig olefination. The phosphonium ylid was prepared in situ with $(Ph)_3PCH_3Br$ and $^tBuOK$, to which nitro-isopropoxy aldehyde (**25**) was added at RT. Complete conversion of the starting aldehyde over 12 h was confirmed by $^1H$ NMR analysis, based on the disappearance of the diagnostic aldehyde peak at 10.45 ppm. The nitrostyrene product **20** was isolated as a viscous yellow oil in 82% yield,[39] as compared to 95% for the Stille cross-coupling step in the original route.

Synthesis of 2-isopropoxy-5-aminostyrene **22** via reduction of nitroarene **20** was reported by the Plenio group in 2010. As shown in Scheme 3.4, yields of 55% were reported on use of $Na_2S_2O_4$ as a reducing agent with 1,1´-dioctyl-4,4´-bipyridinium dibromide to mediate electron transfer.[1] Initial attempts at reduction with $Na_2S_2O_4$ without bipyridinium bromide proceeded in only 12% yield (Scheme 3.4b). The bipyridinium radical thus appears to be critical in assisting electron transfer.[40,41] A potentially chemoselective role has also been noted, and its absence may allow competing reduction of the alkene.[41] As the additional complexity associated with the co-reagent is unattractive, use of $SnCl_2$ as a reducing agent[42–44] (Scheme 3.4c) was attempted despite the toxicity of tin. This effort failed, as tin side-products were formed, and removing them by hydrolysis and precipitation with 0.2 M NaOH or 5% $NaHCO_3$[42] caused degradation of base-sensitive **22**.

**Scheme 3.4.** Synthesis of 2-isopropoxy-5-aminostyrene (**22**) from **20**. (a) Literature route. (b) Attempted reduction without bipyridinium bromide. (c) Attempted reduction with $SnCl_2$.

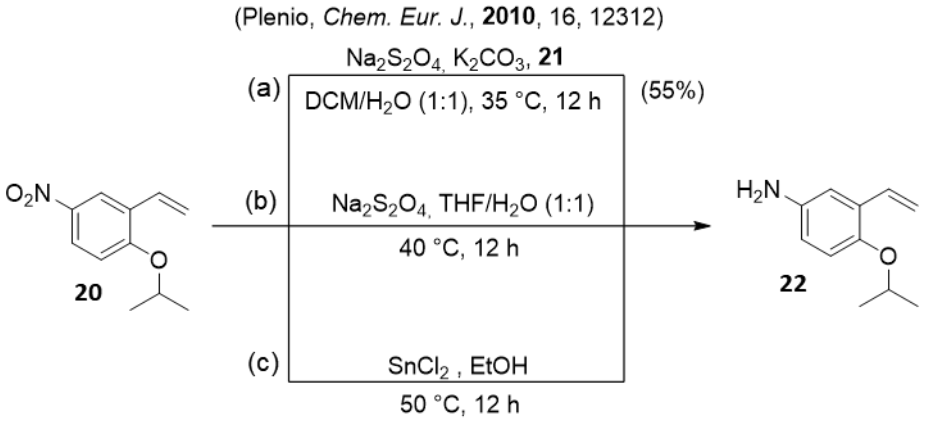


A 2012 patent by Parsy et al. (Scheme 3.5a) describes a more attractive alternative, in which reduction was effected in 86% yield with Zn dust in glacial acetic acid.[45] Parsy's procedure was therefore undertaken for Step 3 with minor modification (Scheme 3.5b). Reduction of **20** proceeded quantitatively, as judged by $^1$H NMR analysis. Diagnostic features are the upfield shift of the signals for the terminal olefin (from 5.86 and 5.39 ppm for **20** to 5.66 ppm and 5.21 ppm for **22**). However, a disconcerting black paste was obtained on workup by filtration through Celite and extraction with EtOAc-water. This was unexpected given the description of **22** as a yellow solid in the original reports.[1,45] Nevertheless, as the $^1$H NMR spectrum showed only the signals expected for **22**, the product was carried forward to the dansyl coupling step (Step 4 of Scheme 3.3). Yields were <10%, suggesting the presence of NMR-silent inorganic contaminants in the black paste. Repeating the reduction of **20** with purification by silica-gel chromatography afforded **22** as a dark yellow oil in 50% yield. This yield is comparable to that reported by Plenio (55%),[1] if disappointingly lower than that described in the original patent.[45]

**Scheme 3.5.** Alternative synthesis of 2-isopropoxy-5-aminostyrene (**22**) from **20**. (a) Patent route. (b) Modified implementation route.

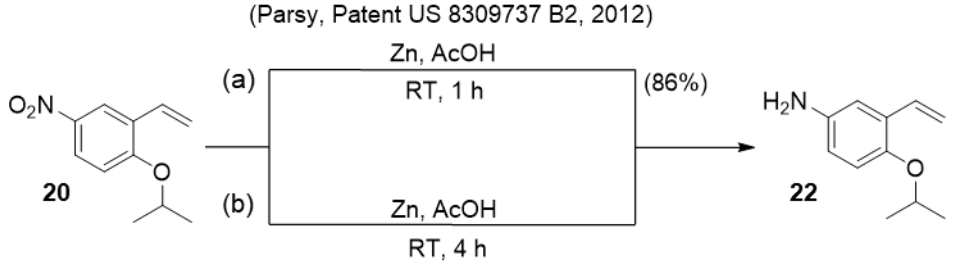


To attach the dansyl fluorophore, the styrene block **22** was reacted with dansyl chloride (**DNS-Cl**) in the presence of $NEt_3$ to take up the acid produced (Figure 3.2). Despite use of the styrene in excess (1.5 equiv), consumption of **DNS-Cl** was only 70% complete, as judged from the $^1$H NMR integration for the diagnostic Ar-H proton (8.69 ppm, black arrow). Increasing the proportion of

styrene **22** to 2 equivalents had no effect. Increasing reaction times beyond 48 h proved deleterious, as $^{1}$H NMR analysis showed new signals for an unknown side product at 8.64 ppm (labelled as **26**). The side-product may be an amine bearing two dansyl groups (see **26**),[17,18] formation of which would be favoured with increases in the concentration of monosubstituted **23**. As increasing reaction time proved unproductive, favouring formation of **26** instead of improving the yield of **23**, this approach was abandoned.

**Figure 3.2.** Intended synthesis of dansylstyrene **23**, with $^{1}$H NMR spectra ($CDCl_3$, 300 MHz), showing the progress of reaction. Top: crude reaction mixture at 48 h. Bottom: At 72 h.

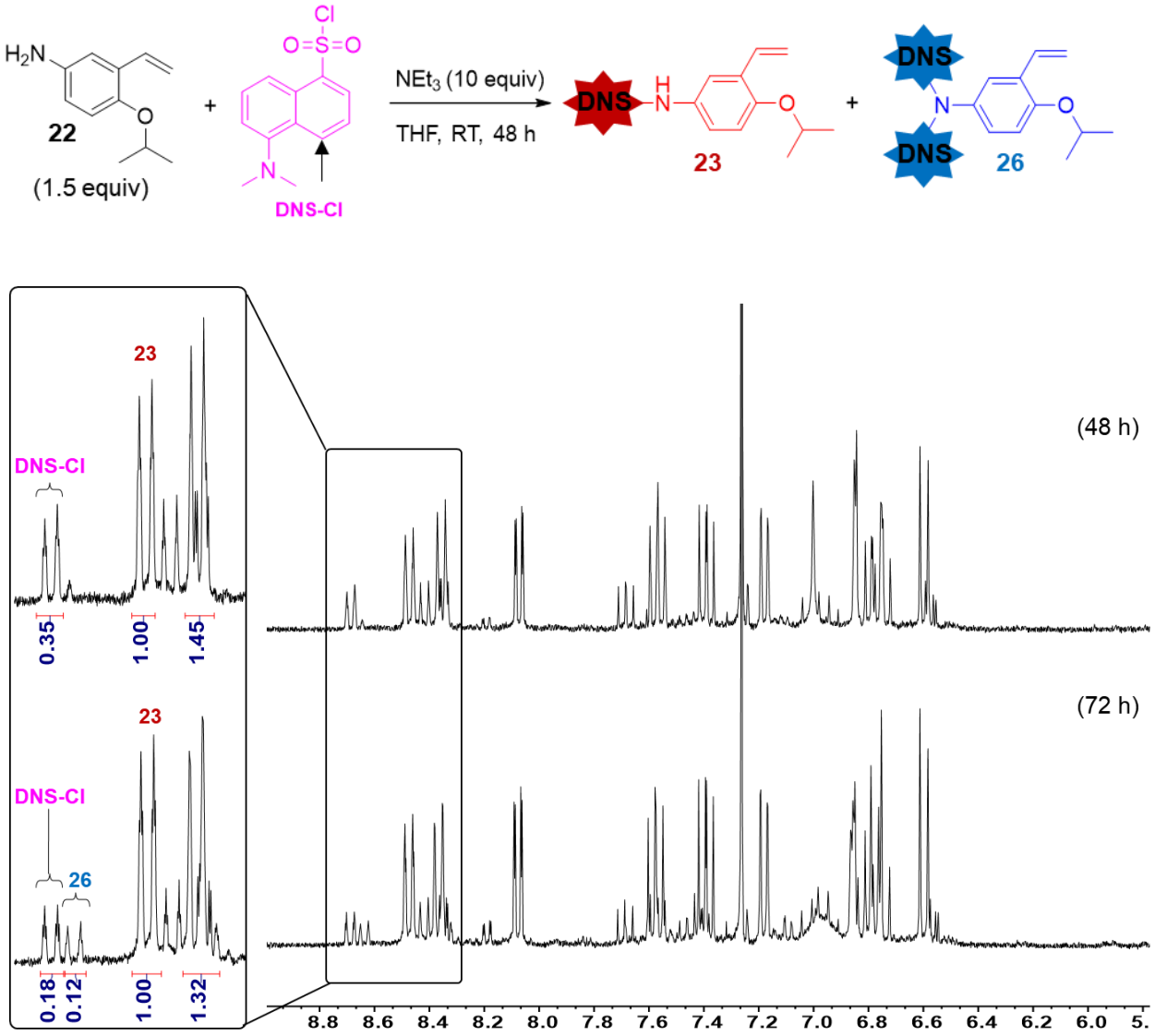


Precedent for formation of a di-dansyl product appears in a report by Ortega-Gutiérrez and co-workers (2010), in which synthesis of disubstituted amines with dansyl fluorophores was deliberately undertaken (Figure 3.3).[17] The Ar-H signal for disubstituted **28** appeared as a doublet of doublets at 8.49 ppm, upfield of the corresponding signal for monosubstituted **29** (8.56 ppm).[17]

Similarly, the signal for **26** appears as a doublet at 8.47 ppm, vs 8.64 ppm for **23** (see bottom spectrum of Figure 3.2). Confirmation of this assignment is unresolved as attempts to isolate the side-product by silica-gel chromatography were unsuccessful, but monosubstituted dansylstyrene was isolated in 45% yield. It may be noted that these yields compare favourably with those reported in the corresponding fluorophore-benzylidene attachment step for the BODIPY-tagged catalysts, where yields range from 12-35%.[4,5]

**Figure 3.3.** Mono- and doubly dansyl-tagged compounds reported by Ortega-Gutiérrez.

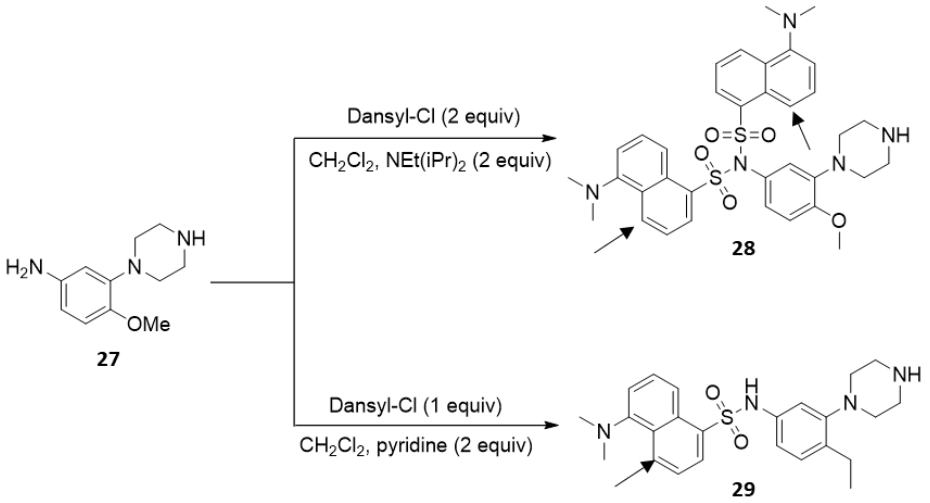


The final step in the synthesis of **HII-Dansyl** in Plenio's original report involved installation of the dansyl-tagged styrenyl ether ligand by cross-metathesis with **GII** in $CH_2Cl_2$. The low yield in this reaction (only 60%) could reflect difficulties in removing the $PCy_3$ coproduct, despite use of CuCl as a phosphine scavenger. While the Grela group has reported yields of 97% for the corresponding reaction of **GII** with 2-isopropoxystyrene in $CH_2Cl_2$,[35], our group has found use of THF to provide better purity,[36,37] because the reaction is driven by precipitation of the CuCl-phosphine product from THF. (Alternatively, a Merrifield resin can be used to scavenge the phosphine, but the reaction is slower).[36] Installation of the fluorophore-tagged ligand was therefore carried out with **GII** and CuCl in THF (Scheme 3.6). Complete conversion of **GII** was observed after 2 h, as judged from disappearance of the $PCy_3$ singlet at 30 ppm.[36] Purification of the crude product by silica-gel chromatography using 1:1 $CH_2Cl_2$/hexanes afforded **HII-Dansyl** in 85% yield, approximately 25% higher than that in the Plenio report.

**Scheme 3.6.** Synthesis of the catalyst **HII-Dansyl**.

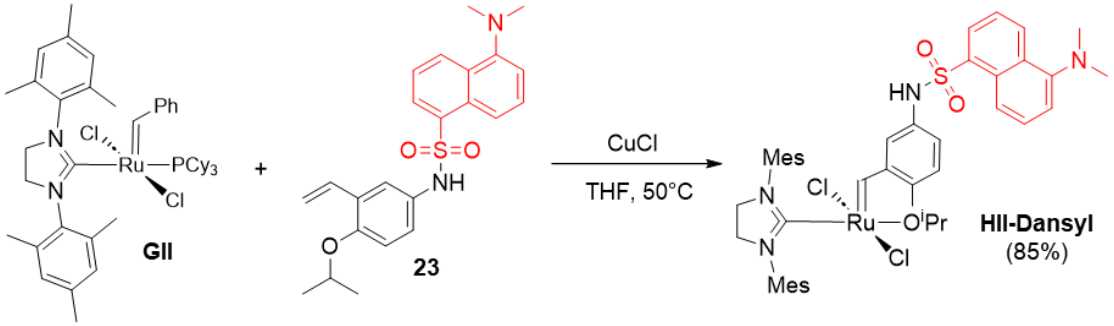


## 3.3 Conclusions

Fluorescence spectroscopy holds great potential in olefin metathesis, and reliable and reproducible routes to fluorophore-tagged catalysts are therefore important. Described in this Chapter is the adaptation of a reported route to **HII-Dansyl**, containing a dansyl-tagged benzylidene ligand.[1] Targeted for improvement were the initial step involving reduction of the nitro functionality, as well as the installation of the isopropoxybenzylidene group. Some success was achieved in the first objective. Use of Zn/HOAc to reduce the nitro group in **20**, in place of Plenio's $Na_2S_2O_4$–bipyridinium bromide, gave more convenient access to the 2-isopropoxy-5-aminostyrene **22**.[45] However, the patent yield of 86% could not be reproduced. The yield of 50% ultimately obtained was similar to that reported by Plenio.[1]

An unexpected problem, even under conditions identical to those reported, was the formation of side-products during synthesis of the dansyl-tagged benzylidene ligand. One of these is tentatively identified as the doubly-substituted dansylamine.

Finally, installation of the dansyl-tagged benzylidene ligand was achieved in ca. 15% higher yield than previously reported. The overall yield of **HII-Dansyl** was 16%, comparable to the 19% reported in Plenio's original route. Improvements in step 3 and 4 are clearly still required, but the methodology developed is reproducible, and will form a foundation for future work.

## 3.4 Experimental Procedures

General procedures are as shown in Chapter 2. Dansyl chloride (97%, ThermoFisher), 2-iodopropane (99%, Sigma-Aldrich), 5-nitrosalicylaldehyde (98%, Sigma-Aldrich), and $Ph_3PCH_3Br$ (98%, Sigma-Aldrich) were used without purification. Dansylstyrene was stored in the glovebox freezer at –35 °C. Catalyst **GII**[36] was prepared by the literature method.

### 3.4.1 Synthesis of 2-isopropoxy-5-nitrobenzaldehyde (25)

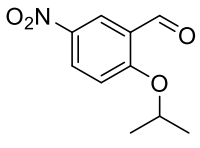


Under a flow of $N_2$, 2-iodopropane (6.10 g, 35.9 mmol, 2 equiv) was added to a suspension of $Cs_2CO_3$ (2.34 g, 7.2 mmol, 0.4 equiv) and $K_2CO_3$ (4.96 g, 35.9 mmol, 2 equiv) in 90 mL DMF. The mixture was stirred for 5 min, after which 5-nitrosalicylaldehyde (3.00 g, 17.9 mmol, 1 equiv) was added, and the reaction

was heated at 40 °C for 24 h. The yellow solution was cooled to RT, and 90 mL of water was added. The product was extracted with EtOAc (5 × 50 mL), then washed with water (50 mL) and brine (3 × 50 mL). The combined organic layers were dried over $MgSO_4$. The solvent was then removed under reduced pressure to yield a yellow solid, which was dried under vacuum for 12 h. Yield: 76%. $^1$H NMR (300 MHz, $CDCl_3$) δ 10.45 (s, 1H, C*H*O), 8.68 (d, $^4J_{HH}$ = 2.9 Hz, 1H, Ar-*H*), 8.39 (dd, $^3J_{HH}$ = 9.2, $^4J_{HH}$ = 2.9 Hz, 1H, Ar-*H*), 7.09 (d, $^3J_{HH}$ = 9.3 Hz, 1H, Ar-*H*), 4.84 (sept, $^3J_{HH}$ = 6.1 Hz, 1H, C*H*Me$_2$), 1.48 (d, *J* = 6.1 Hz, 6H, $^i$PrC*H*$_3$).

### 3.4.2 Synthesis of 2-isopropoxy-5-nitrostyrene (20)

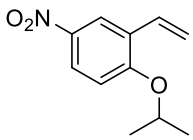

KO$^t$Bu (1.04 g, 9.25 mmol, 1.5 equiv) was suspended in 25 mL of dry THF and cooled to -78 °C and $(Ph)_3PCH_3Br$ (2.9 g, 8.06 mmol, 1.3 equiv) was slowly added as a solid under a flow of $N_2$. The mixture was allowed to warm to RT and stirred for 3 h. 2-Isopropoxy-5-nitrobenzaldehyde (2.9 g, 8.06 mmol, 1.3 equiv) was added at -78 °C. The resulting solution was allowed to warm to RT overnight, after which 30 mL of saturated $NH_4Cl$(aq) was added. The solution was extracted with $Et_2O$ (3 × 30 mL), washed with brine (3 × 30 mL), and the organic fraction was dried over $MgSO_4$. The solvent was removed under reduced pressure and the resulting residue was purified by silica-gel chromatography, eluting with 9:1 hexanes/EtOAc. The yellow fraction was isolated and stripped to a yellow viscous oil. Yield: 82%. $^1$H NMR (300 MHz, $CDCl_3$) δ 8.35 (d, $^4J_{HH}$ = 2.8 Hz, 1H, Ar-*H*), 8.11 (dd, $^3J_{HH}$ = 9.1, $^4J_{HH}$ = 2.9 Hz, 1H, Ar-*H*), 7.00 (dd, $^3J_{HH}$ = 17.7, $^3J_{HH}$ = 11.2 Hz, 1H, Ar-C*H*=Me), 6.90 (d, $^3J_{HH}$ = 9.1 Hz, 1H, Ar-*H*), 5.86 (dd, $^3J_{HH}$ = 17.8, $^2J_{HH}$ = 1.1 Hz, 1H, C=C*H*$_2$), 5.39 (dd, $^3J_{HH}$ = 11.2, $^2J_{HH}$ = 1.1 Hz, 1H, C=C*H*$_2$), 4.70 (sept, $^3J_{HH}$ = 6.1 Hz, 1H, C*H*Me$_2$), 1.41 (d, $^3J_{HH}$ = 6.1 Hz, 6H, $^i$PrC*H*$_3$).

### 3.4.3 Synthesis of 2-isopropoxy-5-aminostyrene (22)

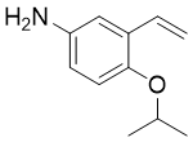

To a Schlenk flask containing Zn powder (3.1 g, 48.20 mmol, 10 equiv) was added glacial acetic acid (5 mL), followed by the dropwise addition of **20** (1.0 g, 4.82 mmol) against a flow of $N_2$. The mixture was stirred at RT for 4 h at which point full conversion confirmed by $^1$H NMR analysis. The reaction mixture was filtered through a Celite plug, and 10 mL of water was added. The resulting solution was extracted with EtOAc (3 × 20 mL), and the organic phase washed with brine (3 × 20 mL) and dried with $MgSO_4$. The combined organic layers were stripped to a thick dark oil and purified by column chromatography (silica gel; hexanes/EtOAc from 10% to 50%). The yellow fraction was isolated to give the product as a brown-yellow oil. Yield: 50%. $^1$H NMR (300 MHz, $CDCl_3$) δ7.01 (dd, $^3J_{HH}$ = 17.8, $^3J_{HH}$ = 11.1 Hz, 1H, Ar-C*H*=Me), 6.85 (d, $^4J_{HH}$ = 2.9 Hz, 1H, Ar-*H*), 6.75 (d, $^3J_{HH}$ = 8.6 Hz, 1H, Ar-*H*), 6.59 (dd, $^3J_{HH}$ = 8.6, $^4J_{HH}$ = 2.9 Hz, 1H, Ar-*H*), 5.66 (dd, $^3J_{HH}$ = 17.8, $^2J_{HH}$ = 1.5 Hz, 1H, C=C*H*$_2$), 5.21 (dd, $^3J_{HH}$ = 11.1, $^2J_{HH}$ = 1.5 Hz, 1H, C=C*H*$_2$), 4.32 (sept, $^3J_{HH}$ = 6.1 Hz, 1H, C*H*Me$_2$), 3.52 (s, 2H, N*H*$_2$), 1.30 (d, $^3J_{HH}$ = 6.1 Hz, 6H, $^i$PrC*H*$_3$).

### 3.4.4 Synthesis of Dansyl-styrene (23)

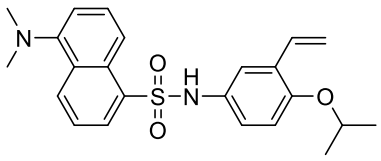

A solution of dansyl chloride (380 mg, 1.40 mmol) in 5 mL of dry THF was added to a 5 mL THF solution of **22** (380 mg, 2.14 mmol, 1.5 equiv) against an $N_2$ flow. Triethylamine (2.0 mL, 14.0 mmol, 10 equiv) was added and the reaction was left to stir at RT for 48 h. The solvent was removed under vacuum and residue was purified by column chromatography (silica gel; hexanes/EtOAc 10% to 30%). The main fraction was isolated and stripped of solvent to afford a yellow solid. Yield: 45%. $^1$H NMR (300 MHz, $CDCl_3$): δ 8.49 (d, $^3J_{HH}$ = 8.5 Hz, 1H), 8.38 (d, $^3J_{HH}$ = 8.6 Hz, 1H), 8.09 (d, $^3J_{HH}$ = 7.3 Hz, 1H), 7.58 (t, $^3J_{HH}$ = 8.1 Hz, 1H), 7.40 (t, $^3J_{HH}$ = 7.9 Hz, 1H), 7.19 (d, $^3J_{HH}$ = 7.5 Hz, 1H), 6.88 – 6.72 (m, 3H), 6.71 (s, 1H), 6.60 (d, $^3J_{HH}$ = 8.7 Hz, 1H), 5.30 (d, $^3J_{HH}$ = 17.7 Hz, 1H), 5.07 (d, $^3J_{HH}$ = 11.3 Hz, 1H), 4.36 (sept, $^3J_{HH}$ = 5.8 Hz, 1H), 2.88 (s, 6H), 1.25 (d, $^3J_{HH}$ = 6.1 Hz, 6H). Values agree with the literature report.[1]

### 3.4.5 Synthesis of $RuCl_2(H_2IMes)(=C_6H_3$-2-$O^iPr$-dansyl), HII-Dansyl

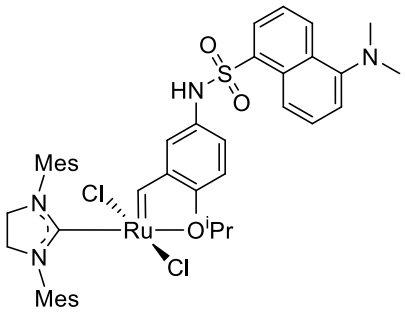

In the glovebox, **GII** (50 mg, 0.06 mmol, 1 equiv) was dissolved in 1.0 mL THF and heated to 50 °C. A solution of the dansyl styrene **23** (30 mg, 0.07 mmol, 1.2 equiv) in 0.5 mL THF was added dropwise. After 45 min CuCl (7 mg, 0.07 mmol, 1.2 equiv) was added. Full conversion of **GII** was confirmed by $^{31}$P NMR analysis in 2 h, and the reaction was allowed to cool to RT. The reaction mixture was filtered through a celite plug, and the solvent was removed from the filtrate by vacuum. The residue was purified by column chromatography in the glovebox, using a silica-gel column and eluting with 1:1 $CH_2Cl_2$/hexanes to afford a dark-green product. Yield: 85%. $^1$H NMR (300 MHz, $CDCl_3$): δ 16.23 (s, 1H, Ru=CH), 8.50 (d, $^3J_{HH}$ = 8.5 Hz, 1H), 8.29 (d, $^3J_{HH}$ = 8.6 Hz, 1H), 8.06 (dd, $^3J_{HH}$ = 7.4, $^4J_{HH}$ = 1.3 Hz, 1H), 7.58 (m, 1H), 7.42 (dd, $^3J_{HH}$ = 8.6, $^3J_{HH}$ = 7.3 Hz, 1H), 7.20 (d, $^3J_{HH}$ = 7.5 Hz, 1H), 7.00 (s, 4H), 6.68 (s, 1H), 6.58 (d, $^3J_{HH}$ = 2.6 Hz, 1H), 6.50 (d, J = 8.8 Hz, 1H), 4.73 (p, $^3J_{HH}$ = 6.1 Hz, 1H), 4.16 (s, 4H), 2.89 (s, 6H), 2.42 (s, br, 12H), 2.33 (s, 6H), 1.16 (d, $^3J_{HH}$ = 6.1 Hz, 6H).Values agree with the literature report.[1]

## 3.5 References


(1) Vorfalt, T.; Wannowius, K. J.; Thiel, V.; Plenio, H. How Important Is the Release–Return Mechanism in Olefin Metathesis? *Chem. – A Eur. J.* **2010**, *16*, 12312–12315.

(2) Sashuk, V.; Schoeps, D.; Plenio, H. Fluorophore Tagged Cross-Coupling Catalysts. *Chem. Commun.* **2009**, No. 7, 770–772.

(3) Godoy, J.; García-López, V.; Wang, L.-Y.; Rondeau-Gagné, S.; Link, S.; Martí, A. A.; Tour, J. M. Synthesis of a Fluorescent BODIPY-Tagged ROMP Catalyst and Initial Polymerization-Propelled Diffusion Studies. *Tetrahedron* **2015**, *71*, 5965–5972.

(4) Schunck, N. S.; Mecking, S. In Vivo Olefin Metathesis in Microalgae Upgrades Lipids to

Building Blocks for Polymers and Chemicals. *Angew. Chem. Int. Ed.* **2022**, *61*, e202211285.

(5) Toussaint, S. N. W.; Calkins, R. T.; Lee, S.; Michel, B. W. Olefin Metathesis-Based Fluorescent Probes for the Selective Detection of Ethylene in Live Cells. *J. Am. Chem. Soc.* **2018**, *140*, 13151–13155.

(6) Higman, C. S.; Lummiss, J. A. M.; Fogg, D. E. Olefin Metathesis at the Dawn of Implementation in Pharmaceutical and Specialty-Chemicals Manufacturing. *Angew. Chem. Int. Ed.* **2016**, *55*, 3552–3565.

(7) Nascimento, D. L.; Fogg, D. E. Origin of the Breakthrough Productivity of Ruthenium–Cyclic Alkyl Amino Carbene Catalysts in Olefin Metathesis. *J. Am. Chem. Soc.* **2019**, *141*, 19236–19240.

(8) Blanco, C. O.; Fogg, D. E. Water-Accelerated Decomposition of Olefin Metathesis Catalysts. *ACS Catal.* **2023**, *13*, 1097–1102.

(9) Nascimento, D. L.; Reim, I.; Foscato, M.; Jensen, V. R.; Fogg, D. E. Challenging Metathesis Catalysts with Nucleophiles and Brønsted Base: Examining the Stability of State-of-the-Art Ruthenium Carbene Catalysts to Attack by Amines. *ACS Catal.* **2020**, *10*, 11623–11633.

(10) Marx, V. M.; Sullivan, A. H.; Melaimi, M.; Virgil, S. C.; Keitz, B. K.; Weinberger, D. S.; Bertrand, G.; Grubbs, R. H. Cyclic Alkyl Amino Carbene (CAAC) Ruthenium Complexes as Remarkably Active Catalysts for Ethenolysis. *Angew. Chem. Int. Ed.* **2015**, *54*, 1919–1923.

(11) Blanco, C. O.; Sims, J.; Nascimento, D. L.; Goudreault, A. Y.; Steinmann, S. N.; Michel, C.; Fogg, D. E. The Impact of Water on Ru-Catalyzed Olefin Metathesis: Potent Deactivating Effects Even at Low Water Concentrations. *ACS Catal.* **2021**, *11*, 893–899.

(12) Gawin, R.; Tracz, A.; Chwalba, M.; Kozakiewicz, A.; Trzaskowski, B.; Skowerski, K. Cyclic Alkyl Amino Ruthenium Complexes—Efficient Catalysts for Macrocyclization and Acrylonitrile Cross Metathesis. *ACS Catal.* **2017**, *7*, 5443–5449.

(13) Bryant, R. G. The NMR Time Scale. *J. Chem. Educ.* **1983**, *60*, 933–935.

(14) Chakraborty, S. K. *Principles of Fluorescence Spectroscopy*; Lakowicz, J. R., Ed.; Springer US: Boston, MA, 2006; Vol. 33.

(15) Brand, L.; Johnson, M. L. *An Introduction to Fluorescence Spectroscopy*; PerkinElmer, 2011.

(16) Wardle, B. *Principles and Applications of Photochemistry*; Wiley, 2009.

(17) Vázquez-Villa, H.; González-Vera, J. A.; Benhamú, B.; Viso, A.; Fernández de la Pradilla, R.; Junquera, E.; Aicart, E.; López-Rodríguez, M. L.; Ortega-Gutiérrez, S. Development of Molecular Probes for the Human 5-HT 6 Receptor. *J. Med. Chem.* **2010**, *53*, 7095–7106.

(18) David, T.; Kotek, J.; Kubíček, V.; Tošner, Z.; Hermann, P.; Lukeš, I. Bis(Phosphonate)-Building Blocks Modified with Fluorescent Dyes. *Heteroat. Chem.* **2013**, *24*, 413–425.

(19) Garg, S. S.; Gupta, J.; Sharma, S.; Sahu, D. An Insight into the Therapeutic Applications of Coumarin Compounds and Their Mechanisms of Action. *Eur. J. Pharm. Sci.* **2020**, *152*, 105424.

(20) Sun, X.; Liu, T.; Sun, J.; Wang, X. Synthesis and Application of Coumarin Fluorescence Probes. *RSC Adv.* **2020**, *10*, 10826–10847.

(21) Hua, C.; Zhang, K.; Xin, M.; Ying, T.; Gao, J.; Jia, J.; Li, Y. High Quantum Yield and PH Sensitive Fluorescence Dyes Based on Coumarin Derivatives: Fluorescence Characteristics and Theoretical Study. *RSC Adv.* **2016**, *6*, 49221–49227.

(22) Sun, M.; Yang, X.; Zhang, Y.; Wang, S.; Wong, M. W.; Ni, R.; Huang, D. Rapid and Visual Detection and Quantitation of Ethylene Released from Ripening Fruits: The New Use of Grubbs Catalyst. *J. Agric. Food Chem.* **2019**, *67*, 507–513.

(23) Noh, H.; Lim, T.; Park, B. Y.; Han, M. S. A Fluorescence-Based High-Throughput Screening Method for Olefin Metathesis Using a Ratiometric Fluorescent Probe. *Org. Lett.* **2020**, *22*, 1703–1708.

(24) Obukhova, O. M.; Mchedlov-Petrossyan, N. O.; Vodolazkaya, N. A.; Patsenker, L. D.; Doroshenko, A. O. Stability of Rhodamine Lactone Cycle in Solutions: Chain–Ring Tautomerism, Acid–Base Equilibria, Interaction with Lewis Acids, and Fluorescence. *Colorants* **2022**, *1*, 58–90.

(25) Smith, S.; Pretorius, W. The Conservative Behaviour of Fluorescein. *Water SA* **2002**, *28*, 403–406.

(26) Fu, Y.; Finney, N. S. Small-Molecule Fluorescent Probes and Their Design. *RSC Adv.* **2018**, *8*, 29051–29061.

(27) Grimm, J. B.; Lavis, L. D. Caveat Fluorophore: An Insiders' Guide to Small-Molecule Fluorescent Labels. *Nat. Methods* **2022**, *19*, 149–158.

(28) Bates, J. M.; Lummiss, J. A. M.; Bailey, G. A.; Fogg, D. E. Operation of the Boomerang Mechanism in Olefin Metathesis Reactions Promoted by the Second-Generation Hoveyda Catalyst. *ACS Catal.* **2014**, *4*, 2387–2394.

(29) Vong, K.; Eda, S.; Kadota, Y.; Nasibullin, I.; Wakatake, T.; Yokoshima, S.; Shirasu, K.; Tanaka, K. An Artificial Metalloenzyme Biosensor Can Detect Ethylene Gas in Fruits and Arabidopsis Leaves. *Nat. Commun.* **2019**, *10*, 5746.

(30) Easter, Q. T.; Blum, S. A. Organic and Organometallic Chemistry at the Single-Molecule, -Particle, and -Molecular-Catalyst-Turnover Level by Fluorescence Microscopy. *Acc. Chem. Res.* **2019**, *52*, 2244–2255.

(31) Reuter, R.; Ward, T. R. Profluorescent Substrates for the Screening of Olefin Metathesis Catalysts. *Beilstein J. Org. Chem.* **2015**, *11*, 1886–1892.

(32) Rix, D.; Clavier, H.; Coutard, Y.; Gulajski, L.; Grela, K.; Mauduit, M. Activated Pyridinium-Tagged Ruthenium Complexes as Efficient Catalysts for Ring-Closing Metathesis. *J. Organomet. Chem.* **2006**, *691*, 5397–5405.

(33) Pagliarani, A.; Nesci, S.; Ventrella, V. Toxicity of Organotin Compounds: Shared and Unshared Biochemical Targets and Mechanisms in Animal Cells. *Toxicol. Vitr.* **2013**, *27*, 978–990.

(34) Barbosa, C. M. de L.; Ferrão, F. M.; Graceli, J. B. Organotin Compounds Toxicity: Focus on Kidney. *Front. Endocrinol. (Lausanne).* **2018**, *9*, 1–7.

(35) Bujok, R.; Bieniek, M.; Masnyk, M.; Michrowska, A.; Sarosiek, A.; Stępowska, H.; Arlt, D.; Grela, K. Ortho- and Para-Substituted Hoveyda−Grubbs Carbenes. An Improved Synthesis of Highly Efficient Metathesis Initiators. *J. Org. Chem.* **2004**, *69*, 6894–6896.

(36) Nascimento, D. L.; Davy, E. C.; Fogg, D. E. Merrifield Resin-Assisted Routes to Second-Generation Catalysts for Olefin Metathesis. *Catal. Sci. Technol.* **2018**, *8*, 1535–1544.

(37) Blanco, C. O.; Nascimento, D. L.; Fogg, D. E. Routes to High-Performing Ruthenium–Iodide Catalysts for Olefin Metathesis: Ligand Lability Is Key to Efficient Halide Exchange. *Organometallics* **2021**, *40*, 1811–1816.

(38) Bieniek, M.; Michrowska, A.; Gułajski, Łu.; Grela, K. A Practical Larger Scale Preparation of Second-Generation Hoveyda-Type Catalysts. *Organometallics* **2007**, *26*, 1096–1099.

(39) Van Veldhuizen, J. J.; Gillingham, D. G.; Garber, S. B.; Kataoka, O.; Hoveyda, A. H. Chiral Ru-Based Complexes for Asymmetric Olefin Metathesis: Enhancement of Catalyst Activity through Steric and Electronic Modifications. *J. Am. Chem. Soc.* **2003**, *125*, 12502–12508.

(40) Cumine, F.; Palumbo, F.; Murphy, J. A. Reduction of Nitroarenes, Azoarenes and Hydrazine Derivatives by an Organic Super Electron Donor. *Tetrahedron* **2018**, *74*, 5539–5545.

(41) Yu, C.; Liu, B.; Hu, L. Samarium(0) and 1,1‘-Dioctyl-4,4‘-Bipyridinium Dibromide: A Novel Electron-Transfer System for the Chemoselective Reduction of Aromatic Nitro Groups. *J. Org. Chem.* **2001**, *66*, 919–924.

(42) Bellamy, F. D.; Ou, K. Selective Reduction of Aromatic Nitro Compounds with Stannous Chloride in Non Acidic and Non Aqueous Medium. *Tetrahedron Lett.* **1984**, *25*, 839–842.

(43) Yrjölä, S.; Parkkari, T.; Navia-Paldanius, D.; Laitinen, T.; Kaczor, A. A.; Kokkola, T.; Adusei-Mensah, F.; Savinainen, J. R.; Laitinen, J. T.; Poso, A.; Alexander, A.; Penman, J.; Stott, L.; Anskat, M.; Irving, A. J.; Nevalainen, T. J. Potent and Selective N-(4-Sulfamoylphenyl)Thiourea-Based GPR55 Agonists. *Eur. J. Med. Chem.* **2016**, *107*, 119–132.

(44) Auzzas, L.; Larsson, A.; Matera, R.; Baraldi, A.; Deschênes-Simard, B.; Giannini, G.; Cabri, W.; Battistuzzi, G.; Gallo, G.; Ciacci, A.; Vesci, L.; Pisano, C.; Hanessian, S. Non-Natural Macrocyclic Inhibitors of Histone Deacetylases: Design, Synthesis, and Activity. *J. Med. Chem.* **2010**, *53*, 8387–8399.

(45) Jacou, C. C. P.; Montpellier, F.-R. A.; Romainville, F. M.-E. B.; Wauthier-Braine, D. S. Phosphinate Ruthenium Complexes. US 8309737 B2, 2012.

## Chapter 4 Conclusions and Future Work

Olefin metathesis holds great promise for its versatility in a wide range of applications: for example, for the production of antiviral and oncology therapeutics in the pharmaceutical industry, for the production of specialty-grade polymers, and for the preparation of essential building-block chemicals from biomass. The ruthenium metathesis catalysts have been widely adopted for metathesis in the research and discovery context, owing to their high functional-group tolerance and their greater resistance to moisture and oxygen relative to catalysts based on early- or mid-transition metals. However, low catalyst productivity has presented a significant challenge to the use of metathesis on production or manufacturing scales. This is now poised to change. A step-change in productivity came with the introduction of catalysts containing cyclic (alkyl)(amino)carbene (CAAC) ligands. Such catalysts dramatically increase efficiency in the bench-scale conversion of unsaturated hydrocarbon chains present in methyl oleate and other FAMEs. The latter are considered carbon-neutral, and thus represent potentially renewable feedstocks, particularly if they can be harvested on scale from non-edible fatty oils such as those produced by microalgae. Olefin metathesis hence emerges as an attractive and potentially viable catalytic process for the transformation of biomass into valuable oleochemical products. Nonetheless, the internal olefins in plant and algal lipids are more problematic substrates than the 1-olefins that dominate olefin metathesis, owing to their reduced accessibility. In short, catalyst performance is diminished by the steric hindrance present even in cis-configured double bonds.

Reducing ligand bulk is believed to play a decisive role in improving performance in the metathesis of internal olefins and, more broadly, in successfully handling crowded substrates. Decreasing the size of the CAAC ligands would thus enhance the capacity of the catalysts to interact with sterically congested substrates. Deployment of such catalysts is hampered, however, by the significant challenges of synthesizing catalysts bearing small CAACs. The work described in Chapter 2 addresses these problems for the smallest current CAAC ligand, **CAAC-10**, in which the carbene carbon is flanked by an N-mesityl group and a dimethyl-substituted carbon. The core problem identified at the outset of this work was the dominance of side-reactions during the attempted liberation and installation of the small carbene on the metal center. More minor challenge in synthesis emerged in the production of the iminium CAAC salts that function as precursors for the carbene. These reactions were found to exhibit sensitivities that are either not operative or are less pronounced for larger CAACs. Addressing these issues (largely unexplored in the reported work) proved essential to success in the cyclization step.

Nevertheless, the central challenge remains installation of small CAAC ligands such as **CAAC-10** on the Hoveyda platform. Current routes to the target catalyst **RuCAAC-10** fail outright, or deliver the product in yields ranging from 14% in a literature report, to 40% in a patent claim. The premise in this thesis work was that the low yields in carbene installation for small CAACs are due to nucleophilic abstraction of the alkylidene ligand, resulting in decomposition of the catalyst in situ during its attempted synthesis. The nucleophilicity of free NHCs is commonly masked by their strong Lewis basicity: that is, ligation quenches their nucleophilicity. However, the electron-

rich free carbenes can also participate as nucleophiles that promote undesired degradation pathways.

To circumvent such reactions, the conventional Ru-dichloride precursor (the first-generation Hoveyda complex **HI**) was converted into its iodide analogue **HI-$I_2$**. The latter was employed as a platform for installation of **CAAC-10**, on the presumption that the bulkier **RuCAAC-10-$I_2$** complex should be sterically protected against nucleophilic attack on the alkylidene. Following isolation of **RuCAAC-10-$I_2$**, transformation into the desired chloride species **RuCAAC-10** was envisaged**,** by salt metathesis in an environment free from $PCy_3$ or a free CAAC. Consistent with the fundamental hypothesis, the synthetic strategy outlined yielded **RuCAAC-10** with an overall yield of 55%, a significant improvement over the maximum of 14% reported in the open literature.

This route offers a practical, efficient, and potentially general methodology for the preparation of catalysts bearing small carbene ligands. One line of future advance would involve extension to synthesis of other catalysts bearing small carbenes, whether CAAC or others. From a mechanistic perspective, the experiments to date are weakened by the absence of evidence for the participation of $PCy_3$ and/or **CAAC-10** in decomposing the Ru-chloride species. Experiments to probe the stability of **RuCAAC-10** to nucleophiles could add weight to the core hypothesis. The availability of the chloride complex via the synthetic route developed in Chapter 2 permits these ideas to be explicitly tested. Recommended as priority experiments are the addition of $PCy_3$ and small carbenes to isolated, clean **RuCAAC-10**, with an internal NMR standard present to enable tracking of benzylidene loss over time. Mass spectrometric analysis could confirm formation of the putative $[ArCH_2PCy_3]Cl$ product of $PCy_3$ attack, while addition of pyridine could help trap the Ru products.

Confirming nucleophilic attack by the small CAAC is more difficult. A first attempt could involve flooding a solution of **RuCAAC-10** with free **CAAC-01**. This approach would build on current efforts by Ms. Eliza-Jayne Boisvert of this research group to maximize in situ yields of free CAACs. The proposed reaction would involve immediate addition of the free **CAAC-10**, without isolation, to **RuCAAC-10**. Shown in Scheme 4.1a are two possible products: **A1**, formed by nucleophilic attack and ensuing deprotonation of a ligand or other proton source, and N-heterocyclic olefin (NHO) **A2**, precedent for which comes from prior work by our group with a small free NHC.[1] Use of excess **CAAC-10** may also enable trapping of a $RuCl_2$(**CAAC-10**)$_4$ product.

**Scheme 4.1.** Proposed experiments to confirm degradation of **RuCAAC-10** by nucleophiles.

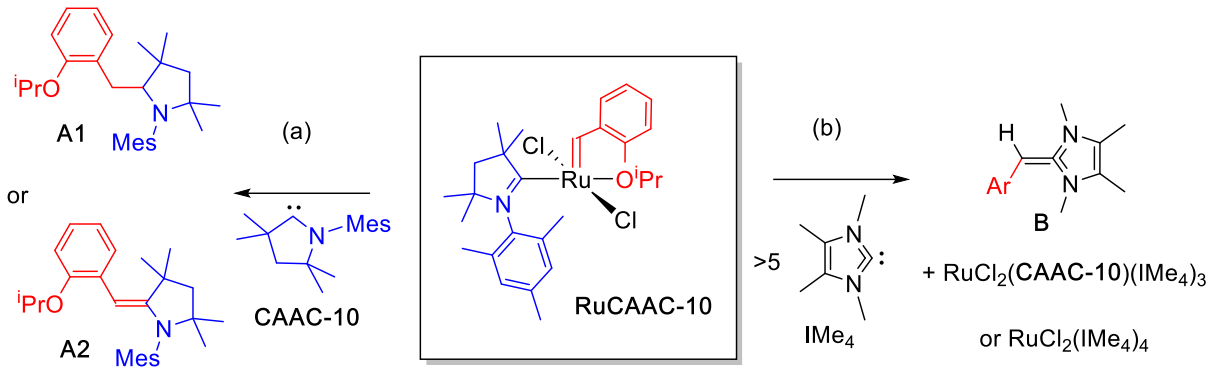


However, competing reaction with the excess base used to generate free **CAAC-10** may cloud the results. An alternative approach could therefore involve the proxy use of the small NHC $IMe_4$, in which the carbene carbon is flanked by two NMe groups (Scheme 4.1b). $IMe_4$ is readily isolated and handled as the free carbene, and was shown in earlier work from our group to engage in nucleophilic attack on the methylidene ligand of $RuCl_2(PCy_3)_2(=CH_2)$.[1] By analogy to the latter work, attack on **RuCAAC-10** may produce the NHO **B**, $IMe_4$=CHAr. Positive evidence would not be a clear-cut demonstration that attack of **CAAC-10** could occur, as $IMe_4$ is even less bulky than **CAAC-10**, but would nevertheless provide insight into possible products to aid in analysis of the experiment with **CAAC-10** proposed above. Failed reaction of $IMe_4$ with clean **RuCAAC-10** would be strong evidence against the proposed nucleophilic degradation.

The capacity of the **RuCAAC-10** catalyst to aid in the metathesis of crowded olefins was confirmed by undertaking the self-metathesis of methyl oleate (**MO**), a potentially renewable feedstock. Self-metathesis avoids the formation of methylidene species during catalysis, and hence limits decomposition via bimolecular coupling, a pathway to which our group has shown that the CAAC catalysts are particularly susceptible.[2,3] The intermediates in the self-metathesis reaction are bulky alkylidene derivatives, which are stabilized against BMC despite the small size of the CAAC ligand. **RuCAAC-10** demonstrated exceptional performance, achieving 430,000 TON with complete selectivity for the target Z-olefin. It surpassed both its diiodide analogue **RuCAAC-10-I$_2$** (as expected) and **RuCAAC-3**. The latter is identical to **RuCAAC-10** but for the presence of an *o*-CMePh group flanking the carbene carbon, supporting the hypothesis that reduced steric bulk is an asset. It also outperforms not only the well-established NHC catalyst **HII**, but the best catalysts reported to date. This outstanding performance underscores the advantage of reducing catalyst size in metathesis of the cis-olefins ubiquitous in nature, as well as more crowded substrates.

Future work should undertake expansion to the highly desired 'ethenolysis' of **MO**, a reaction that cleaves long-chain fatty acids into two smaller 1-alkenes of high market value. The challenge in such reactions, as noted above, is that metathesis with ethylene generates methylidene intermediates. Bimolecular decomposition of the latter is anticipated to be especially fast given the small size of **RuCAAC-10**. That is, the same steric feature that makes the catalyst so desirable for metathesis with internal olefins is expected to severely degrade catalyst lifetime. If, as expected,

BMC suppresses the performance of **RuCAAC-10** even at the lowest possible (sub-micromolar) catalyst concentrations, immobilization on solid support may enable its impressive performance to be maintained even in 'ethenolysis' reactions.

Chapter 3 tackles the very different synthetic challenges involved in the preparation of fluorophore-tagged catalysts for olefin metathesis. Catalysts labelled with fluorophores have great potential as a tool for visualizing and monitoring catalyst behaviour, including decomposition, throughout a reaction. They also facilitate real-time monitoring of reactions, providing mechanistic insights under authentic operating conditions. In particular, they could enable monitoring of catalysts at concentrations unattainably low for observation by NMR analysis. The utilization of fluorophore-tagged metathesis catalysts has the capacity to boost advances in the fields of materials science, renewable feedstocks, industrial processes, and pharmaceutical chemistry.

The synthesis of **HII-Dansyl**, in which the benzylidene ligand is tagged with a dansyl fluorophore, was selected due to the exceptional chemical stability of the dansyl group, and its high quantum yield, large Stokes shift, and minimal interference with catalyst activity. The literature route to **HII-Dansyl** is limited low yields in several key reactions. Planned improvements focused on two main aspects: the first step, in which a yield of ca. 50% was reported for reduction of the nitro group by $Na_2S_2O_4$/bipyridinium bromide, and the 65% yield of the final reaction, incorporation of the dansyl-tagged isopropoxy benzylidene group. Some progress was made in the first objective. Reduction of the nitro group with Zn/HOAc was pursued in light of a patent claiming a yield of 86%. Despite exhaustive attempts, this yield could not be replicated even under conditions identical to those described. An unexpected issue was the appearance of a side product, possibly the doubly-substituted dansylamine. Confirmation and mitigation of this reaction is a priority.

Greater success was achieved in incorporation of the dansyl-tagged benzylidene ligand, accomplished in 15% higher yield compared to the literature report. Although the overall yield remained comparable to that originally established, the route in this thesis work offers more convenient access to **22** and the dansyl-tagged catalyst. While there is still room for improvement in the reduction step, in particular, the methodology developed is reproducible and provides a solid foundation for future research advances.

## 4.1 References


(1) Rufh, S. A.; Goudreault, A. Y.; Foscato, M.; Jensen, V. R.; Fogg, D. E. Rapid Decomposition of Olefin Metathesis Catalysts by a Truncated N-Heterocyclic Carbene. *ACS Catal.* **2018**, *8*, 11822–11826.

(2) Occhipinti, G.; Nascimento, D. L.; Foscato, M.; Fogg, D. E.; Jensen, V. R. The Janus Face of High Trans-Effect Carbenes in Olefin Metathesis: Gateway to Both Productivity and Decomposition. *Chem. Sci.* **2022**, *13*, 5107–5117.

(3) Nascimento, D. L.; Foscato, M.; Occhipinti, G.; Jensen, V. R.; Fogg, D. E. Bimolecular Coupling in Olefin Metathesis: Correlating Structure and Decomposition for Leading and Emerging Ruthenium−Carbene Catalysts. *J. Am. Chem. Soc.* **2021**, *143*, 11072–11079.

# Appendices

## NMR Spectra

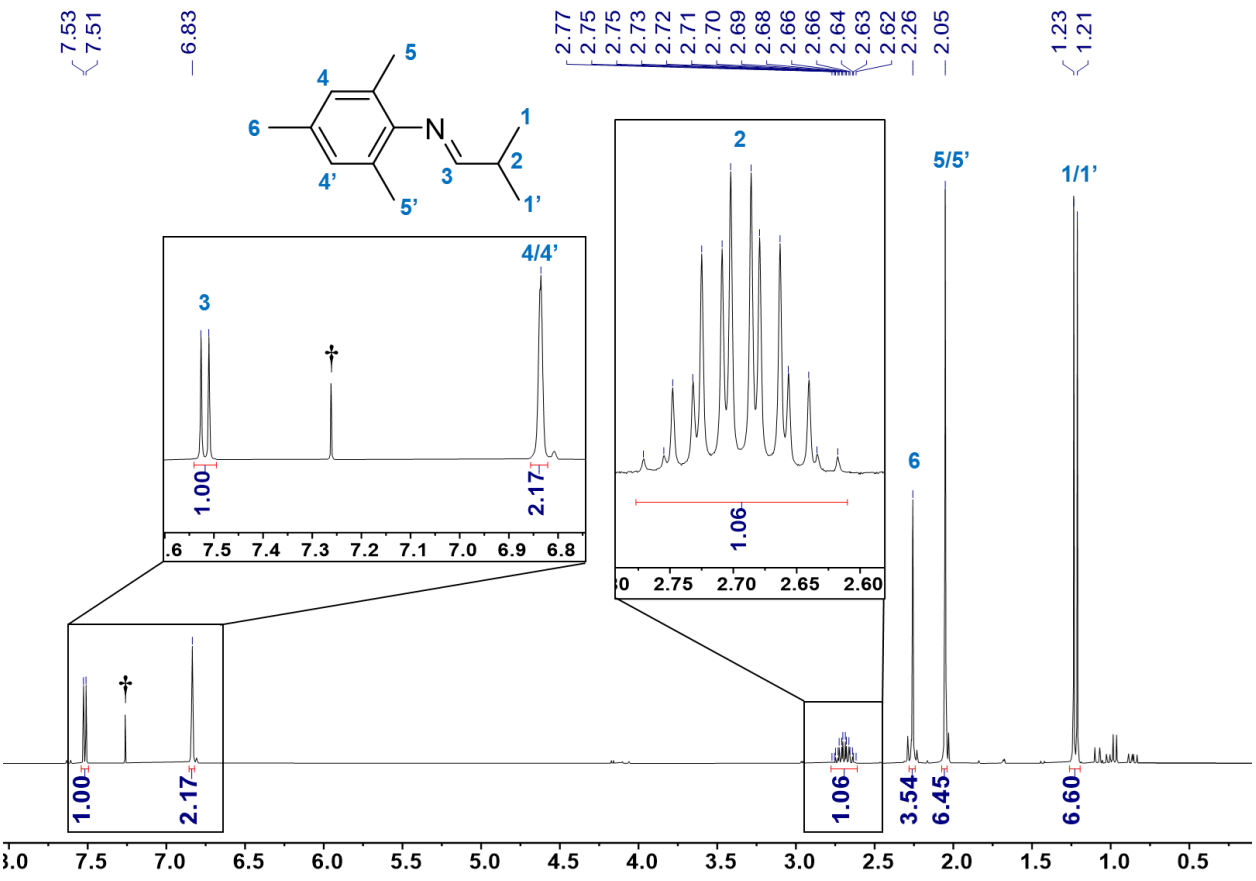


**Figure A.1.** $^{1}H$ NMR spectrum (300 MHz, $CDCl_3$) of aldimine **10a** († = residual proton of the deuterated solvent).

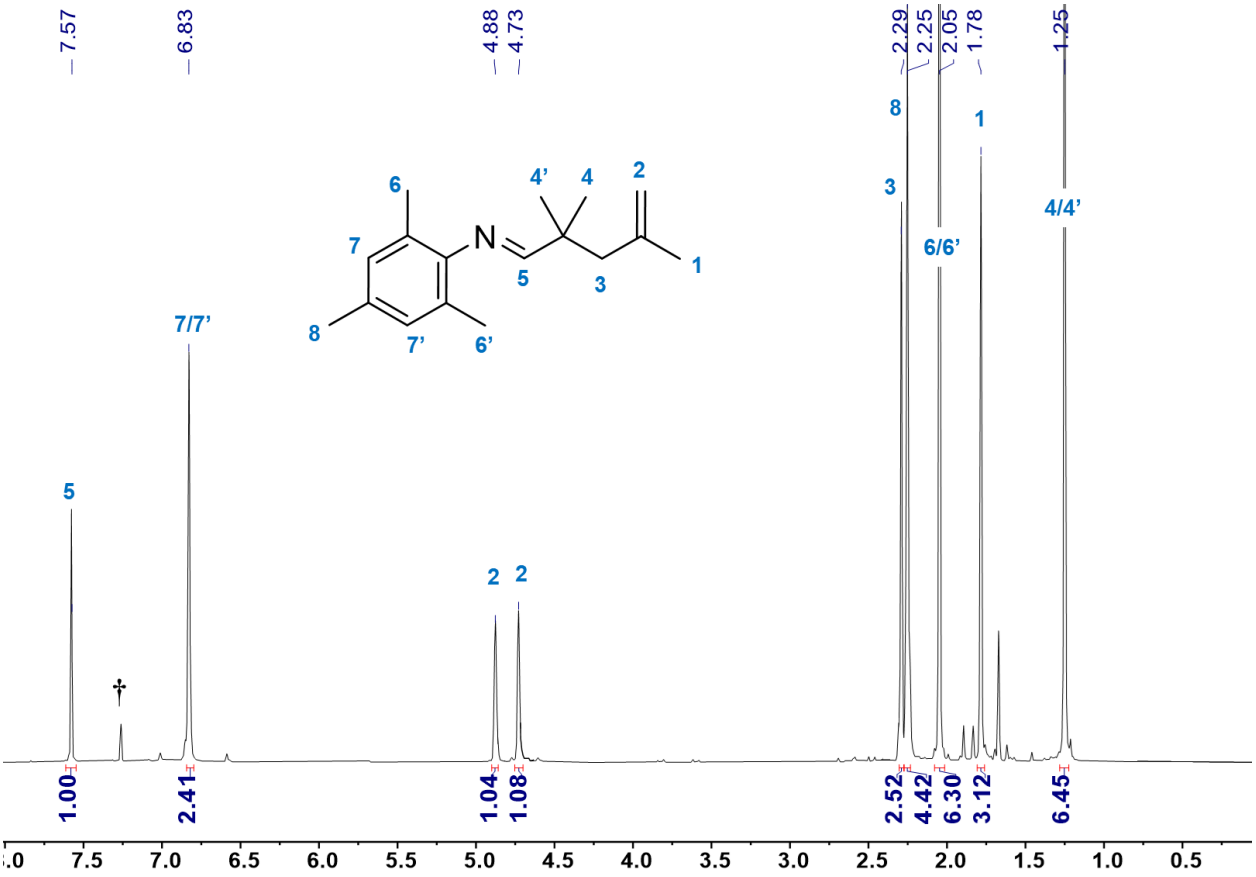


**Figure A.2.** $^{1}$H NMR spectrum (300 MHz, $CDCl_3$) of alkenyl imines **11a** († = residual proton of the deuterated solvent).

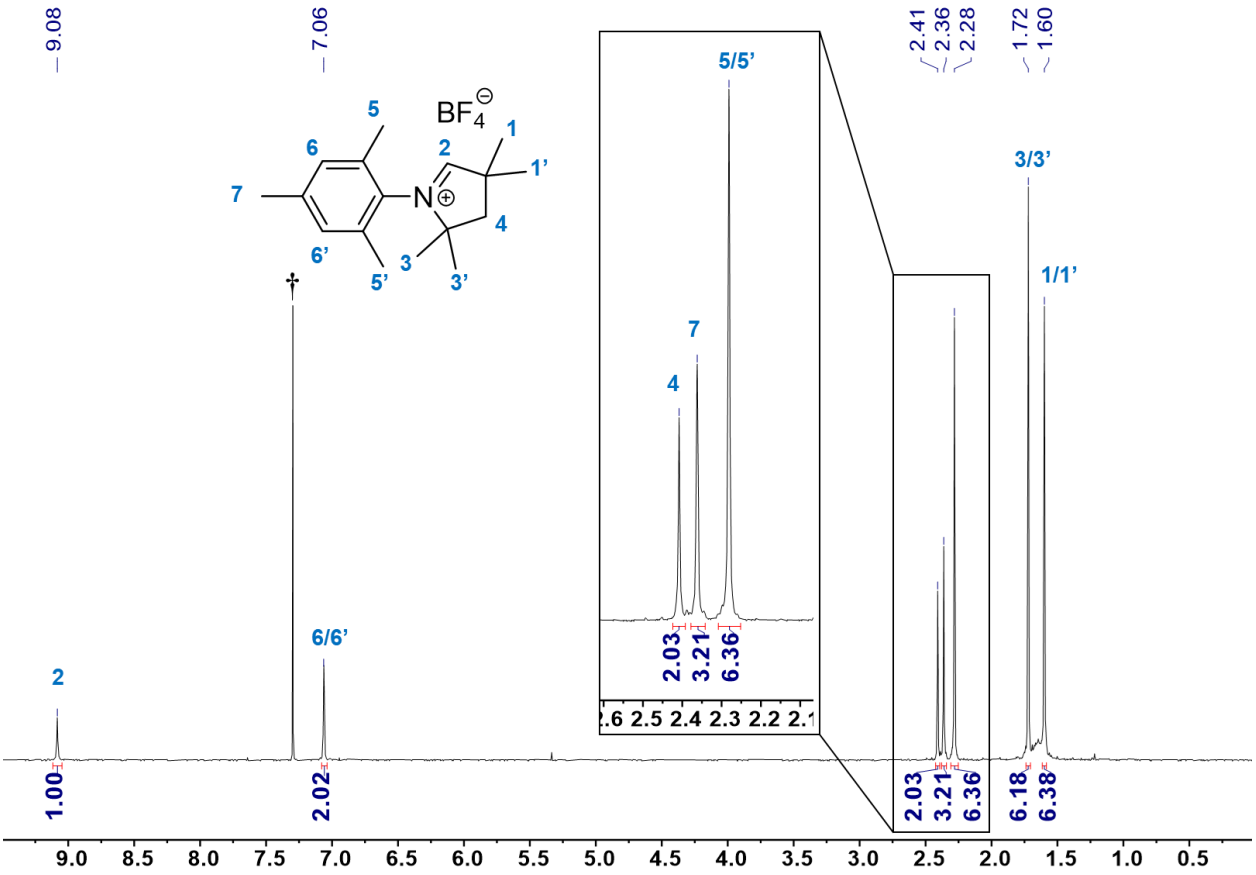


**Figure A.3.** $^{1}$H NMR spectrum (300 MHz, $CDCl_3$) of **CAAC-10•HBF$_4$** († = residual proton of the deuterated solvent).

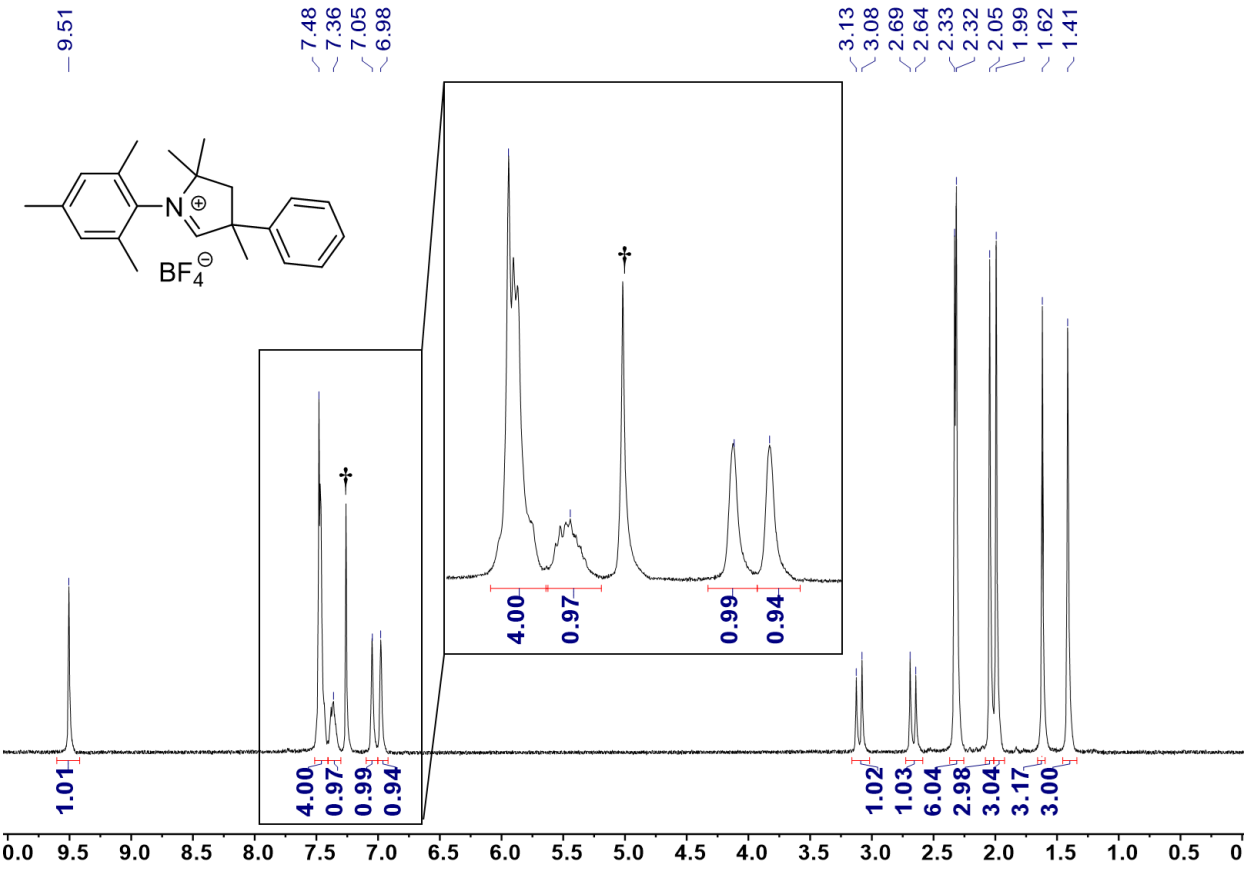


**Figure A.4.** $^{1}$H NMR spectrum (300 MHz, $CDCl_3$) of **CAAC-3•HBF$_4$** († = residual proton of the deuterated solvent).

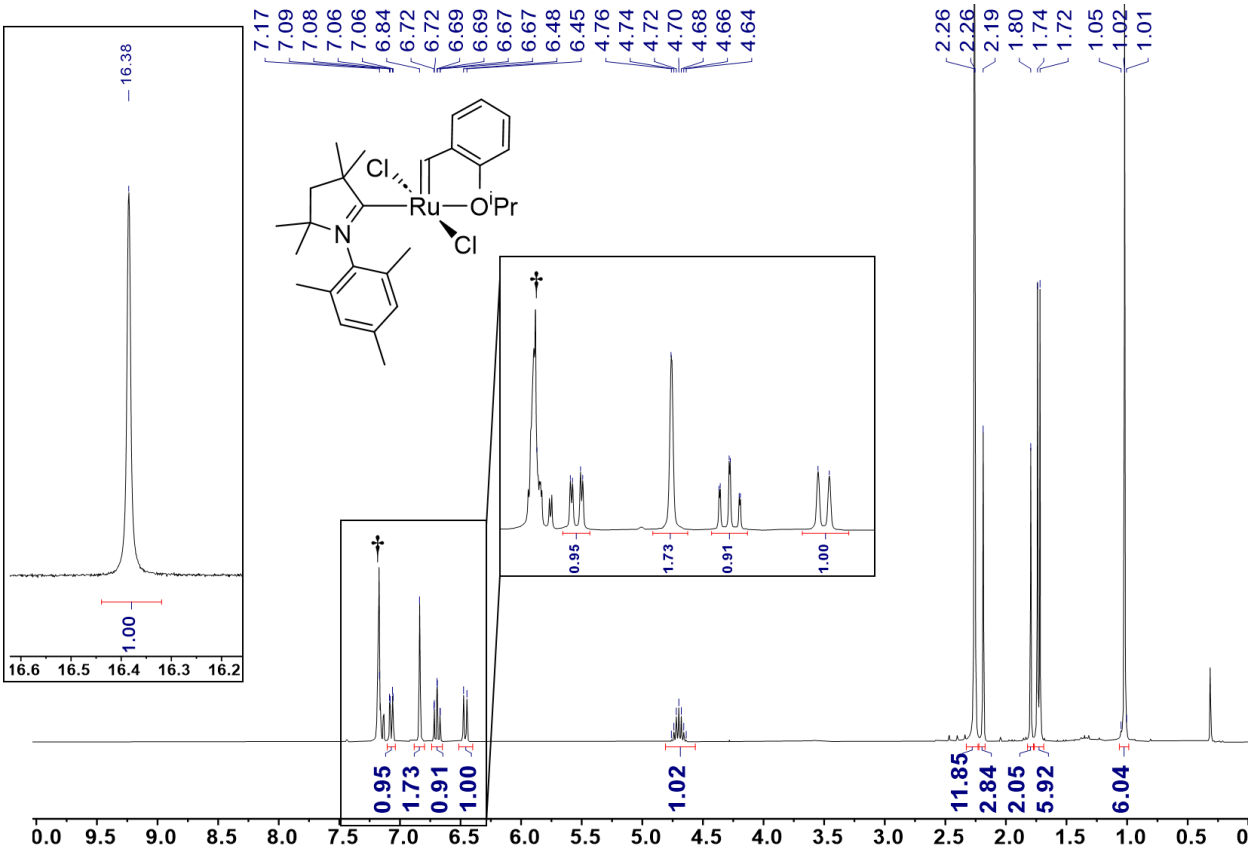


**Figure A.5.** $^{1}$H NMR spectrum (300 MHz, $C_6D_6$) of **RuCAAC-6** († = residual proton of the deuterated solvent).

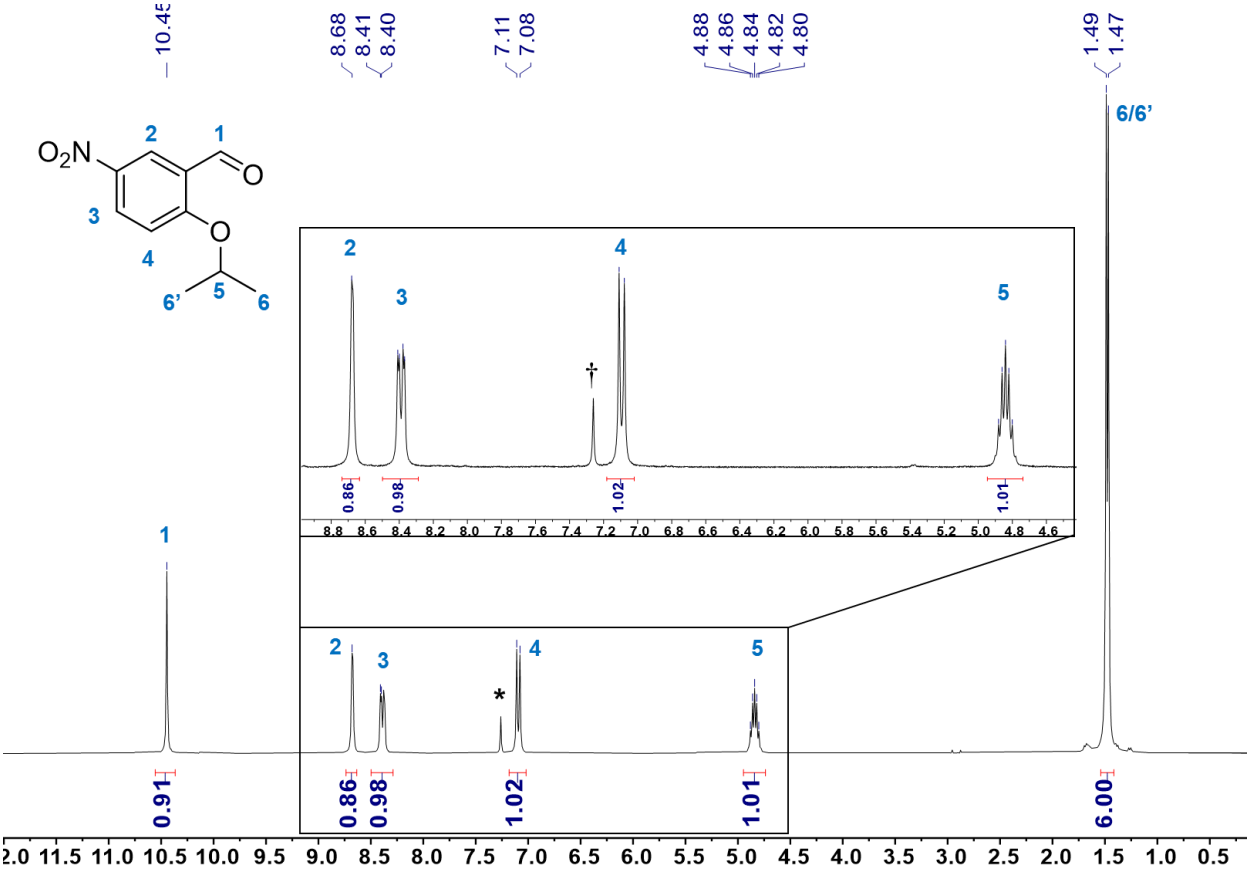


**Figure A.6.** $^{1}H$ NMR spectrum (300 MHz, $CDCl_3$) of 2-isopropoxy-5-nitrobenzaldehyde (**25**) († = residual proton of the deuterated solvent).

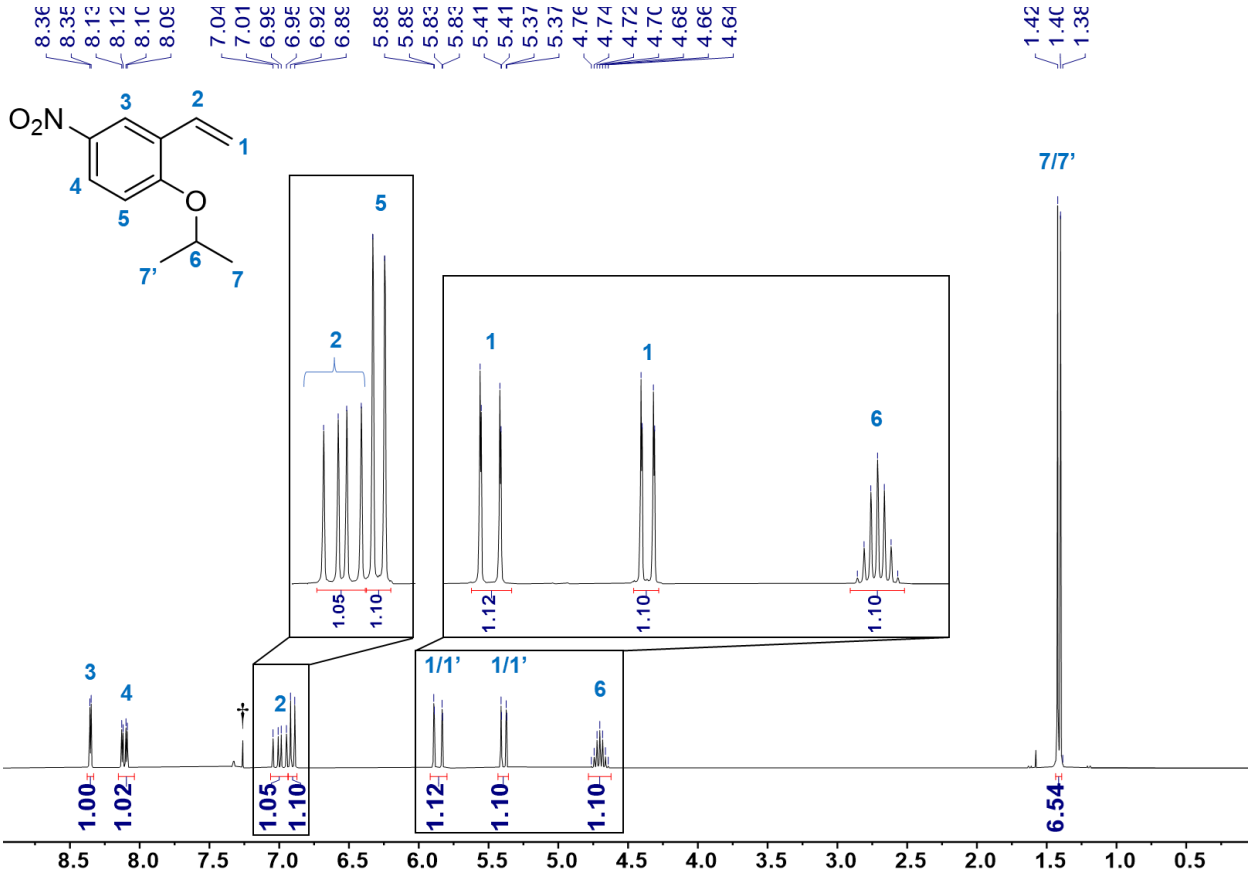


**Figure A.7.** $^{1}H$ NMR spectrum (300 MHz, $CDCl_3$) of 2-isopropoxy-5-nitrostyrene (**20**) († = residual proton of the deuterated solvent).

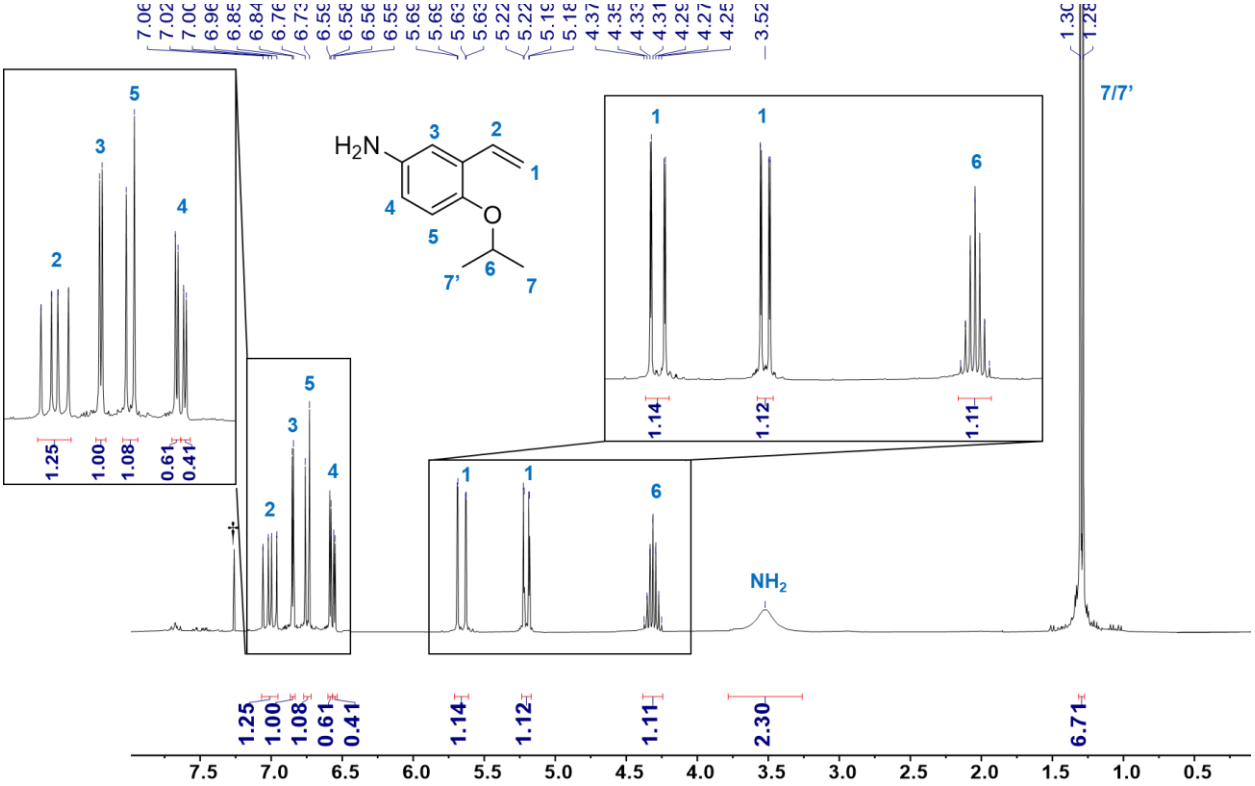


**Figure A.8.** $^{1}H$ NMR spectrum (300 MHz, $CDCl_3$) of 2-isopropoxy-5-aminostyrene (**22**) († = residual proton of the deuterated solvent).

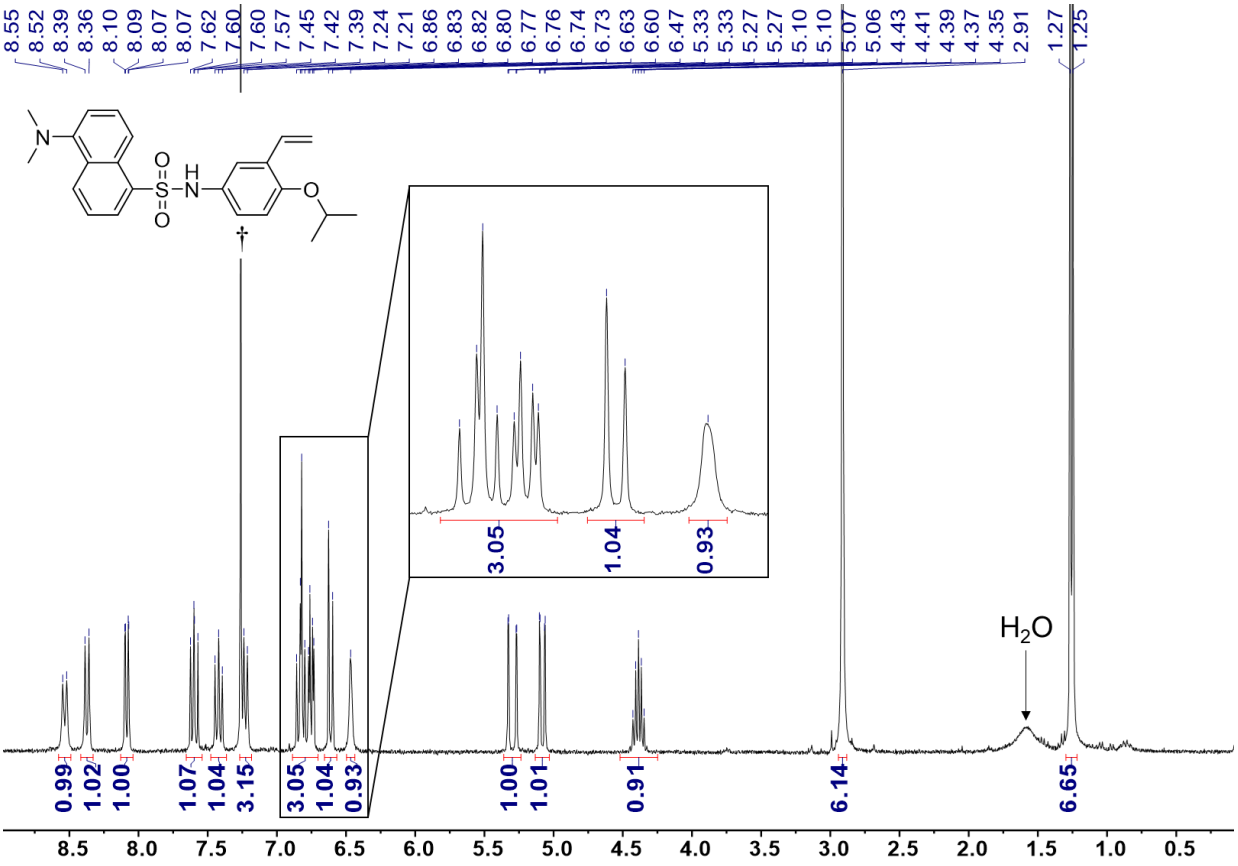


**Figure A.9.** $^{1}H$ NMR spectrum (300 MHz, $CDCl_3$) of dansyl-styrene (**23**) († = residual proton of the deuterated solvent).

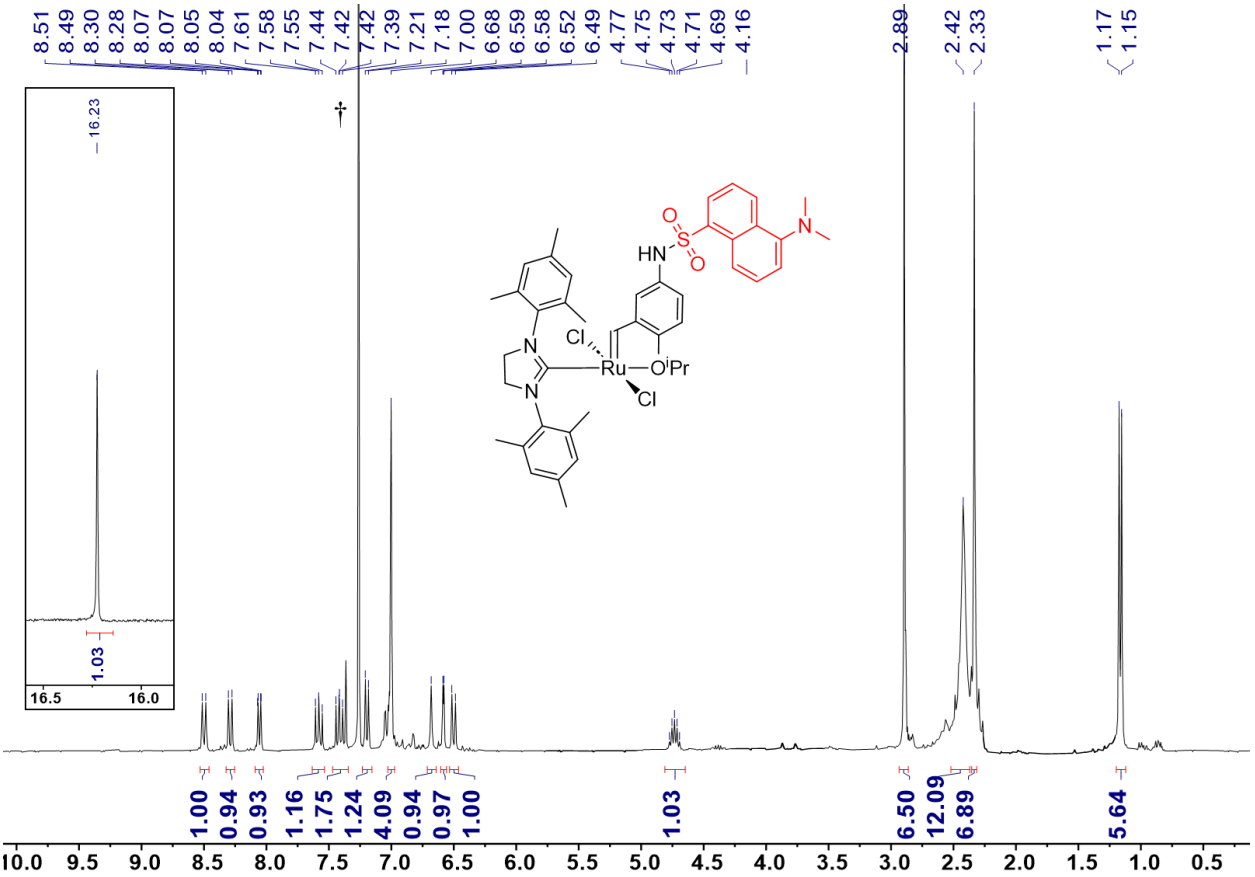


**Figure A.10.** $^1$H NMR spectrum (300 MHz, $CDCl_3$) of **HII-Dansyl** († = residual proton of the deuterated solvent).